

Daniel Solheim Haugsvær

# Steel lazy wave riser system in deep water and harsh environment

Master's thesis in Marine Technology

Supervisor: Bernt Johan Leira

June 2024





Daniel Solheim Haugsvær

# **Steel lazy wave riser system in deep water and harsh environment**

Master's thesis in Marine Technology  
Supervisor: Bernt Johan Leira  
June 2024

Norwegian University of Science and Technology  
Faculty of Engineering  
Department of Marine Technology







## Master Thesis Spring 2024

for

**Stud. Tech. Daniel Haugsvær**

### **Steel lazy wave riser system in deep water and harsh environment**

*Lazy wave stigerørsystem i stål på dypt vann med utfordrende havmiljø*

Oil and gas production and exploration moves towards larger water depths, subjected to harsh environmental conditions. Riser technology has been introduced to carry out the retrieval of deep water oil and gas resources. The design of the systems that connect the surface floater to the subsea installation must satisfy a set of criteria due to the load the system is subjected to. This is to ensure a safe design as failure of the system can have major consequences in the form of human injury and fatalities, and also with respect to environmental damage and financial loss. The commonly used production riser configuration comprised of a steel catenary pipe can be subjected to low fatigue life at the touch down point when connected to a floater with large heave motions. The Steel lazy wave riser configuration is presented as a more robust configuration when it comes to being subjected to harsh environments. This configuration will be investigated as a part of this thesis.

The following subjects are to be addressed as part of this work:

1. An overview of different types of riser systems is to be given.
2. An outline of the static, dynamic and fatigue analysis methods is to be presented.
3. Relevant design guidelines and codes for riser systems are to be reviewed and key design limit states should be summarized (i.e. SLS, ULS, FLS and ALS).
4. A model of a steel lazy wave riser connected to a semi-submersible platform is to be created in order to be applied for static and dynamic response and fatigue analysis.
5. A parametric study of the buoyancy section of the steel lazy wave riser is to be carried out. If time allows, design issues related to the top end termination of the riser at the connection to the platform are to be addressed.

The work scope may prove to be larger than initially anticipated. Subject to approval from the supervisors, topics may be deleted from the list above or reduced in extent. This is to be notified to the reader in the introduction.

In the master report, the candidate shall present his/her personal contribution to the resolution of problems within the scope of the master work



Theories and conclusions should be based on mathematical derivations and/or logic reasoning identifying the various steps in the deduction.

The candidate should utilise the existing possibilities for obtaining relevant literature.

### **Master report format**

The master report should be organised in a rational manner to give a clear exposition of results, assessments, and conclusions. The text should be brief and to the point, with a clear language. Telegraphic language should be avoided.

The report shall contain the following elements: A text defining the scope (this document to be included), preface, list of contents, summary, main body of thesis, conclusions with recommendations for further work, list of symbols and acronyms, references and (optional) appendices. All figures, tables and equations shall be numerated.

The supervisors may require that the candidate, in an early stage of the work, presents a written plan for the completion of the work.

The original contribution of the candidate and material taken from other sources shall be clearly defined. Work from other sources shall be properly referenced using an acknowledged referencing system.

The report shall be submitted in electronic format (.pdf):

- Signed by the candidate
- The text defining the scope shall be included (this document)
- Drawings and/or computer models that are not suited to be part of the report in terms of appendices shall be provided on separate (.zip) files.

### **Ownership**

NTNU has according to the present rules the ownership of the master reports. Any use of the report has to be approved by NTNU (or external partner when this applies). The department has the right to use the report as if the work was carried out by a NTNU employee, if nothing else has been agreed in advance.

### **Thesis supervisors:**

Prof. Bernt J. Leira, NTNU, [bernt.leira@ntnu.no](mailto:bernt.leira@ntnu.no)

**Deadline: June 10, 2024**

Trondheim, January 14 , 2024

Bernt J. Leira

Candidate – date and signature:

14.01.2024 Daniel S. Haugseter

---

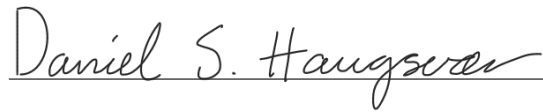
## Preface

This master's thesis is written by Stud. Techn. Daniel Solheim Haugsvær at the Norwegian University of Science and Technology (NTNU). This thesis is a mandatory assignment in order to obtain the Master of Science degree in Marine Technology with specialization in Marine structures. The thesis work was carried out in the spring of 2024. The focus of the study was to investigate the SLWR configuration in deep water subjected to harsh environments. During the work of this thesis I have obtained knowledge of riser systems and riser technology as well as modeling in the SIMA computer program. My supervisor during the Master's thesis work has been Professor Bernt Johan Leira.

I want to thank professor Bernt Johan Leira for the guidance during the work with the thesis. As he has shared his expertise and been available to help by providing relevant feedback and guidance.

I also want to thank Ph.D. candidate Veronica Liverud Krathe at the Department of Marine Technology, NTNU. As Veronica has helped me when I have had problems in the SIMA software by providing possible solutions to my problem.

I want to thank my fellow students for five great years in Trondheim. Finally, I want to thank my parents for always supporting me.



---

**Daniel Solheim Haugsvær**

---

## Abstract

Oil and gas production and exploration moves towards larger water depths, subjected to harsh environmental conditions. Riser technology has been introduced to carry out the retrieval of deep water oil and gas resources. The design of the systems that connects the surface floater to the subsea installation must satisfy a set of criteria due to the load the system is subjected to. This is to ensure a safe design as failure of the system can have major consequences both financially and environmentally.

In the development of deep water riser technology, the steel catenary riser (SCR) configuration has emerged as a preferred solution due to its simplicity as well as being cost effective. The main drawback with the SCR is that it can be subjected low fatigue life at the touch down point (TDP) when paired with a floater with high heave motions such as a Semi-submersible platform or a floating production storage and offloading (FPSO) ship (Q. Bai and Y. Bai 2005).

The steel lazy wave riser (SLWR) configuration is presented as a riser configuration that is better suitable for harsh environments. The configuration is also stated to be better suited for large floater motions. This is due to the buoyancy section of the SLWR configuration decouples the floater motions from the TDP (Cheng et al. 2020). As a part of this thesis the SLWR configuration will be investigated when it is subjected to harsh environmental conditions.

A general description of riser systems is carried out as a part of the thesis. Where geometry of riser configuration, riser materials and riser components are described. The methods used to carry out static, dynamic and fatigue analysis are presented. The computer program SIMA RIFLEX is used to analyse the SLWR configuration. In order to ensure a safe design, design codes are used to determine if the system can be described as safe. DNV-ST-F201 and API STD 2RD are design codes that are used for riser systems.

A case study of a SLWR configuration at a water depth of 1500 meter subjected to harsh environment was carried out. The floater used for the analysis is a semi-submersible platform. The global analysis of the riser configuration was carried out in SIMA RIFLEX. In the dynamic analysis of the riser configuration were irregular waves applied using the JONSWAP spectrum. The waves applied were 100 year North sea wave conditions with a  $H_s = 17\text{m}$  and  $TP = 18.8\text{s}$ . The configuration was also subjected to a 10 year North sea current. This load condition combination is assumed to be the ULS load condition. The slow drift floater offset is assumed to be 8% of the water depth in the ULS condition and 10% for the ALS condition.

The combined load criteria from DNV-ST-F201 was applied to determine if the SLWR configuration has sufficient strength against environmental and functional loads. In order to determine the worst sea state was the 90th percentile largest downward velocity at the hang-off applied. The static and dynamic analysis of the SLWR configuration was used to calculate the utilization of the riser system. From the calculations, it was found that the most critical areas of the riser were near the hang-off, at the sag bend and at the TDP. The largest utilization was located near the hang-off point in the mean ULS offset condition. The largest utilization value was 0.817. This means that the SLWR has sufficient strength to withstand harsh environmental conditions as the utilization calculated from the design code was less than 1.

The fatigue analysis of the SLWR configuration was carried out with respect to wave induced fatigue. The sea state conditions used for the analysis was obtained from a omni-directional scatter diagram. The scatter diagram was blocked in order to reduce the computational load. The analysis was carried out for 18 sea states in 12 different wave directions. The effect of having a taper section was investigated and it was found that including a taper section to the riser hang-off increase the fatigue life at the hang-off substantially. It was found from the fatigue analysis that the critical areas of the SLWR configurations was near the hang-off and at the TDP. The lowest fatigue life for the system was found at the TDP and was 1057 years. This means that the SLWR configuration has a sufficient fatigue life for a 25 year design life according to the DNV-ST-F201.

The parametric study was carried out to see the effect of changing the buoyancy section of the SLWR configuration. The parameters investigated were the buoyancy section length and the buoyancy module geometry. It was found that the largest utilization was located at the TDP in

---

the ULS near offset for the smallest buoyancy module geometry. The largest utilization value was found to be 0.885. This means that all the configuration investigated had sufficient strength to be subjected to harsh environmental conditions. In the fatigue analysis of the configurations, it was found that the buoyancy section had a large effect on the fatigue life of the system. The buoyancy section had little effect on the fatigue life near the hang-off. The fatigue life at the TDP was greatly effected by the buoyancy section. It was found that the fatigue life of the smallest buoyancy module geometry only had a fatigue life of 33 years at the TDP. From the parametric study, it was found that modeling a sufficient buoyancy section greatly improve the fatigue life of the SLWR configuration subjected to wave induced fatigue.

---

## Sammendrag

Olje og gass produksjon og utvinning flytter seg mot dypere vanddyb, utsatt for sterke værtilstander. Stigerør teknologi har blitt utviklet for å kunne få tak i olje og gass fra dype vanddyb. Stigerørsystemet fungerer som ein link mellom flyteren og havbunnsinstallasjoner må tilfredsstillende en rekke kriterier som et resultat av kreftene systemet er utsatt for. Grunnen til at disse kriteriene blir fulgt er for å sikre et sikkert system. Da feil på stigerørsystemet kan føre til store miljømessige og økonomiske konsekvenser.

I utviklingen av stigerørsystem til dypvannsløkasjoner har SCR oppstått som et gunstig alternativ grunnet at den er en enkel konstruksjon samtidig som å være pris effektiv. Det som har vist seg å være et av hovedproblemene med SCR er at det kan forekomme utmattning i stigerøret ved TDP. Dette er spesielt for SCR som er kombinert med flytere med relativt store hev bevegelser. Eksempel på slike flytere semi-submersible plattformer og FPSO skip (Q. Bai and Y. Bai 2005).

SLWR konfigurasjonen har blitt presentert som et alternativ til SCR da denne konfigurasjonen har bedre forutsetninger for å bli utsatt for sterke værtilstander. Konfigurasjonen blir også fremstilt å bedre kunne håndtere store bevegelser i flyteren. Grunnen til dette er at flyteseksjonen til stigerøret absorberer flyterbevegelser slik at de påvirker stigerøret ved TDP i mindre grad. Som en del av denne avhandlingen vil en SLWR konfigurasjon bli undersøkt i sterke værtilstander.

En beskrivelse av de generelle stigerørsystemene med fokus på geometri, material og stigerørkomponenter. Teorien for hvordan å utføre statiske, dynamiske og utmattingsanalyser vil bli presentert. For å utføre denne typen analyser på SLWR konfigurasjonen har programmet SIMA RIFLEX blitt brukt. For å sikre et sikkert design brukes regelverk for å sjekke at systemet har tilstrekkelig styrke. Noen regelverk som blir brukt for stigerør er DNV-ST-F201 og API STD 2RD.

Et casestudie av en SLWR konfigurasjon på 1500 meters vanddyb utsatt for sterke værtilstander ble gjennomført. Flyteren som ble brukt som en del av studiet var en semi-submersible plattform. De globale analysene av stigerørkonfigurasjonen ble utført med bruk av SIMA RIFLEX analyse programmet. Den dynamiske analysen ble utført i irregulære bølger presentert gjennom JONSWAP spekteret. 100 års bølgetilstand fra Nordsjøen ble satt som  $H_s = 17\text{m}$  og  $T_p = 18.8\text{s}$ . En 10 års strømningstilstand ble brukt for å beskrive de sterke værtilstandene. Disse lastkombinasjonene ble brukt som ULS lasten. Lavfrekvent drift av flyteren ble satt som 8% for ULS tilstanden og 10% for ALS tilstanden.

Det kombinerte last kriteriet fra DNV-ST-F201 ble brukt for å evaluere om SLWR konfigurasjonen har tilstrekkelig styrke til å tåle funksjonelle og miljølast. Den maksimale nedover hastigheten i hang-off punktet ble brukt for å bestemme den verste sjøtilstanden. Resultatet fra den statiske og dynamiske analysen ble brukt til å kalkulere utnyttelsen av stigerørkonfigurasjonen. Ut fra disse utrekningene ble det funnet at de mest kritiske punktene for systemet var ved hang-off, i sag bøyn og i TDP. Den største utnyttelsen av stigerøret ble funnet i nærheten av hang-off punktet for den gjennomsnittlige flyter posisjonen i ULS tilstanden. Den største utnyttelsesverdien var 0.817 som betyr at SLWR konfigurasjonen har tilstrekkelig styrke i streke værtilstander da utnyttelsen var under 1.

Utmattingsanalysen av SLWR konfigurasjonen ble utført med hensyn på bølgeindusert utmattning. Sjøtilstandene som ble brukt i analysen ble reknet ut fra et omni-direksjonelt scatter diagram. Scatter diagrammet ble blokket for å redusere den beregningsmessige størrelsen. Utmattingsanalysen ble gjennomført for 18 sjøtilstander i 12 forskjellige bølgeretninger. Det ble undersøkt effekten av å ha en konisk seksjon ved hang-off punktet. Det ble funnet at den koniske seksjonen hadde stor effekt på utmattingslevetiden ved hang-off punktet. I utmattingsanalysen ble det funnet at de kritiske punktene i SLWR konfigurasjonen var ved hang-off og i TDP. Den laveste utmattingslevetiden ble funnet i TDP og var på 1057 år, som betyr at SLWR konfigurasjonen har tilstrekkelig utmattingsliv for et stigerør med design levetid på 25 år.

Et parameterstudie ble utført av flyteseksjonen til SLWR konfigurasjonen. Flyteseksjonlengden og flytemodulgeometrien var parameterene som ble undersøkt. Den største utnyttelsen av stigerøret ble funnet i TPD i den nære ULS offseten for den konfigurasjonen med de minste flytemodulene. Der den største utnyttelsesverdien av stigerøret var 0.885. Dette betyr at alle konfigurasjonene som



---

ble utforsket har tilstrekkelig styrke til å motstå sterke værtilstander. Som en del av utmatting-sanalysen ble det funnet at flyteseksjonen har stor effekt på utmattingslevetiden til stigerøret. Det kommer frem at flyteseksjonen har lite effekt på utmattingslevetiden i nærheten av hang-off punktet. Det som også kom frem var at flyteseksjoenen har stor effekt på utmattingslevetiden i TDP. I analysen ble det funnet at den laveste utmattingslevetiden var 33 år for konfigurasjonen med de minste flytemodulene i TDP. Fra parameterstudiet ble det funnet at det å ha en tilstrekkelig flyteseksjon for en SLWR konfigurasjon vil føre til økt utmattingslevetid for stigerørssystemet.

---

## List of abbreviations

ALS Accidental Limit State  
API American Petroleum Institute  
AR Arbitrary Riser  
CAPEX Capital Expenditure  
DFF Design Fatigue Factor  
DNV Det Norske Veritas  
FCAW Flux core arch weld  
FEM Finite Element Method  
FLS Fatigue Limit State  
FPSO Floating, Production, Storage and Offloading  
GMAW Gas metal arch weld  
GTAW Gas tungsten arch weld  
ISO International Organization for Standardization  
LRFD Load and Resistance Factor Design  
NDT Non Destructive Testing  
JONSWAP Joint North Sea Wave Project  
RAO Response Amplitude Operator  
SAW Submerged arch weld  
SCR Steel Catenary Riser  
SLS Serviceability Limit State  
SLWR Steel Lazy Wave Riser  
SMAW Shielded metal arch weld  
SN Standard Norge  
TDP Touchdown Point  
TLP Tension-Leg Platform  
TSJ Taper Stress Joint  
TTR Top Tension Riser  
ULS Ultimate Limit State  
VIV Vortex Induced Vibrations  
WSD Working stress design

---

## List of symbols

### Greek symbols

- $\omega$  Angular frequency
- $\gamma$  Peakedness factor
- $\omega_p$  Peak frequency
- $\sigma$  Determined from  $\omega$  and  $\omega_p$
- $\rho$  Density of element
- $\alpha_1$  Mass proportional damping coefficient
- $\alpha_2$  Stiffness proportional damping coefficient
- $\lambda$  Eigenvalue matrix
- $\chi$  Eigenvectors
- $\omega$  Eigenfrequency
- $\epsilon$  Bandwidth factor
- $\gamma_F$  Functional load factor
- $\gamma_E$  environmental load factor
- $\gamma_A$  Accidental load factor
- $\gamma_{SC}$  Consequence of failure factor
- $\gamma_m$  Material safety factor
- $\alpha_c$  Strain hardening and wall thinning factor
- $\nu$  Poisson ratio
- $\Lambda$  Vector for safety factor
- $\Delta_p$  Local pressure differential
- $\alpha$  Location parameter in Gumbel distribution
- $\beta$  Scale parameter in Gumbel distribution
- $\Delta\sigma$  Stress range
- $\Delta\sigma_0$  Nominal stress range
- $\eta$  Usage factor
- ### Latin symbols
- a Connectivity matrix
- A Quadratic matrix
- c material dependent factor
- C Damping matrix
- $C_a$  Added mass coefficient
- $C_d$  Drag coefficient

---

$C_m$  Mass coefficient

D Damage

$D_0$  Intended pipe diameter

$D_{fat}$  Accumalated damage

$D_{max}$  Maximum pipe diameter

$D_{min}$  Minimum pipe diameter

dn Crack growth

dN Numner of cycles

E Youngs modulus

$f_0$  Out of roundness of pipe

$F_d$  Design factor

g Gravity acceleration

g Generalized load effect

Hs Significant wave height

$Hs_{block}$  Hs for a given block

$Hs_i$  Hs for a singel sea state

I Irregularity factor

k Material property

k Number of stress blocks

K Stiffness matrix

$\Delta K$  Stress intensity factor

$K_E$  External stiffness matrix

$K_G$  Geometric stiffness matrix

$k_i$  Local stiffness matrix

$K_I(r)$  Tangential stiffness matrix

m Material dependent factor

m Negative inverse slope of S-N curve

m Element mass martix

M Global mass matrix

M Bending moment

$M_d$  Design bending moment

$M_k$  Plastic bending moment resistance

$m_n$  Spectral moment

$M_y$  Yield bending moment

N Interpolation function

---

---

$n_i$  Numbers of cycles in block i  
 $n_i$  Numbers of a single sea state  
 $N_{eg}$  Number of cycles needed to go from initial to critical defect size  
 $N_i$  Numbers of sea states in a block  
 $N_{tot}$  Total number of stress cycles  
 $p_b$  Burst pressure  
 $p_c$  Collapse pressure  
 $p_d$  Design pressure  
 $p_e$  External pressure  
 $p_{el}$  Elastic collapse pressure  
 $p_i$  Local internal pressure  
 $p_{li}$  Local incidental pressure  
 $p_{min}$  Minimum internal pressure  
 $P_y$  Yield collapse pressure  
r Nodal displacement vector  
 $R_F$  Generalized resistance  
 $R_E(r)$  External force vector  
 $R_S(r)$  Internal structural reaction force  
S Minimum yield strength  
 $S_A$  Accidental load  
 $S_E$  Environmental load  
 $S_F$  Functional load  
 $S_P$  Pressure load  
 $\Delta S$  Stress range  
t Plate thickness  
t Time  
t Wall thickness  
 $t_{corr}$  Corrosion criteria  
 $t_{fab}$  Fabrication criteria  
 $t_{nom}$  Nominal wall thickness  
 $t_{ref}$  Reference plate thickness  
T Transformation matrix  
T Effective tension  
 $T_{ed}$  Design effective tension  
 $T_k$  Plastic effective tension resistance

---

---

$T_y$  Yield effective tension  
Tp Spectral epeak period  
 $Tp_{block}$  Tp for a given block  
 $Tp_i$  Tp for a single sea state  
U Minimum ultimate strength  
v Displacement vector  
 $\dot{v}$  Velocity vector  
 $\ddot{v}$  Acceleration vector  
V Wind speed at 19.5 meter over the surface

---

# Table of Contents

<b>List of Figures</b>	<b>xvii</b>
<b>List of Tables</b>	<b>xxi</b>
<b>1 Introduction</b>	<b>1</b>
1.1 Background . . . . .	1
1.2 Objective . . . . .	1
1.3 Thesis structure . . . . .	2
<b>2 Riser systems</b>	<b>3</b>
2.1 Introduction . . . . .	3
2.2 Top tensioned risers . . . . .	4
2.3 Compliant risers . . . . .	4
2.3.1 Single catenary risers . . . . .	4
2.3.2 Double catenary risers . . . . .	5
2.4 Hybrid risers . . . . .	8
2.5 Riser components . . . . .	8
2.6 Steel Lazy Wave Riser Configuration . . . . .	9
2.7 Riser material . . . . .	10
2.7.1 Flexible risers . . . . .	10
2.7.2 Rigid risers . . . . .	11
2.8 Riser fabrication and installation . . . . .	11
2.8.1 Riser fabrication . . . . .	12
2.8.2 Rigid riser installation . . . . .	12
2.9 Deep water challenges . . . . .	15
2.10 Riser design loads . . . . .	16
2.10.1 Functional and pressure loads . . . . .	16
2.10.2 Environmental loads . . . . .	16
2.10.3 Waves loads . . . . .	17
2.10.4 Current loads . . . . .	18
2.10.5 Floater motion . . . . .	18
2.10.6 Accidental loads . . . . .	18
<b>3 Analysis methodology</b>	<b>20</b>
3.1 Finite element model . . . . .	20

---

3.1.1	Mass matrix . . . . .	21
3.1.2	Damping matrix . . . . .	21
3.1.3	Stiffness matrix . . . . .	22
3.2	Static analysis . . . . .	23
3.3	Eigenvalue Analysis . . . . .	25
3.4	Dynamic analysis of riser systems . . . . .	25
<b>4</b>	<b>Fatigue theory</b>	<b>27</b>
4.1	Load history . . . . .	28
4.2	S-N curves . . . . .	29
4.3	Cycle counting . . . . .	30
4.4	Miner-Palmgren Summation . . . . .	32
<b>5</b>	<b>SIMA RIFLEX</b>	<b>34</b>
5.1	Structure of RIFLEX program . . . . .	34
5.2	Riser system modeling in RIFLEX . . . . .	36
5.3	Main components in riser system modeling in RIFLEX . . . . .	36
<b>6</b>	<b>Design codes</b>	<b>39</b>
6.1	DNV-ST-F201 . . . . .	39
6.1.1	Load and resistance factor design (LRFD) . . . . .	41
6.1.2	Limit states . . . . .	43
6.1.3	Serviceability Limit State . . . . .	44
6.1.4	Ultimate Limit State . . . . .	45
6.1.5	Accidental Limit State . . . . .	48
6.1.6	Fatigue Limit State . . . . .	48
6.2	Limit states in API STD 2RD . . . . .	49
6.2.1	Internal Pressure . . . . .	49
6.2.2	External Pressure . . . . .	50
6.2.3	Combined loads . . . . .	51
6.2.4	Fatigue . . . . .	52
<b>7</b>	<b>Design basis</b>	<b>53</b>
7.1	Environmental data . . . . .	53
7.1.1	Wave conditions . . . . .	53
7.1.2	Design current . . . . .	55
7.1.3	Floater motions and offset . . . . .	55

---



---

7.1.4	Riser soil interaction . . . . .	56
7.1.5	Hydrodynamic parameters . . . . .	57
7.2	Riser configuration . . . . .	58
7.2.1	Riser material and cross section . . . . .	58
7.2.2	Buoyancy modules . . . . .	58
7.2.3	Riser coating . . . . .	59
7.2.4	Internal fluid . . . . .	60
7.2.5	Riser hang off modeling . . . . .	60
<b>8</b>	<b>Analysis of SLWR in ULS and ALS environmental conditions</b>	<b>61</b>
8.1	Load case selection . . . . .	61
8.1.1	Wave and current direction . . . . .	61
8.1.2	Significant wave height and spectral peak period . . . . .	63
8.2	Static analysis of the SLWR . . . . .	64
8.3	Dynamic analysis of the SLWR . . . . .	66
8.4	Utilization of the SLWR . . . . .	71
8.5	Buckling . . . . .	72
8.6	Summary of the ULS and ALS limit state analysis . . . . .	72
<b>9</b>	<b>Fatigue analysis of the SLWR configuration</b>	<b>73</b>
9.1	Introduction . . . . .	73
9.1.1	Wave fatigue . . . . .	73
9.1.2	VIV fatigue . . . . .	73
9.2	Wave fatigue analysis . . . . .	74
9.2.1	S-N curve . . . . .	74
9.2.2	Stress concentration factor . . . . .	75
9.2.3	Damage . . . . .	75
9.2.4	Wave scatter diagram blocking . . . . .	76
9.2.5	Effect of the tapered section . . . . .	78
9.2.6	Effect of simulation time . . . . .	79
9.3	Results of the SLWR wave induced fatigue analysis . . . . .	79
<b>10</b>	<b>Parametric study of the buoyancy section of the SLWR configuration</b>	<b>81</b>
10.1	SLWR configuration conditions . . . . .	81
10.1.1	Geometry of the different configurations . . . . .	81
10.1.2	ULS capabilities . . . . .	82

---

---

10.1.3 Fatigue life of different SLWR configurations . . . . .	88
10.2 Summary of the parametric study . . . . .	89
<b>11 Conclusion and further work</b>	<b>91</b>
11.1 Conclusion . . . . .	91
11.2 Further work . . . . .	92
<b>Bibliography</b>	<b>93</b>
<b>Appendix</b>	<b>96</b>
A Programfiles . . . . .	96
B Python file used for utilization calculations . . . . .	97
C Python file used for Gumbel distribution of the downward velocity at the hang-off point . . . . .	99
D Python program used to calculate the fatigue life from several wave sectors . . . . .	102
E RAO file used in the SIMA RIFEX program . . . . .	104
F Parametric study ULS limit state results . . . . .	112
F.1 Buoyancy module geometry 1 . . . . .	112
F.2 Buoyancy module geometry 2 . . . . .	114
F.3 Buoyancy module geometry 3 . . . . .	116
F.4 Buoyancy module geometry 4 . . . . .	118
F.5 Buoyancy module geometry 5 . . . . .	120
F.6 Buoyancy section length 500 meters . . . . .	122
F.7 Buoyancy section length 525 meters . . . . .	124
F.8 Buoyancy section length 550 meters . . . . .	126
F.9 Buoyancy section length 575 meters . . . . .	128
F.10 Buoyancy section length 600 meters . . . . .	130

---

## List of Figures

1	Riser systems (DNV 2001). . . . .	3
2	Top tensioned riser system (DNV 2001) . . . . .	4
3	Single catenary riser system (Q. Bai and Y. Bai 2005) . . . . .	5
4	Lazy S riser system (Q. Bai and Y. Bai 2005) . . . . .	6
5	Steep S riser system (Q. Bai and Y. Bai 2005) . . . . .	6
6	Lazy wave riser system (Q. Bai and Y. Bai 2005) . . . . .	7
7	Steep wave riser system (Q. Bai and Y. Bai 2005) . . . . .	7
8	The Pliant wave riser system (Q. Bai and Y. Bai 2005) . . . . .	8
9	Hybrid riser system (Athisakul et al. 2014) . . . . .	8
10	Typical flex joint configuration (Hui et al. 2019) . . . . .	9
11	Typical flexible pipe cross section (Sævik 2017). . . . .	11
12	J-Lay method (DrillingFormulas 2024a). . . . .	13
13	S-Lay method (DrillingFormulas 2024b). . . . .	14
14	Reel Lay method (Hu et al. 2012). . . . .	15
15	Euler-Cauchy method with equilibrium correction (Moan 2003) . . . . .	24
16	Newton-Raphson method (Moan 2003) . . . . .	25
17	The different stages of crack growth (Ray 2001) . . . . .	27
18	Different parts of a load history (Wægter 2024) . . . . .	28
19	Representation of S-N curve with constant amplitued fatigue limit (Berge 2006) . .	29
20	Example of a bilinear S-N curve (Berge 2006) . . . . .	30
21	An example of the relation between the strain history and the stress strain response using rainflow counting (Almar-Næss 1985) . . . . .	31
22	Presentation of the pagoda roof analogy for raiflow counting (Almar-Næss 1985) .	32
23	Structure of the RIFLEX program system (SINTEF 2024b) . . . . .	35
24	System definition in INPMOD (SINTEF 2024b). . . . .	36
25	Description of a line in RIFLEX (SINTEF 2024b) . . . . .	37
26	The design approach of a riser system described by DNV ST-F201 (DNV 2021) . .	40
27	Typical load types (DNV 2021) . . . . .	42
28	Load effect factors (DNV 2021) . . . . .	42
29	Safety class resistance factor (DNV 2021) . . . . .	42
30	Safety class resistance factor (DNV 2021) . . . . .	42
31	Accidental load resistance factor (DNV 2021) . . . . .	43
32	Typical limit states for a riser system (DNV 2001) . . . . .	44

---

33	100 year Hs and Tp sea state of the North sea based on the NORA10 data (NORSOK-Standard 2018) . . . . .	54
34	Omni-directional scatter diagram from Haltenbanken (Johnsen 2020)) . . . . .	55
35	Friction coefficient for different types of seafloor soil (Q. Bai and Y. Bai 2014) . . .	57
36	External wrapping in SIMA RIFLEX (SINTEF 2024a) . . . . .	59
37	Nonlinear flex joint stiffness plot (Hui et al. 2019) . . . . .	60
38	Largest bending moment for different wave and current directions . . . . .	62
39	Largest effective tension for different wave and current directions . . . . .	62
40	Largest bending moment for different Hs and TP combinations . . . . .	63
41	Largest effective tension for different Hs and Tp combinations . . . . .	63
42	SLWR configuration in the mean, near and far ULS and ALs offset position . . . .	64
43	Largest bending moment in the mean, near and far ULS and ALS offsets . . . . .	65
44	Largest effective tension in the mean, near and far ULS and ALS offsets . . . . .	65
45	Vertical displacement waveseed 1 . . . . .	66
46	Vertical displacement waveseed 2 . . . . .	67
47	Largest bending moment for 20 different waveseeds . . . . .	67
48	Largest effective tension for 20 different waveseeds . . . . .	68
49	Gumbel distribution presenting the 90th percentile . . . . .	69
50	Largest bending moment for waveseed 19 in the mean, near and far ULS and ALS offset position . . . . .	70
51	Largest effective tension for waveseed 19 in the mean, near and far ULS and ALS offset position . . . . .	70
52	Utilization of the SLWR configuration in the mean, near and far ULS and ALS offset	71
53	Smallest effective tension for waveseed 19 in the mean, near and far ULS and ALS offset position . . . . .	72
54	Example of helical strakes on a pipe (Ranjith et al. 2016) . . . . .	74
55	S-N curves presenetd in the design code DNV-RP-C203 . . . . .	75
56	Blocking used for the fatigue analysis of the SLWR configuration . . . . .	76
57	Fatigue life of the SLWR configuration near the hang-off with and without a taper section . . . . .	79
58	Fatigue life of the SLWR configuration subjected to wave induced fatigue . . . . .	80
59	Static configuration for 5 different buoyancy section length . . . . .	82
60	Static configuration for 5 different buoyancy section geometries . . . . .	82
61	Static bending moment for the worst cases of the 5 different buoyancy section length configurations in the mean, near and far ULS offset . . . . .	83
62	Static bending moment for the worst case of the 5 different buoyancy module geometry configurations in the mean, near and far ULS offset . . . . .	83

---

---

63	Effective tension for the worst case of the 5 different buoyancy section length configurations in the mean, near and far ULS offset . . . . .	84
64	Effective tension for the worst case of the 5 different buoyancy module geometry configurations in the mean, near and far ULS offset . . . . .	84
65	Dynamic bending moment for the worst case of the 5 different buoyancy section length configurations in the mean, near and far ULS offset . . . . .	85
66	Dynamic bending moment for the worst case of the 5 different buoyancy module geometry configurations in the mean, near and far ULS offset . . . . .	85
67	Effective tension for the worst case of the 5 different buoyancy section length configurations in the mean, near and far ULS offset . . . . .	86
68	Effective tension for the worst case of the 5 different buoyancy module geometry configurations in the mean, near and far ULS offset . . . . .	86
69	The worst utilization found for the worst case of the 5 different buoyancy section length configurations in the mean, near and far ULS offset . . . . .	87
70	The worst utilization found for the worst case of the 5 different buoyancy section geometries in the mean, near and far ULS offset condition . . . . .	87
71	Fatigue life for the 5 different buoyancy section length configurations . . . . .	88
72	Fatigue life for the 5 different buoyancy module geometry configurations . . . . .	89
73	Static results . . . . .	112
74	Dynamic results . . . . .	112
75	Utilization of buoyancy module geometry for different offsets . . . . .	112
76	Static results . . . . .	114
77	Dynamic results . . . . .	114
78	Utilization of buoyancy module geometry for different offsets . . . . .	114
79	Static results . . . . .	116
80	Dynamic results . . . . .	116
81	Utilization of buoyancy module geometry for different offsets . . . . .	116
82	Static results . . . . .	118
83	Dynamic results . . . . .	118
84	Utilization of buoyancy module geometry for different offsets . . . . .	118
85	Static results . . . . .	120
86	Dynamic results . . . . .	120
87	Utilization of buoyancy module geometry for different offsets . . . . .	120
88	Static results . . . . .	122
89	Dynamic results . . . . .	122
90	Utilization of buoyancy section length for different offsets . . . . .	122
91	Static results . . . . .	124
92	Dynamic results . . . . .	124

---

---

93	Utilization of buoyancy section length for different offsets . . . . .	124
94	Static results . . . . .	126
95	Dynamic results . . . . .	126
96	Utilization of buoyancy section length for different offsets . . . . .	126
97	Static results . . . . .	128
98	Dynamic results . . . . .	128
99	Utilization of buoyancy section length for different offsets . . . . .	128
100	Static results . . . . .	130
101	Dynamic results . . . . .	130
102	Utilization of buoyancy section length for different offsets . . . . .	130

---

## List of Tables

1	API 5L material strength properties (API 2018) . . . . .	11
2	Design factor FD for different load cases (API 2020) . . . . .	50
3	Design factor FD for different limit states (API 2020) . . . . .	51
4	Design factor FD for different limit states (API 2020) . . . . .	52
5	Damage that is allowed for different limit states (API 2020) . . . . .	52
6	Design current D.N. Karunakaran and Baarholm 2013 . . . . .	55
7	Summary of the offset conditions used in the extreme response analysis . . . . .	56
8	Riser soil interaction (D.N. Karunakaran and Baarholm 2013) . . . . .	57
9	Hydrodynamic coefficient used for the riser configuration (Felisita et al. 2017) (D.N. Karunakaran and Baarholm 2013) . . . . .	57
10	Riser material and cross section properties . . . . .	58
11	Buoyancy module parameters . . . . .	59
12	Safety factors for the combined loading criteria in ULS and ALS conditions (DNV 2021) . . . . .	61
13	Summary of the results from the static analysis . . . . .	66
14	Maximum downward vertical velocity . . . . .	68
15	Summary of the results from the dynamic analysis . . . . .	71
16	Largest utilization along the riser configuration . . . . .	72
17	Sea states calculated for the different scatter diagram blocks . . . . .	77
18	Probability of waves from different directions (Johnsen 2020) . . . . .	78
19	Fatigue life of the SLWR configuration for different simulation lengths . . . . .	79
20	Important locations with respect to fatigue life . . . . .	80
21	Buoyancy section length cases . . . . .	81
22	Buoyancy module geometry cases . . . . .	81
23	Largest utilization along the riser parameter configurations . . . . .	88
24	Summary of the results from the dynamic analysis . . . . .	89
25	Summary of the loads and utilization of the mean offset . . . . .	113
26	Summary of the loads and utilization of the near offset . . . . .	113
27	Summary of the loads and utilization of the far offset . . . . .	113
28	Summary of the loads and utilization of the mean offset . . . . .	115
29	Summary of the loads and utilization of the near offset . . . . .	115
30	Summary of the loads and utilization of the far offset . . . . .	115
31	Summary of the loads and utilization of the mean offset . . . . .	117
32	Summary of the loads and utilization of the near offset . . . . .	117

---

33	Summary of the loads and utilization of the far offset . . . . .	117
34	Summary of the loads and utilization of the mean offset . . . . .	119
35	Summary of the loads and utilization of the near offset . . . . .	119
36	Summary of the loads and utilization of the far offset . . . . .	119
37	Summary of the loads and utilization of the mean offset . . . . .	121
38	Summary of the loads and utilization of the near offset . . . . .	121
39	Summary of the loads and utilization of the far offset . . . . .	121
40	Summary of the loads and utilization of the mean offset . . . . .	123
41	Summary of the loads and utilization of the near offset . . . . .	123
42	Summary of the loads and utilization of the far offset . . . . .	123
43	Summary of the loads and utilization of the mean offset . . . . .	125
44	Summary of the loads and utilization of the near offset . . . . .	125
45	Summary of the loads and utilization of the far offset . . . . .	125
46	Summary of the loads and utilization of the mean offset . . . . .	127
47	Summary of the loads and utilization of the near offset . . . . .	127
48	Summary of the loads and utilization of the far offset . . . . .	127
49	Summary of the loads and utilization of the mean offset . . . . .	129
50	Summary of the loads and utilization of the near offset . . . . .	129
51	Summary of the loads and utilization of the far offset . . . . .	129
52	Summary of the loads and utilization of the mean offset . . . . .	131
53	Summary of the loads and utilization of the near offset . . . . .	131
54	Summary of the loads and utilization of the far offset . . . . .	131



---

# 1 Introduction

## 1.1 Background

Oil and gas production and exploration moves towards larger water depths, subjected to harsh environmental conditions. Riser technology has been introduced to carry out the retrieval of deep water oil and gas resources. The design of the systems that connects the surface floater to the subsea installation must satisfy a set of criteria due to the load the system is subjected to. This is to ensure a safe design as failure of the system can have major consequences both financially and environmentally.

In development of deep water locations, Spar platform, semi-submersible platform, tension leg platform (TLP) and floating production storage and offloading (FPSO) ships floaters are used. Regardless of the floater that is used for the development, there is a need of a riser system to connect the surface and the subsea equipment. The function of the riser system is to provide a transfer of the fluid from the seabed to the surface floater. The function of a riser system can be divided into categories such as drilling risers, workover risers and production risers.

When choosing a riser system to be applied for deep water development there are many parameters that need to be considered. Some of the parameters to be considered are if a flexible or a rigid riser should be used. Which riser configurations should be applied top tension riser, single or double catenary riser or a hybrid riser system. The riser concept that is chosen must therefore be able to withstand the loads and forces that act on the system for the given location.

In the development of deep water riser technology. the steel catenary riser (SCR) configuration has emerged as a preferred solution due to its simplicity as well as being cost effective. The main drawback with the SCR is that it can be subjected to low fatigue life at the touch down point (TDP) when paired with a floater with high heave motions such as a Semi-submersible platform or a FPSO ship (Q. Bai and Y. Bai 2005).

The steel lazy wave riser (SLWR) configuration is presented as a riser configuration that is better suited for harsh environments. The configuration is also stated to be better suited for large floater motions. This is due to the buoyancy section of the SLWR configuration decouples the floater motions from the TDP (Cheng et al. 2020). As a part of this thesis the SLWR configuration will be investigated when it is subjected to harsh environmental conditions.

## 1.2 Objective

The main objective of this master thesis is to investigate the capabilities of the SLWR configuration in deep water and subjected to harsh environmental conditions. The capabilities of the SLWR configuration subjected to wave induced fatigue. This will be investigated by carrying out analysis in the SIMA RIFLEX analysis program. This is to see if the SLWR is a suitable alternative to the SCR when connected to a floater with large floater motions. A parametric study is carried out to investigate the effects on the riser system when changes are made to the buoyancy section of the SLWR configuration.

---

### 1.3 Thesis structure

- **Chapter 1 Introduction** gives a background of the topic as well as the thesis objective and the structure of the thesis.
- **Chapter 2 Riser system** present different riser systems, material and installation methods. The chapter also gives a brief description of the most common riser components and riser design loads.
- **Chapter 3 Analysis methodology** is a description of the theory used in static and dynamic analysis that are used in global analysis.
- **Chapter 4 Fatigue theory** is a description of fatigue theory.
- **Chapter 5 SIMA RIFLEX** describes the SIMA RIFLEX program and presents some of the most important components used to model a riser system.
- **Chapter 6 Design codes** describes design codes that are used for riser design. The design codes DNV-ST-F201 and API STD 2RD are described.
- **Chapter 7 Design basin** introduces the design parameters used in the riser system modeling. This includes the environmental conditions and the riser configuration dimensions.
- **Chapter 8 Analysis of SLWR in ULS and ALS environmental conditions** contains the static and dynamic analysis of the SLWR configuration. The riser configuration is investigated for mean, far and near ULS and ALS offsets. The results from these analysis are used to calculate the utilization of the riser configuration.
- **Chapter 9 Fatigue analysis of the SLWR** presents the wave induced fatigue analysis of the SLWR configuration. The fatigue analysis is based on the wave induced fatigue.
- **Chapter 10 Parametric study of the buoyancy section of the SLWR configurations** is a parametric study of the riser buoyancy section length and buoyancy module geometry. The effect the configurations have on the utilization and fatigue life of the riser.
- **Chapter 11 Conclusion and further work** summarizes the main results of the thesis and proposes further work that can be carried out.

The investigation of the problem presented as a part of this thesis was initiated in the fall of 2023. Some of the theory presented is based on the theory that was presented as a part of the project thesis.

---

## 2 Riser systems

### 2.1 Introduction

The riser system makes it possible to transport fluid from the seabed to the floater. Where the riser system acts as the connection between the seabed and the floater. As a result of this, the riser system is an important component in the development of the oil and gas fields. The riser system is therefore an essential factor for success in the operational phase of the of subsea production. The riser systems can be applied for different phases of the development of oil and gas fields. These include the drilling, workover, production and export phase.

A riser system can be described as an assembly of components. This is the description of a riser system according to the American Petroleum Institute (API) (API 2020). Examples of riser components include buoyancy modules, tensioner systems and flexible-joints. A riser system comes in many shapes and sizes. Which system is chosen is highly dependent on the task it is supposed to fill. A description of some of the most common riser configurations will be described in this chapter. In figure (1) below can some of the riser systems be seen with different floaters.

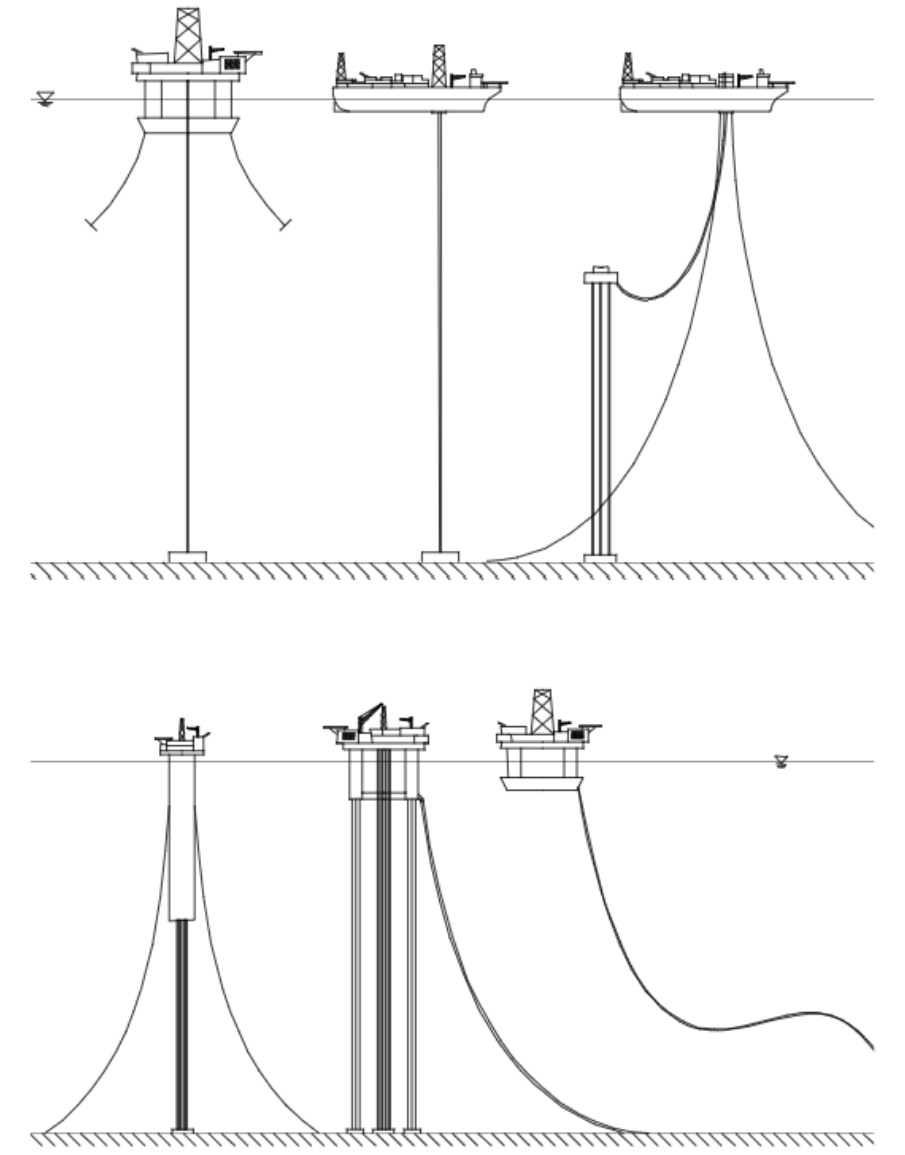


Figure 1: Riser systems (DNV 2001).

---

## 2.2 Top tensioned risers

A top tension riser (TTR) configuration will often consist of a vertical steel pipe. The riser is supported by the floater as well as a tensioning system. The tensioning system creates a top tension force that gives the riser system bending lateral stiffness. This stiffness makes it possible to have relative vertical motion between the riser system and the floater. As a result of the connection between the riser system and the floater, the riser system will follow the floater motion. TTR configurations are often paired with floaters that have relatively small heave motions such as Spar and TLPs. One of the governing design criteria for the TTR configuration is that the riser system can not be subjected to compressive forces (Q. Bai and Y. Bai 2005). Extensive compression force can lead to buckling in the riser. This is one of the main reasons to use a floater with small heave motions when designing a riser system with the TTR configuration.

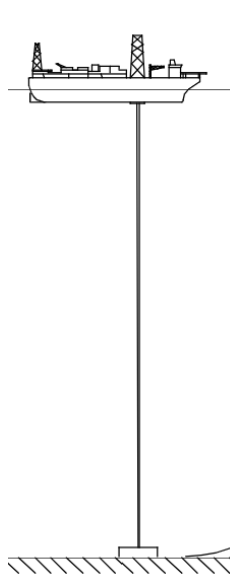


Figure 2: Top tensioned riser system (DNV 2001)

## 2.3 Compliant risers

Compliant riser systems are designed in a way that are able to absorb floater motion by change in the riser geometry. This makes tension control and heave compensation less relevant. At smaller water depths, flexibility of the riser system are obtained by using flexible pipes. Using a pipe with this kind of cross section makes it possible for the system to have a small bending radius. This kind of configuration can often handle high axial tensile forces. For larger water depths a metallic pipe will behave in a flexible manner making an arrangement of pipes act in a compliant manner.

Compliant riser systems are often subjected to larger static and dynamic excursions compared to a top tensioned riser systems. Environmental loads will also often be taken more into account for a compliant riser system. A compliant riser system can be dividend into two sub categories which are single and double catenaries.

### 2.3.1 Single catenary risers

The single catenary riser configuration can be described as a single catenary hanging from the floater as shown if figure (3). The geometry of the system comes from the weight of the riser. The single catenary riser is a simple configuration that requires minimal subsea infrastructure, and is therefore a cheap configuration compared to other types of riser configurations. The main drawback of the single catenary riser configuration is that it can be exposed to significant loading because of floater motions. This is due to the limited amount of geometry available to account

---

for the floater motions. The main concern for this type of configuration is the TDP, as the riser will be lifted off or lowered down on the seabed. The single catenary riser configuration is likely to suffer compression buckling at the TDP if the system is subjected to high floater motions. For larger water depths, the top tension of the riser system will become larger as the length of the riser in the water column increases (Q. Bai and Y. Bai 2005). As a result of this, the single catenary riser configuration is often paired with floaters that have relatively small floater motions such as Spar and TLP platforms.

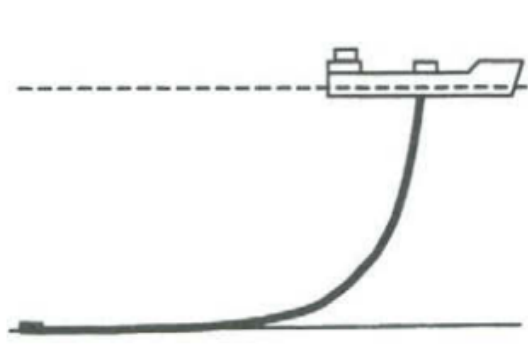


Figure 3: Single catenary riser system (Q. Bai and Y. Bai 2005)

### 2.3.2 Double catenary risers

A double catenary riser configuration can be described as riser system consisting of two catenaries in the water column. This type of configuration is obtained by applying buoyancy elements to the riser system. Creating one catenary from the floater to the buoyancy elements, and another from the buoyancy elements to the seabed. There are several types of double catenary configurations, some of the most common will be described below.

#### Lazy S

The lazy S configuration uses a subsea buoy to create the geometry of the configuration as seen in figure (4) below. This buoy is either fixed to a structure at the seabed or it is a buoyant buoy that is positioned by using chains. The main reason to use this type of configuration is the absorption of the tension variations created from floater motion, and thereby reducing the tension variations in the TDP. This means that the addition of the buoy can remove the problems with the TDP described for the single catenary riser configuration (Q. Bai and Y. Bai 2005). The lazy S configuration is often used for cases with severe environmental loads, where the connection point at the seabed is located some distance from the floater.

Lazy S configurations are only considered if the single catenary riser or any of the wave configurations are not suited to use for the particular field. This is due to the complexity of the installation of a lazy S configuration, as it requires a mid-water arch. The riser response depend on the buoy hydrodynamics. Due to the large inertia forces present, complex modelling must be carried out (Q. Bai and Y. Bai 2005).

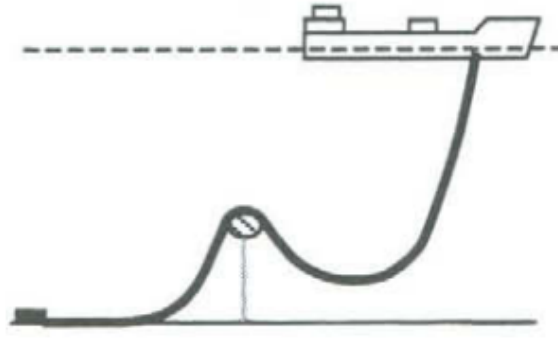


Figure 4: Lazy S riser system (Q. Bai and Y. Bai 2005)

### Steep S

In the Steep S configuration, a buoy is used in the same manner as in the Lazy S configuration. The main difference between the Steep S and the lazy S configuration is the seabed connection. As the Lazy S lays on the seabed for some distance before the connection point. The Steep S configuration uses a bend stiffener at the connection point at the seabed making a constant TDP for the system. This can be seen in figure (5) below. The Steep S configuration can be used in cases where there are compression problems at the TDP due to large floater motions even for the Lazy S configuration (Q. Bai and Y. Bai 2005).

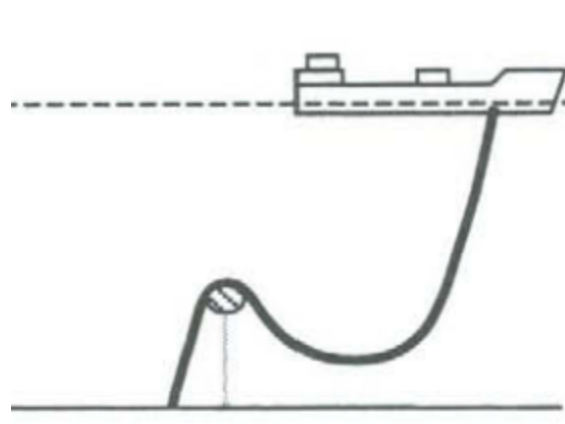


Figure 5: Steep S riser system (Q. Bai and Y. Bai 2005)

### Lazy wave

The lazy wave configuration uses buoyancy elements and weights over a length of the riser system. This is done in order to decouple the floater motions from the TDP of the system. The added buoyancy creates the wave shape of the riser system as seen in figure (6) below. The lazy wave is often preferred to the steep wave due to it being a simpler configuration. Something to consider when choosing a lazy wave configuration is the density of the fluid that is to be transported. This is due to the lazy wave configuration being prone to change in configuration if the density of the fluid being transported changes over the lifetime of the riser system (Q. Bai and Y. Bai 2005).

The buoyancy modules used in the lazy wave configurations are made from syntactic foam. The foam is chosen with respect to having low water absorption. This property is important because the buoyancy modules lose buoyancy over time. Lazy wave configurations are then designed in order to accommodate for a 10% loss in buoyancy. The buoyancy modules are clamped tightly to the riser. This is to ensure that there is no slipping by the modules. If the buoyancy modules slip, it can lead to changes in the configuration that can induce high stress in the riser. It is also

---

important that the modules are not clamped so hard that it damages the riser system (Q. Bai and Y. Bai 2005).

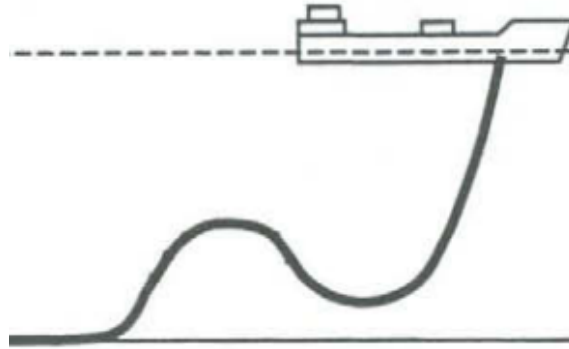


Figure 6: Lazy wave riser system (Q. Bai and Y. Bai 2005)

### Steep wave

In the Steep wave configurations, buoyancy modules and weights are used in the same manner as in the Lazy wave configurations. The main difference between the Steep wave and the lazy wave configurations is the seabed connection. As the Lazy wave lays on the seabed for some distance before the connection point. The Steep wave configuration uses a bend stiffener at the connection point at the seabed making a constant TDP for the system. This can be seen in figure (7) below. The Steep wave configuration is able to maintain its configuration despite changes in the fluid density (Q. Bai and Y. Bai 2005).

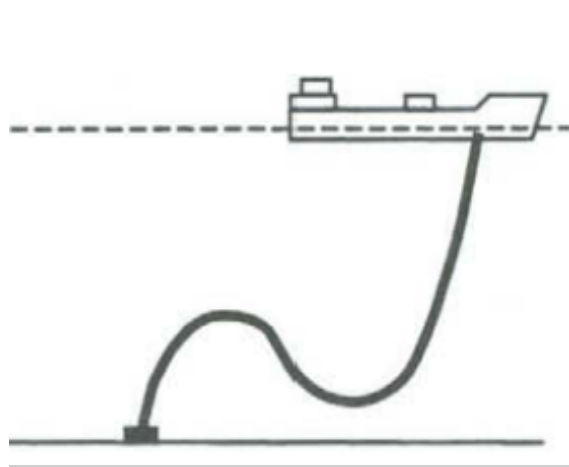


Figure 7: Steep wave riser system (Q. Bai and Y. Bai 2005)

### The Pliant wave

The pliant wave configuration shares many similarities with the steep wave configuration. The main difference is that in the pliant wave, the TDP is controlled by an anchor. The TDP is controlled due to the tension in the riser being transferred to the anchor instead of the TDP. One of the main reasons for using the pliant wave is the configurations ability to operate with a wide range of fluid density, as well as being subjected to floater motion, without major changes to the configuration. The main drawback to this configuration is the complexity of the subsea installation needed. Therefore is the pliant wave only used if the simple catenary or the wave configurations are not sufficient (Q. Bai and Y. Bai 2005).

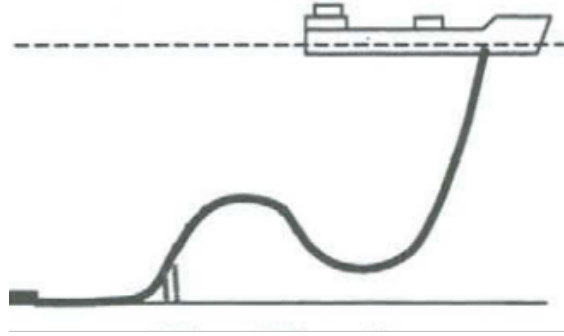


Figure 8: The Pliant wave riser system (Q. Bai and Y. Bai 2005)

## 2.4 Hybrid risers

The hybrid riser configuration can be divided into three parts; the rigid vertical section, the jumper and the submerged buoy as seen in figure (9) below. This type of riser systems allows the riser to be installed either before or after the floater. One of the main advantages of this type of riser configuration is that it is possible to isolate the riser from the floater motions. This is due to the jumper being made from flexible pipes that are capable of absorbing the floater motions. The rigid part of the riser system consists of a rigid pipe that goes from the seabed to the submerged buoy. The buoy creates top tension in the rigid section, as well as supporting some of the weight of the jumper. The buoy is often made from buoyant tanks that are connected to the top riser assembly using a tethering mechanism (Miller 2017).

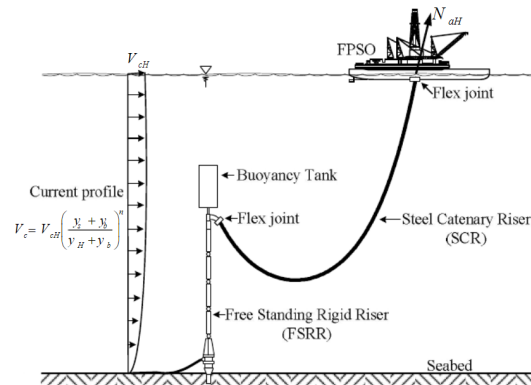


Figure 9: Hybrid riser system (Athisakul et al. 2014)

## 2.5 Riser components

A riser configuration is an assembly of a number of components. A description of some of the most used riser components are given below:

### Flex joint

Flex joints can be located both at the upper and lower part of the riser systems. In catenary risers, flex joints are often applied at the hang of region of the riser. The purpose of the flex joint is to reduce stress due to bending and motions, as well as resisting internal pressure. A flex joint makes riser system able to rotate with a reduced bending moment. The flex joint will often exhibit strong nonlinear behavior for small rotation angles. As a result of this, the flex joint should be modeled as nonlinear rotation spring or as a short beam that has a nonlinear rotational stiffness (Q. Bai and Y. Bai 2018). Figure (10) below shows a typical flex joint component.



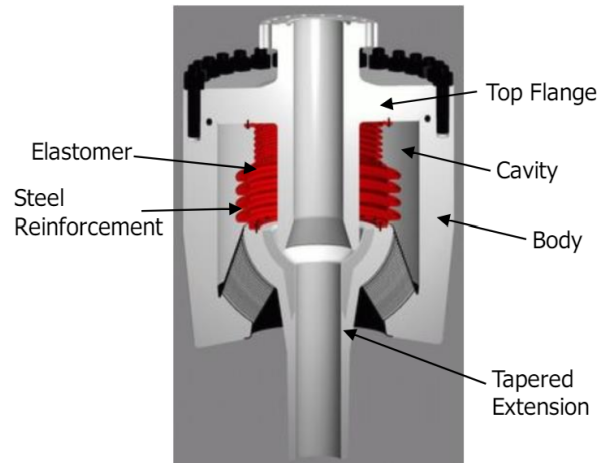


Figure 10: Typical flex joint configuration (Hui et al. 2019)

### Tapered stress joint

The steel catenary and lazy wave riser systems can be subjected to high bending moments at the hang-off point. This type of bending moment can be accommodated with a special joint where the wall thickness gradually increases towards the hang off point. This type of joint is known as the tapered stress joint (TSJ). The geometry of the TSJ include the overall length, wall thickness as well as the taper profile. The TSJ geometry is highly influenced by the global floater motions as well as the riser structural response (Arikan 2024).

### Bend stiffeners

The purpose of bend stiffeners is to increase and distribute bending stiffness in localized areas in the pipe. This is done when the configuration is subjected to bending moments that would be unacceptable. The increased stiffness reduces curvature and strain in the configuration. A typical application for a bend stiffener is at the top of a riser configuration. Bend stiffeners are often made of a polymeric molded material surrounding the pipe and attached to the end fitting (Q. Bai and Y. Bai 2005).

### Buoyancy modules

Buoyancy modules come in two main forms either as air cans or as foam modules. Air can buoyancy modules are a central component often used in buoyancy based tensioning systems. These are often used to provide top tension to risers in deep draft vessel applications. The foam buoyancy modules are often used to provide lift and thereby reduce the submerged weight of the riser. This type of buoyancy module can therefore be used in deep water applications (Q. Bai and Y. Bai 2005). The buoyancy modules are also used to change the riser configuration in order to have a more favourable configuration with respect to the load that the riser system is subjected to.

## 2.6 Steel Lazy Wave Riser Configuration

The compliant riser configurations can be made from either rigid or flexible pipes. The lazy wave configuration made from rigid steel pipes is known as the SLWR. This type of riser configuration can be used as an effective deep water oil and gas production system. The system is able to provide low cost and good reliability. One of the main advantages with SLWR compared to the often used SCR is the resultant top loads and fatigue life are significantly improved (Cheng et al. 2020). This is due to the SCR having poor fatigue performance when it is connected to a floater with large floater motions (Karunakara et al. 2005). Resulting in the most vulnerable parts of the SCR configuration, being located at the hang-off and at the TDP.

The SLWR type of riser is presented as a viable solution for deep water and ultra-deep water

---

applications. This is a result of the elimination of partial tension, and is achieved with the buoyancy modules that are added to the system. The buoyant section of the riser system creates a second arc to the riser system. The function of this arc is to isolate the riser motions from the floater motions. Thus the amplification of dynamic response is avoided. As a result of this, the dynamic response of the riser system can be independently analysed because of the decoupling between the top end of the riser and the TDP (Cheng et al. 2020).

The SLWRs are often hung from the floater without a motion compensating system, which is the norm for the different compliant riser configurations. This means that the self weight of the riser system is creating the tension in the configuration. A hang-off arrangement can include components such as flex joint, stress-joint and pull-tube arrangement. The flex joint is a widely used hang-off configuration used in deep water catenary risers. This is due to the large rotation and load bearing capacity (Hui et al. 2019). The top angle of the riser configuration will fluctuate as a result of the wind, wave, and current generated motions.

## 2.7 Riser material

When choosing a riser material, several parameters must be considered. Sævik (2017) states that the main purpose in pipeline material selection is to choose a material that ensures an economic and safe product transport. Some of the most important parameters when choosing a riser material are; the external environment the riser is subjected to, the service life of the riser as well as the functional, environmental and accidental loads. The riser systems can be divided in two different cross sectional configurations, these are flexible risers and rigid risers.

### 2.7.1 Flexible risers

The flexible riser is made from flexible pipes. Flexible pipes are made from several materials that are combined in several layers. A polymeric sealing material is used to contain the bore fluid. Several helical armor layers are applied in order to provide the strength of the flexible pipe. The flexible pipe has a polymer outer layer that has the function to prevent seawater from interacting with the armor wires. The cross section configuration of the flexible pipes provide a lower bending radius compared to the rigid riser. It is found that a flexible riser with the same pressure capabilities as a rigid riser has a 25 times lower required bending radius (Fergestad and Løtveit 2017).

In some cases, flexible risers are more favourable than rigid risers. There are two main reasons to use flexible risers over the rigid riser. These reasons can be summarized by the following (Fergestad and Løtveit 2017):

- The flexible riser allows for a permanent connection between a floater, with large floater motions, and the subsea installation.
- The transportation and installation of the flexible pipes are simpler. This is because of the possibility to prefabricate the flexible pipe in long lengths. The pipes can also be stored on a limited sized reel due to the flexibility of the pipes.



Figure 11: Typical flexible pipe cross section (Sævik 2017).

### 2.7.2 Rigid risers

Rigid risers can be made from materials such as steel, aluminium alloys and titanium. It is preferred that risers made from steel pipelines are made of carbon steel alloys if possible. This is due to the carbon steel pipes provide a favourable strength to cost ratio (Sævik 2017). The low carbon steels can be divided into different grades. Some examples of steel grades that are used in rigid riser configurations are API 5L X60, X65, and X70. Pipes made from different steel grades are made in different diameters and wall thicknesses. The rigid risers have a higher tensile strength compared to a flexible pipe. As a result of the rigid riser being made from pipe sections it is less flexible than a riser made from flexible pipe. Material properties of some of the most commonly used steel grades are stated in table (1) below.

Steel grade	Yield strength MPa	Tensile strength MPa
API 5L X60	415	520
API 5L X65	450	535
API 5L X70	485	570

Table 1: API 5L material strength properties (API 2018)

## 2.8 Riser fabrication and installation

In order to understand the overall picture of the design of a riser concept, this section will look into the fabrication and installation methods of rigid steel risers. One of the main reasons that the fabrication and installation methods are of interest is because of the capital expenditure (CAPEX). Q. Bai and Y. Bai (2005) states that the CAPEX of a pipeline project can be divided into the following categories:

- Materials and fabrication 55%
- Installation 29%
- Miscellaneous 8%
- Management and design 5%

- 
- Insurance 2%
  - Commissioning 1%

These numbers are only an estimate and will vary from project to project. However, it shows that the materials, fabrication and installation make up a majority of the CAPEX. With this in mind, it is clear that there is money to be saved by choosing the correct material, use an effective fabrication technique and install the riser with the right method.

### 2.8.1 Riser fabrication

Rigid risers can be made from a range of different materials such as carbon steel, aluminium or titanium. Low carbon steels are often used in offshore industry due to the low cost of the material compared to other options. Of these low carbon steels are API 5L X65 widely used. The main drawback to using low carbon steels is that they are subject to corrosion. In cases where the well fluid consists of CO<sub>2</sub> and H<sub>2</sub>S, the riser should be made from corrosion resistant alloys in order to reduce the risk of internal corrosion (Karunakara et al. 2005).

The fabrication of rigid risers consists of welding a series of pipes. This operation can be carried out both offshore and onshore. The main advantage to onshore fabrication is that the risers is produced in a controlled environment. With controlled environment it means that the weld inspections is preformed in an suitable environment. The main drawback with onshore production of rigid rises is that it becomes hard to transport.

The rigid riser is a series of welded pipes, and therefore the quality of the fabrication will have a direct effect on the quality of the riser. Some of the main factors when it comes to the quality of the fabrication are the material quality, which welding procedure is being used, as well as the quality of the weld (D. Karunakaran et al. 2013). Some of the welding techniques used in the fabrication of pipelines are stated below (Q. Bai and Y. Bai 2005).

- Flux core arch weld (FCAW)
- Gas metal arch weld (GMAW)
- Gas tungsten arch weld (GTAW)
- Shielded metal arch weld (SMAW)
- Submerged arch weld (SAW)

The material grade has an impact on the preparation that has to be made before starting welding. This is to ensure that the weld quality is of the required quality. Some of the measures that can be carried out are preheating of the pipes, joint preparation, as well as inter-run grinding. This is the case for higher strength grades of low carbon steels such as API 5L X70 and above (Q. Bai and Y. Bai 2005). In order to test if the weld is of the required quality, non-destructive tests (NDT) are applied. NDT of welds shall be carried out from agreed procedures with respect to the NDT standards from the international organization for standardization (ISO). In addition to this, requirements and acceptance criteria from the recommended practices will also be carried out (DNV 2020).

### 2.8.2 Rigid riser installation

There are several ways to install a rigid riser. The installation method that is chosen is based on the environment the riser is installed in. This is based on parameters such as maximum bending stress, axial stress in the riser, as well as preventing the riser from kicking. Three of the most common methods used for riser installation are the following:

- J-Lay
- S-Lay
- Reel Lay

### J-Lay

The J-Lay method gets its name due to the shape of the pipe that is being installed resembles a “J”. The riser is installed as a catenary where the riser enters the water at a certain angle. The angle of entry is determined by the water depth, the submerged weight of the riser and the horizontal tension acting on the riser. The angle of entry is mostly in the range of 0-15 degrees. High horizontal tension results in a larger angle. In the case of a larger angle, the layback length will increase. The layback length is the distance from the laying vessel to the TDP. The J-Lay method is a favourable method when the installation is located at large water depth. This is due to the methods ability to provide a large top angle which helps reducing the horizontal tension acting on the riser (Sævik 2017).

The main characteristics of a J-lay vessel is that the riser is installed from a steep tower. Due to the steep water entry, this method does not require either an overbend section or a stringer. The main drawback with this method is that the pipes are welded in the steep tower making the lay rate slow compared to other methods. The J-lay vessels are often equipped with collars that act as buckle arrests during the installation by holding the pipes (Sævik 2017). A typical J-lay operation is shown in figure (12) below.

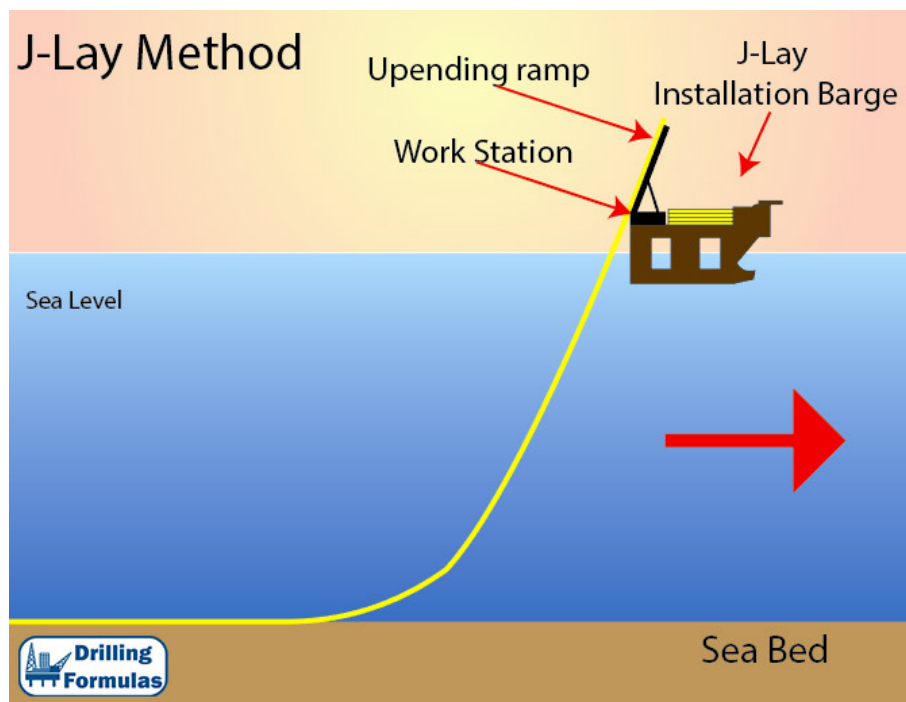


Figure 12: J-Lay method (DrillingFormulas 2024a).

### S-Lay

The S-lay method gets its name from the shape of the pipe being installed resembles a “S”, as a result of the sag bend and the overbend. The method is performed by easing the pipe of the laying vessel through a stringer as the vessel moves forward. The function of the stringer is to create a smooth transition until the pipe gets to a certain angle. This angle is known as the departure angle. From the departure angle, the pipe will behave similar to a J-lay. The S-lay vessel is often a dynamic positioning vessel or an anchored lay barge (Sævik 2017).

---

The S-lay method is the best method to use when installing long lengths of large diameter pipelines at moderate water depth. The limitation of the S-lay method is that it is not suited for deeper water. This is due to the limitation in stringer length as it becomes hard to create a stringer that provides a sufficient departure angle. As a result of the higher top angle, the pipe will be subjected to a larger horizontal tension. This increase in tension leads for the J-lay method to be required (Sævik 2017).

The main characteristics of a S-lay vessel is that the riser is welded in a horizontal position, to then be fed into a overbend created by the stringer. At the ramp of the vessel there are several tensioners places. The function of the tensioners is to create tension in the pipe. This tension is used to control the sag bend part of the pipe. The pipes are typically installed empty. This is done in order to increase the laying rate (Q. Bai and Y. Bai 2005).

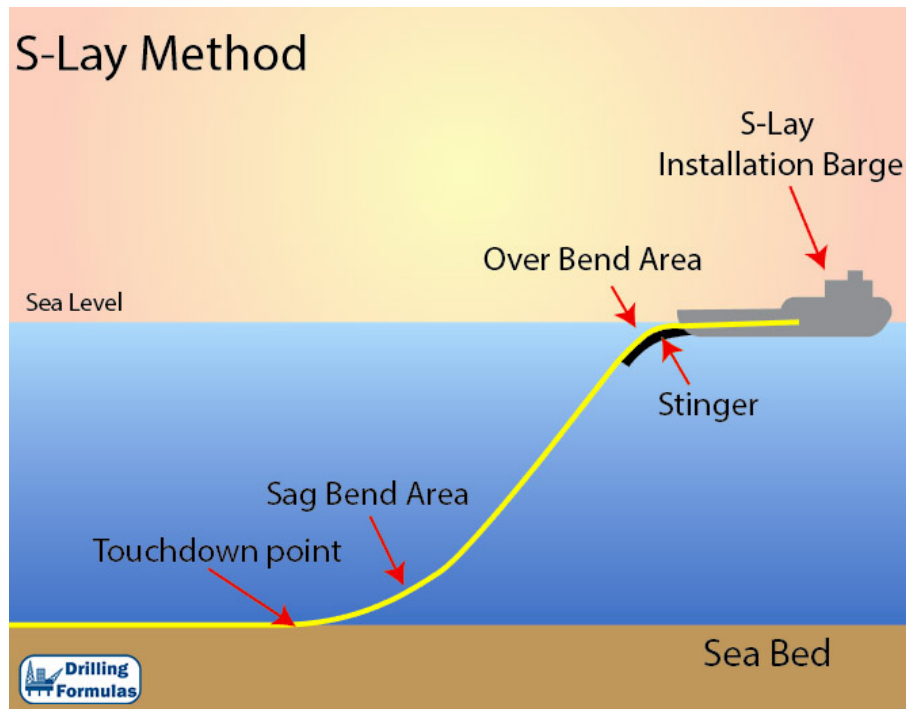


Figure 13: S-Lay method (DrillingFormulas 2024b).

### Reel-lay

In the reel-lay method, the pipe that is to be installed is already welded onshore. By using this method, the pipe can be welded in a controlled environment for example at the spool base. After the fabrication of the pipe, it is spooled onto a reel on the lay vessel. During this operation plastic deformation of the pipe will often occur. As a result of the plastic deformation there are limitations of what type of pipe that can be laid using the reel-lay method. The limitation covers what diameter of pipe that can be used. From the plasticity, the maximum diameter that can be laid with the reel lay method is about 18 inches in diameter. During the installation of the pipe can a J-lay or a S-lay configuration be used depending on the environment of the installation (Sævik 2017).

The main advantage of using the reel lay method is that the pipes are welded onshore in a controlled environment. This also saves time during the installation as there is no welding operation during the installation.

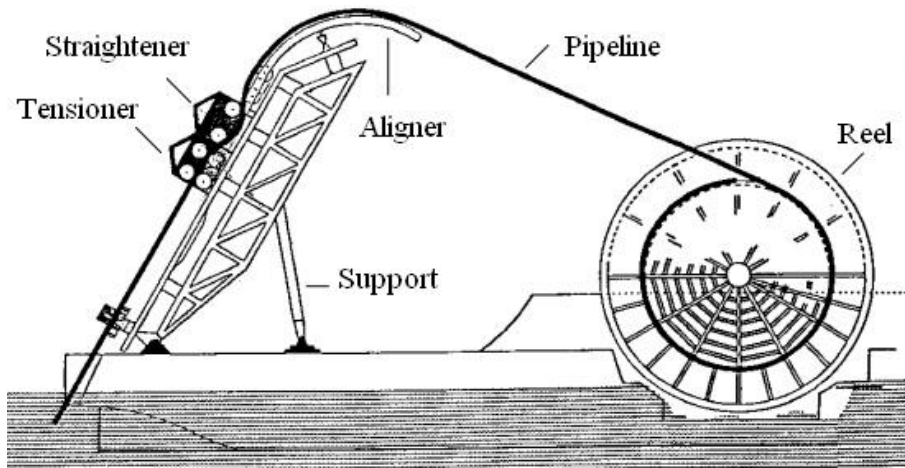


Figure 14: Reel Lay method (Hu et al. 2012).

## 2.9 Deep water challenges

For a riser system being applied for larger water depths, deep water challenges will occur for the riser design. Chakrabarti (2005a) defines deep water as water depths greater than 1000 ft (305 m). Water depths exceeding 5000 ft (1524 m) can be described by the term “ultra-deep water”. Some of the important deep water challenges are presented below:

### Floater motions

Subjecting riser systems to deeper waters, the environmental challenges will become more significant. The floater offset can contribute to deep water challenges (DNV 2021). Floater motions in heave and surge can contribute to high bending moment and low fatigue life in the riser at the TDP. The large water depth makes it possible for larger floater motions. The low frequency drift is often defined as a percentage of the water depth. This makes for a larger near and far load case as a result of floater drift.

### Hydrostatic pressure

With increased water depth, the external hydrostatic pressure acting on a system increase. The main risk of the increased hydrostatic pressure is that it can lead to a collapse of the system (DNV 2021). This issue can be especially important in the system installation if the system is installed in an empty condition. One of the solutions to this challenge is to increase the wall thickness of the riser. Changing the wall thickness of the riser can cause other challenges of the riser design.

### Increased riser weight

With larger water depth, the amount of riser in the water column will increase. For compliant risers without tensioning systems will this lead to an increased tension at the hang-off point. This is due to the weight of the riser increasing. The weight increase of the riser system result in increased tension force acting in the top of the system.

### Current profile

On increased water depths, larger current forces can be applied to the riser system. Another challenge that can occur for larger water depths is the vortex shedding due to certain current speeds. If the vortex shedding frequency is close to the eigenfrequency of the riser, this will lead to Vortex-Induced Vibrations (VIV) (Chakrabarti 2005b). Helical strakes can be applied to reduce the VIV motions and thereby increase the fatigue life of the riser. The main drawback of the helical strakes is that they create increased drag forces acting on the riser configuration (Faltinsen 1990).

---

## 2.10 Riser design loads

An important component of describing the riser system is the prediction of the loads acting on the system. The load components acting on the riser system can be described as design loads acting on the riser or the floater motions creating loads. Design codes are often used to define the loads acting on the riser system. The DNV-ST-F201 classify the loads acting on a riser system as (DNV 2021):

- Functional and Pressure Loads
- Environmental Loads
- Accidental Loads

Functional loads can be defined as loads that are coming from the riser configuration. This can be seen as the static loads acting on the system. Environmental loads can be defined as loads that effect the riser configuration from the surrounding environment. Accidental loads are loads resulted from unplanned occurrences.

### 2.10.1 Functional and pressure loads

Functional loads are defined as the loads that are a result of the riser system. These are load that occur without the presence of either environmental or accidental loads. The functional loads are a result of the physical configuration of the riser system. The pressure loads are a result of the combined load of internal pressure and external pressures (DNV 2021). Some of the main loads that contribute to the functional and pressure loads are presented in the list below:

- Weight of riser
- Nominal top tension
- Buoyancy sections on the riser
- Internal pressure
- External pressure

### 2.10.2 Environmental loads

The environmental loads can be describes as the loads that are applied directly or indirectly to the riser system as a result of environmental conditions (DNV 2021). Some of the most severe environmental conditions that the riser system can be subjected to are presented in the following sections.

- Wave loads
- Current loads
- Vessel motions
- Wind loads



---

### 2.10.3 Waves loads

One of the major dynamic environmental forces acting on the riser system are due to wind driven surface waves. The surface waves are irregular, and as a result of this are the waves varying in height and length. As a result of this irregularity of the sea, the wave can impact the riser configuration from several directions at the same time (DNV 2021).

The wave conditions acting on a riser system can be described in two ways; either by a deterministic design wave or by using stochastic methods. A stochastic method can be applied by using a wave spectra. A wave spectra is often defined by a set of parameters. Some of the most common parameters used to describe a wave spectrum are; the significant wave height ( $H_s$ ), spectral peak period ( $T_p$ ), the spectrum shape factor and the direction of the waves. Some of the most common spectra used for modeling of offshore structures are presented below.

#### Pierson-Moskowitz

The Pierson-Moskowitz spectrum is valid for fully developed sea states and unlimited fetch. This spectrum is a one peak spectrum that has a steep front for low frequencies. The original Pierson-Moskowitz spectrum was parameterized using the average wind speed at 19.5m above sea level. The spectral shape has later been re-parameterized into two parameters,  $H_s$  and  $T_p$ , and can be described by the following equation (Haver 2020):

$$S(\omega) = \frac{\alpha g^2}{\omega^5} \exp(-\beta (\frac{\omega_0}{\omega})^4) \quad (1)$$

$$\omega_0 = \frac{g}{V} \quad (2)$$

The parameters from the Pierson-Moskowitz spectrum equation are presented in the following list:

- $\alpha$ : is 0.0081
- $\beta$ : is 0.74
- $\omega$ : angular frequency
- $g$ : is gravity acceleration
- $V$ : is wind speed at 19.5 meters

#### Joint North Sea Wave Project

In the early seventies, a study of wave growth under growing wind conditions was executed by full scale measurements. This study was carried out in the southern North Sea. A result of this study was the proposal of the Joint North Sea Wave Project (JONSWAP) spectrum (Haver 2020). From the equation below, it can be seen that the JONSWAP spectrum is based on the Pierson-Moskowitz spectrum. The difference between the spectra is that the JONSWAP spectrum is described with a peak enhancement factor. The most common way to present the JONSWAP spectrum for practical calculations is given in the following equations (Larsen et al. 2021):

$$S(\omega) = \frac{\alpha g^2}{\omega^5} \exp(-\frac{5}{4} (\frac{\omega_p}{\omega})^4) \gamma^r \quad (3)$$

$$r = \exp[-\frac{(\omega - \omega_p)^2}{2\sigma^2 \omega_p^2}] \quad (4)$$

$$\omega_p = 0.87 \frac{g}{V} \quad (5)$$

The parameters from the JONSWAP spectrum equation are presented in the following list:

- 
- $\gamma$ : is a peakedness factor
  - $\omega_p$ : is the peak frequency
  - $\sigma$ : is determined from the relation between  $\omega$  and  $\omega_p$

#### 2.10.4 Current loads

The current loads can create significant loads to the riser system. This can either be from the drag forces from the current or from VIV forces from the motion excitation. The reason these are the main current load components are due to the riser structure being long and slender. Faltinsen (1990) presents that current can be described by six current components that create a resulting current. The current components are presented in the following list.

- Tidal current
- Local wind-generated current
- Stokes drift-generated current
- Ocean circulation
- Set-up phenomenon and storm surges
- Local density driven current

#### 2.10.5 Floater motion

The forces acting on the riser system are effected by the surface forces. The surface forces will create floater motions that will be transferred to the riser system. The floater offset will contribute to the static and dynamic loads acting on the riser system. For a compliant riser system is tensioning systems most commonly not applied, as the configurations uses the weigh of the riser to create tension. The heave motion of the floater can create a reduction of tension in the riser at the TDP. If the tension is sufficiently reduced, it can lead to instability of the riser and potential buckling issues. The floater motions that are of interest can be described by the following (DNV 2021):

- Static offset
- Wave frequency motions
- Low frequency motions

The floater motion can be analysed by either carrying out a coupled or a decouple analysis. The coupled analysis is assumed to be more accurate, but has the main drawback of requiring a much larger computational effort. The decoupled analysis is therefore assumed to be more efficient but less accurate (Kim et al. 2017).

#### 2.10.6 Accidental loads

The accidental loads acting on a riser system can be described by load cases that has an annual probability of less then  $10^{-4}$ . These include cases of abnormal environmental conditions, technical failures or incorrect operations. The accidental loads are often a result of unplanned occurrences due to the low annual probability. DNV (2021) presents some of the most common accidental loads.

- Fires and explosions

- 
- Impact and collision
  - Hook or snag loads
  - Environmental events

---

### 3 Analysis methodology

A global riser analysis is carried out in order to describe the static and dynamic structural behaviour of the riser system. This is achieved by loading the riser system with a stationary environmental load condition. As a part of the analysis are a global cross-section description carried out. This description is based on the resulting force and displacement relations of the system. The different global response quantities can be grouped into four main categories (DNV 2021). These are described in the following list.

- The resulting cross-section forces including the effective tension, bending moments as well as the torsional moments.
- The global riser deflections these can be described as the curvature, elongation and angular orientation of the riser system.
- The global riser position is represented by the riser coordinates, translations, position of touch down point on seafloor and more.
- The support forces at termination to rigid structures that are represented by the resulting force and moments.

The finite element method (FEM) is the most common approach in order to carry out a global analysis of a riser system. In order to create an adequate model of the riser system, there are several parameters that should be considered. DNV (2021) presents a list of parameters that should be considered when modelling a deep water riser configuration. The list of features that should be considered can be seen below.

- The seabed riser contact formulations
- The structural damping formulation
- The current profile modelling
- A 3D formulation to allow unlimited translations and rotations
- Small strain slender beam or bar elements that include the material and geometric stiffness that allow non-linear material properties
- Special features for modelling of riser components such as flex-joints and buoyancy modules
- Using the Morison equation to express the hydrodynamic loading
- Regular and irregular loading from waves and the floater motions
- Using non-linear static analysis
- Using non-linear time domain dynamic analysis

#### 3.1 Finite element model

The dynamic equilibrium equation can be presented by the following equation (Langen and Sigbjörnson 1979).

$$M\ddot{v} + C\dot{v} + Kv = Q(t) \tag{6}$$

The parameters from the equilibrium equation represent:

- M: Mass matrix

- C: Damping matrix
- K: Stiffness matrix
- $\ddot{v}$ : Acceleration vector
- $\dot{v}$ : Velocity vector
- $v$ : Displacement vector
- Q External load vector

An explanation of the matrix terms in the dynamic equilibrium equation will be carried out in the following sections.

### 3.1.1 Mass matrix

The mass matrix consists of the structural mass and the added mass. The matrix can be sorted as a consistent matrix or a lumped matrix. In a lumped matrix the mass and added mass are assigned to the the system nodes. The main advantage of using the lumped mass matrix is more efficient calculations. (Langen and Sigbjörnson 1979).

The lumped matrix terms of a 6 degree of freedom beam element can be expressed with the following equation:

$$m_i = \frac{\rho Al}{420} \begin{bmatrix} 140 + 70 & 0 & 0 & 0 & 0 & 0 \\ 0 & 156 + 54 & 0 & 0 & 0 & 0 \\ 0 & 0 & \alpha(4l^2 - 3l^2) & 0 & 0 & 0 \\ 0 & 0 & 0 & 140 + 70 & 0 & 0 \\ 0 & 0 & 0 & 0 & 156 + 54 & 0 \\ 0 & 0 & 0 & 0 & 0 & \alpha(4l^2 - 3l^2) \end{bmatrix} \quad (7)$$

The consistent matrix of an element can be expressed by the following equation:

$$m_i = \int_{V_i} \rho N^T N dV \quad (8)$$

The  $m_i$  term is the mass matrix for a given element.  $\rho$  represent the density of the of the element. N is the interpolation function used over the length of the unit. v represent the displacement vector of the system. Langen and Sigbjörnson (1979) presents that the mass matrix of an entire structure can be written on the following form.

$$M = \sum_i a_i^T m_i a_i \quad (9)$$

Where M represents the total stiffness matrix as a sum of the element mass matrices transformed to the global system using the connectivity matrix represented as a (Langen and Sigbjörnson 1979).

### 3.1.2 Damping matrix

The damping matrix consists of a combination of the structural damping and the hydrodynamic damping acting on the system. The Rayleigh damping formulation is often applied to model the structural damping. The Rayleigh damping formulation can be expressed by the following equation (Langen and Sigbjörnson 1979).

---


$$C = \alpha_1 M + \alpha_2 K \quad (10)$$

$\alpha_1$  represents the mass proportional damping coefficient.  $\alpha_2$  represents the stiffness proportional damping coefficient. Using the Rayleigh damping formulation makes the damping matrix orthogonal with the eigenvectors of the system. In the case of a linear dynamic system, orthogonality can be used to express the damping coefficient. The damping coefficient can be represented by the following equation (Langen and Sigbjörnson 1979).

$$\lambda_i = \frac{1}{2} \left( \frac{\alpha_1}{\omega_i} + \frac{\alpha_2}{\omega_i} \right) \quad (11)$$

### 3.1.3 Stiffness matrix

In modeling of a riser system, a beam element is often utilized. In the case of a 6 degree freedom element, where the shear deformations are neglected, can the stiffness matrix be derived from Euler Bernoulli beam theory. From this, the elastic stiffness matrix can be expressed by the following equation (Langen and Sigbjörnson 1979):

$$k_E = \begin{bmatrix} \frac{EA}{l} & 0 & 0 & \frac{-EA}{l} & 0 & 0 \\ 0 & \frac{12EA}{l^3} & \frac{-6EA}{l^2} & \frac{-12EA}{l^3} & \frac{6EA}{l^2} & 0 \\ 0 & \frac{-6EA}{l^2} & \frac{4EA}{l} & 0 & \frac{6EA}{l^2} & \frac{2EA}{l} \\ \frac{-EA}{l} & 0 & 0 & \frac{EA}{l} & 0 & 0 \\ 0 & \frac{-12EA}{l^3} & \frac{6EA}{l^2} & 0 & \frac{12EA}{l^3} & \frac{6EA}{l^2} \\ 0 & \frac{-6EA}{l^2} & \frac{2EA}{l} & 0 & \frac{6EA}{l^2} & \frac{4EA}{l} \end{bmatrix} \quad (12)$$

The contribution of the geometric stiffness to the global stiffness matrix can be found by applying non-linear theory. The geometric stiffness is found by looking at the strain equation with second order terms. The equation of strain is shown in the following equation (Moan 2003).

$$e_x = u_{,x} - z * w_{,xx} + \frac{1}{2} w_{,x}^2 \quad (13)$$

In order to get the geometric stiffness matrix in a more suitable form, it can be linearized. The linearized geometric stiffness matrix can be expressed by the following equation (Gavin 2012).  $P$  represent the axial force acting on the element.

$$k_G = \begin{bmatrix} 0 & 0 & 0 & 0 & 0 & 0 \\ 0 & \frac{6P}{5l} & \frac{-P}{2Pl} & 0 & \frac{-6P}{5l} & \frac{-P}{2Pl} \\ 0 & \frac{-P}{10} & \frac{2Pl}{15} & 0 & \frac{P}{10} & \frac{-Pl}{30} \\ 0 & 0 & 0 & 0 & 0 & 0 \\ 0 & \frac{-6P}{5l} & \frac{P}{2Pl} & 0 & \frac{6P}{5l} & \frac{P}{2Pl} \\ 0 & \frac{-P}{10} & \frac{-Pl}{30} & 0 & \frac{P}{10} & \frac{Pl}{15} \end{bmatrix} \quad (14)$$

The total stiffness matrix for a given element is therefor a combination of the elastic and the geometric stiffness matrix. This can be written as the following equation:

$$k_i = k_{E,i} + k_{G,i} \quad (15)$$

Langen and Sigbjörnson (1979) states therefore that the total stiffness matrix can be represented by the following equation:

---


$$K = \sum_i a_i^T T_i^T k_i a_i \quad (16)$$

$a_i$  represents the connectivity matrix, and together with the transformation matrix  $T_i$  is the local stiffness matrix  $k_i$  transformed to fit in the global stiffness matrix.

### 3.2 Static analysis

The static analysis is used to establish the static equilibrium configuration from static loading. This is done by ensuring that the system is in static equilibrium by obtaining the nodal displacements (Moan 2003). The static analysis is often described as the first step of the global analysis. This is a result of the static analysis being the starting point of the dynamic and eigenvalue analysis. The static analysis of a riser system is often carried out using a nonlinear finite element approach. For convenience the basic loading components are often divided into the following groups (DNV 2021).

- Volume forces represent the forces from the riser weight and buoyancy
- Specified forces that can be described as the applied top tension
- Prescribed displacements that can be described as displacement from the terminal points from the stress free position to specified positions
- Displacement dependant forces are often described as the current loading

The discretized finite element model of the system is determined by the nodal displacement vector. The static analysis is used to determine the displacement vector. The static equilibrium configuration is found as the solution of the following system of equations (SINTEF 2024h).

$$R^S(r) = R^E(r) \quad (17)$$

In this case:

- $r$  is the nodal displacement vector with all degrees of freedom of the system
- $RS(r)$  is the internal structural reaction force vector determined by assembly of element contributions.
- $RE(r)$  is the external force vector from all elements.

Moan (2003) states that the static equilibrium equation can be written on a differential form:

$$\frac{d}{dr}(K(r)r)dr = dR \quad (18)$$

$$\frac{d}{dr}(K(r)r) = K_I(r) \quad (19)$$

$K_I(r)$  represent the tangential stiffness matrix. This matrix is a combination of the material, geometry and external stiffness matrices (Moan 2003).

The external loading and internal reaction force are often described as nonlinear functions of the nodal displacement vector. The static equilibrium is often found by applying an incremental loading procedure. This procedure finds the static equilibrium numerically by carrying out equilibrium iterations for each of the load steps. The incremental iterative procedure can often use a Euler-Cauchy incrementation (SINTEF 2024h).

---

## Euler-Cauchy

The Euler-Cauchy incrementation method is used to solve the non-linear problem. This is done by applying a step wise application of the external loading. The displacement of the system is predicted by adding the displacement increments from the step wise application. The incremental stiffness matrix  $K$  is calculated from the system displacement and stress condition from the previous iteration. These calculations are carried out before a new load iteration can be applied. The incremental stiffness matrix is kept constant during an increment. The load increment number  $(m+1)$  can be expressed with the following equation (Moan 2003).

$$\Delta R_{m+1} = R_{m+1} - R_m \Delta r_{m+1} = K_I(r_m)^{-1} \Delta R_{m+1} r_{m+1} = r_m + \Delta r_{m+1} \quad (20)$$

Using the Euler-Cauchy formulation can the load be incremented until the desired level is obtained. The main drawback of the Euler-Cauchy method is that it will not fulfill the total equilibrium as a result of the drift of effect. In order to achieve a sufficient level of equilibrium is a term implemented in the next time step. This term is able to account for drift off between the internal and the external loads.

$$\Delta R_{m+1} = R_{m+1} - R_m R_{eq} = R(r_m) - R(r_m) \Delta r_{m+1} = K_I(r_m)^{-1} (\Delta R_{m+1} + R_{eq}) \quad (21)$$

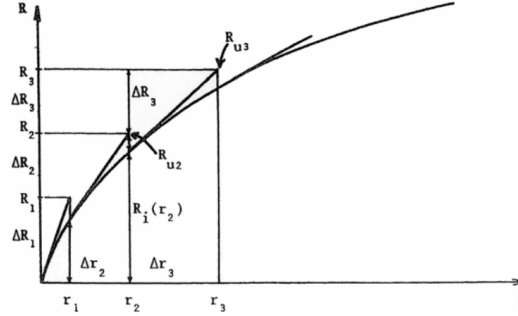


Figure 15: Euler-Cauchy method with equilibrium correction (Moan 2003)

## Newton-Raphson

Newton-Raphson is the most frequently used iteration method to solve non-linear structural problems. The main advantage of the Newton-Raphson method is that it has a quadratic convergence rate. The Newton-Raphson method is not subjected to the drift off problem. Newton-Raphson method formulation can be described by the following equation (Moan 2003).

$$r_{m+1} - r_m = \Delta r_{m+1} = K_I^{-1}(r_n)(R - R_{int}) \quad (22)$$



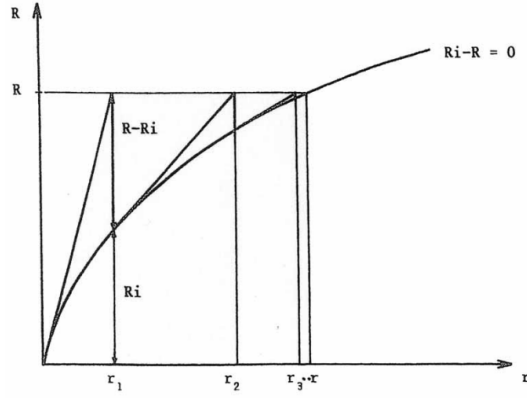


Figure 16: Newton-Raphson method (Moan 2003)

### 3.3 Eigenvalue Analysis

The eigenvalue problem can be written on two forms. These are the eigenvalue problem on the general form and the special eigenvalue formulation. The eigenvalue problem is therefore the solution of either (Langen and Sigbjörnson 1979):

$$(\omega^2 M - K) = 0 \quad (23)$$

$$(A - \lambda I)x = 0 \quad (24)$$

The parameters in the two equations above can be described by the following:

- M is the mass matrix
- K is the stiffness matrix
- $\omega$  is the eigenfrequency
- A is the quadratic matrix
- $\lambda$  is the eigenvalue matrix
- x is the corresponding eigenvectors

The eigenvalues and corresponding eigenvectors can be solved using a truncated Lanczos method (SINTEF 2024i).

### 3.4 Dynamic analysis of riser systems

In some cases, a time domain analysis can be sufficient to find an exact solution of a system. In most cases, the problem will be solved by other types of finite element methods or by using other types of time incremental methods. The global dynamic analysis of a riser system are normally performed by considering the forced excitation from parameters such as wave frequency, floater motions and direct wave and current loading. The most common dynamic finite element analysis methods are often described as the; linearized time domain analysis, the nonlinear time domain analysis and the frequency domain analysis (DNV 2021).

#### Linearized time domain analysis

---

A linearization of the dynamic equilibrium equation is carried out as a part of the linearized time domain analysis. This is done by taking the inertia, damping and stiffness force from the static equilibrium position into account. As a part of this analysis, the mass, damping and stiffness matrices are kept constant during the duration of the analysis. This is done such that the displacement vector can be found by using back substitution of every time step (DNV 2021)

The nonlinear hydrodynamic loads acting on the system from Morison equation still being applied. It is found that the linearized method approach is more efficient than nonlinear analysis methods. The linearized method is therefore seen as an alternative for cases where major nonlinear contributions come from the hydrodynamic loading (DNV 2021)

### **Nonlinear time domain analysis**

In the nonlinear time domain analysis method, a step by step numerical integration of the incremental dynamic equilibrium equation is carried out. In this analysis method, an equilibrium iteration is used for every time step. The main advantage of the nonlinear time domain method is that it gives a description of the nonlinear effect acting on the system. The method can also present possible non-Gaussian responses acting on the system (DNV 2021)

The systems where a non-linear simulation often are applied are systems with; large displacements, large rotations or variations in tension. The method is also applied for systems where material non-linearities are important or for systems with variable TDP (DNV 2021). An example of such a system is a catenary riser system.

### **Frequency domain analysis**

In order to carry out a frequency domain analysis, a linearization of the inertia, damping, stiffness and external forces from the static equilibrium position is applied. In order to carry out an irregular analysis, a stochastic linearization of the combined wave and current loading is required. The method is used to obtain Gaussian response. The method is not suited to carry out extreme response predictions (DNV 2021)

The frequency domain analysis method is mainly used for fatigue calculations or to obtain long-term response statistics. This analysis can be used to identify the design conditions that should be applied for a time domain analysis. One of the main advantages with the frequency domain analysis method is that the computational time is low compared with the time domain methods (DNV 2021).

## 4 Fatigue theory

Fatigue damage is accumulated when a structure is subjected to a cyclic load. These loads are predominantly lower compared to the yield stress of the material. Fatigue will not cause a fast failure as the fatigue damage is accumulated from the cyclic loading that leads to an eventual failure. Berge (2006) states that the fatigue history of a structure can be divided into three different stages.

- Initiation
- Crack growth
- Final failure

For unwelded components, the initiation phase are the dominating phase. For welded components such as a rigid riser, there will be crack growth and initial flaws due to the production of the component, generally the crack growing phase will be the dominating phase. The different phases are governed by different types of stresses. An example of this is that the initiation phase is governed by the yield stress and the von Mises stress due to the phase representing the crack initiation. The crack growth phase is governed by the cyclic stress that is applied to the structure. Crack growth is described as the crack propagation rate. This is measured by measuring the change in crack length during a set number of cycles,  $da/dN$  where  $da$  is the change in crack length and  $dN$  representing the number of cycles (Almar-Næss 1985). (Berge (2006)) states that crack growth can be divided into three regions as presented in the crack growth curve presented in the figure (17) below.

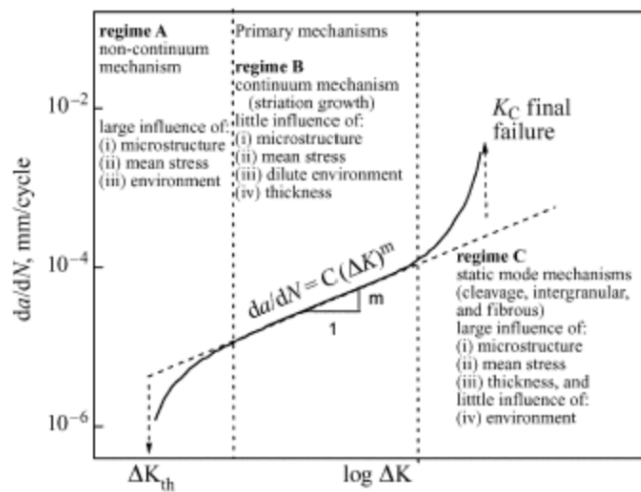


Figure 17: The different stages of crack growth (Ray 2001)

The regions are described as (A) threshold, (B) intermediate and (C) failure. From the crack growth curve, it can be seen that the intermediate region is linear, this represents a stable crack growth in this region. This can be described using Paris law (Almar-Næss 1985):

$$\frac{da}{dN} = C(\Delta K)^m \quad (25)$$

- $da$ : Crack growth
- $dN$ : Number of cycles
- $\Delta K$ : stress intensity factor

- C: material dependent factor
- m: material dependent factor

## 4.1 Load history

The load history of a system is obtained from a dynamic analysis. During the dynamic analysis, the variation in force is created from waves, current and wind these forces create a variable amplitude (Almar-Næss 1985). In fatigue damage calculations, the amplitude of the load history are important. The load range is used in order to calculate the fatigue damage. Using the load range can the load history be divided into blocks. A load history can be represented as shown I figure (18) below.

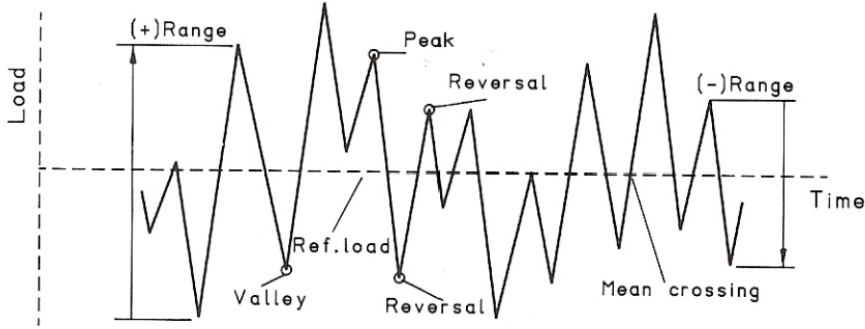


Figure 18: Different parts of a load history (Wægter 2024)

Almar-Næss (1985) states that the main features of a load history can be described by the following characteristics:

- Reversal: The reversal is when the first derivative of the load history changes sign
- Peak: When the reversal sign changes from positive to negative
- Valley: When the reversal sign changes from negative to positive
- Range: The difference between following peak or valley load
- Mean crossing: The number of times the load history crosses the mean load level.

The bandwidth and irregularity factor of the load history is defined the by ratio between the mean crossings compared to the number of the peaks and valleys. The irregularity factor can be linked to the spectral bandwidth factor  $\epsilon$  that can be described as (Almar-Næss 1985):

$$I = (1 - \epsilon^2)^{0.5} \quad (26)$$

$$\epsilon = \left(1 - \frac{m_2^2}{m_0 m_4}\right)^{0.5} \quad (27)$$

$$m_n = \int_{-\infty}^{\infty} \omega^n S(\omega) d\omega \quad (28)$$

I represent the irregularity factor. In a narrow banded process will the bandwidth factor  $\epsilon$  be close to 0.  $m_n$  is the spectral moment calculated from the wave spectrum.

---

## 4.2 S-N curves

S-N curves also known as Wohler curves describe the fatigue properties for a material by using the load range as a function to calculate the cycles until failure. The S-N curves was created using experimental data to describe the relation between load range and cycles (Almar-Næss 1985).

$$N(\Delta S)^m = a \quad (29)$$

- $\Delta S$ : Stress range
- N: Number of cycles
- a: constant
- m: constant

The equation is analogue with Paris law in the intermediate crack growth range. The S-N curve is plotted logarithmicly. By doing this, the S-N curve will be displayed as linear and the equation above can be rewritten as (DNV 2019a):

$$\log a = \log a * m * \log(\Delta S) \quad (30)$$

The S-N curve that is used for design is the mean curve minus two standard deviations, presented by DNV (2019a) as the following equation:

$$\log a = \log a - 2 * \sigma_{\log N} \quad (31)$$

A S-N curve describing the fatigue life of a structure subjected to a constant cyclic loading can describe a fatigue limit. The fatigue limit is the load that is needed to cause the failure in the structure. From this it is assumed that the structure has “infinite” fatigue life, as it is assumed that damage cannot be accumulated from stress lower than the fatigue limit.

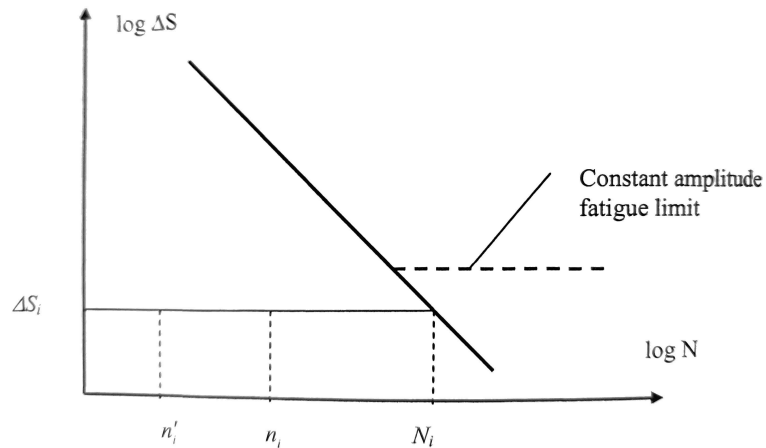


Figure 19: Representation of S-N curve with constant amplitude fatigue limit (Berge 2006)

In cases where the structure is subjected to variable loading, the S-N curve will not have an “infinite” fatigue life. This is due to loads larger than the fatigue limit that contribute to the crack growth and therefore gradually reducing the fatigue limit (Berge 2006). Haibach’s model is used in order to express the slope of the bilinear S-N curve. Haibach model used the fracture mechanic

model that assumes the Paris-Erdogan crack growth law. The model describes the slope of the S-N curve below the original fatigue limit as  $(1/(2m-1))$  making the S-N curve bilinear. This is the S-N curve that has been adopted for design (Berge 2006). An example of a bilinear S-N curve is presented in figure (20) below.

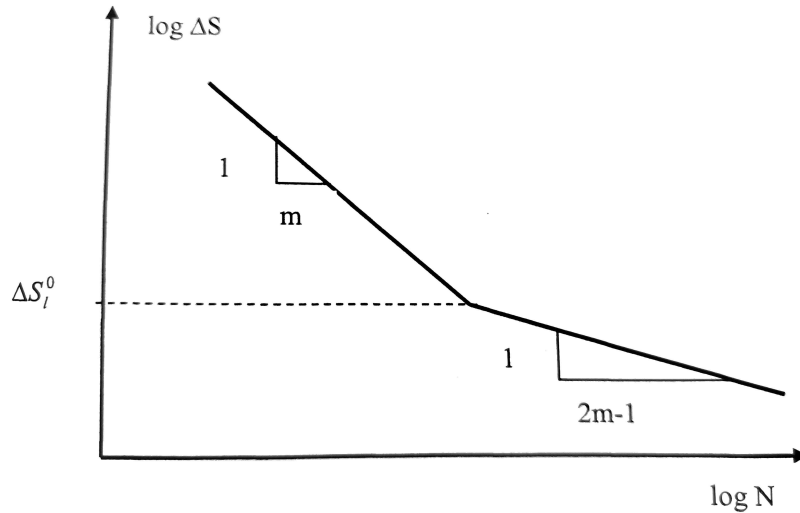


Figure 20: Example of a bilinear S-N curve (Berge 2006)

The fatigue life of welded joints decreases for larger plate thickness, as a result of the local geometry of the weld toe with the welded plates (DNV 2019a). In order to account for this, a thickness correction is added to the S-N curve in the cases where the plate thickness is larger than a reference thickness. The S-N curve can then be represented as:

$$\log a = \log a * m * \log\left(\Delta S \left(\frac{t}{t_{ref}}\right)^k\right) \quad (32)$$

- $t$ : Plate thickness
- $t_{ref}$ : Reference thickness
- $k$ : Thickness exponent

As stress concentration can occur at holes and sharp corners, and in order to account for this can the nominal stress range be corrected with a stress concentration factor (SCF) (DNV 2019a).

$$\Delta = SCF * \Delta S_{nominal} \quad (33)$$

### 4.3 Cycle counting

In order to compare the effect of variable amplitude loading that causes fatigue, cyclic counting can be used. Cycle counting can be done from data presented in a histogram. In a time series each cycle can be divided into individual cycles, these loads can be added together in order to create a load histogram. Some of the most common counting methods are; level crossing counting, rainflow counting, peak counting and simple range counting. The number of cycles is dependent on the fact if the process is narrow or broad banded, as different counting methods count different. The difference in the counting methods are how low cycles affecting the larger cycles are taken into

account. Rainflow counting is an often used method, as it is a representation that is similar to the physical process (Almar-Næss 1985).

Rainflow counting count the turning points in the load history from the stress-strain response. In rainflow counting, the individual cycles does not affect the rest of the stress-strain curve. The stress-strain curve makes a closed hysteresis loop. For every closed loop, another cycle is counted. Unless the load history is rearranged with the maximum or minimum value as the starting peak or valley will unpaired half cycles occur. These half cycles can be difficult to account for when it comes to calculating cumulative damage (Almar-Næss 1985).

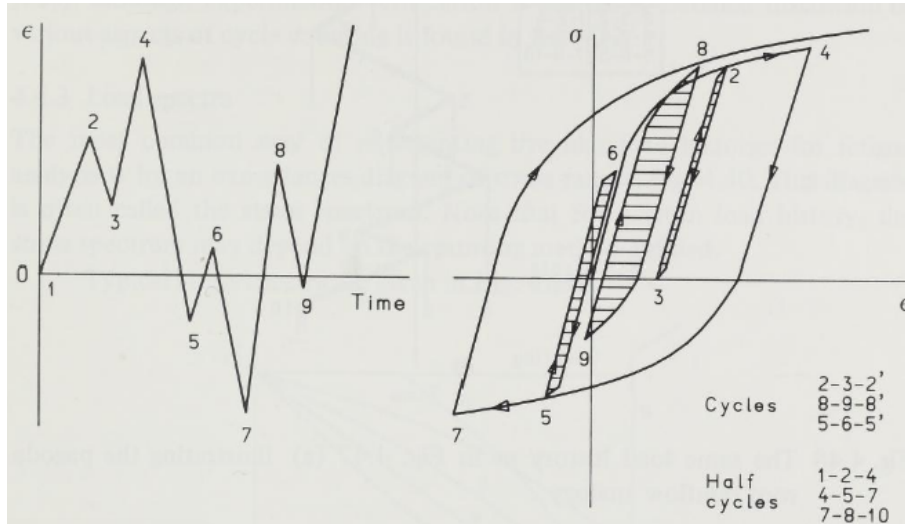


Figure 21: An example of the relation between the strain history and the stress strain response using rainflow counting (Almar-Næss 1985)

Rainflow counting is based on the idea of tuning the strain history 90 degrees and looking at it as rain running down a pagoda roof. The rain flows along the roof until it reaches the edge of the roof representing the peak or valley. The rain flows of the roof and stops when it lands on another flow from above. When this happens the cycle is complete. The cycle start from a peak or a valley and is complete when a lager peak or valley comes along. Figure (22) is a visual representation of how rainflow counting is carried out (Almar-Næss 1985).

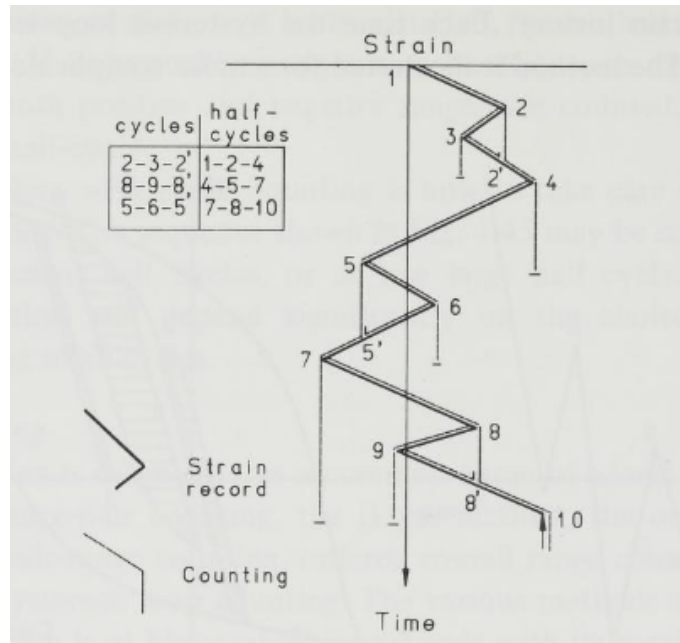


Figure 22: Presentation of the pagoda roof analogy for rainflow counting (Almar-Næss 1985)

#### 4.4 Miner-Palmgren Summation

Miner-Palmgren summation is used to calculate the cumulative fatigue damage. The method uses the data from the S-N curve in order to calculate the cumulated damage. Miner-Palmgren summation uses a constant damage per load cycle and is represented by the equation (Almar-Næss 1985):

$$D_{fat} = \frac{1}{N} \quad (34)$$

$D_{fat}$  represents the accumulated damage.  $N$  represents the constant amplitude endurance. This can be used to calculate number of cycles until failure for a constant stress. In order to account for variable loading, the equation above can be rewritten by dividing the loading into blocks (Almar-Næss 1985):

$$D_{fat} = \sum_{i=1}^k \frac{n_i}{N_i} \quad (35)$$

$k$  represents the number of blocks the loading is divided into, where  $n_i$  is the number of load cycles in block  $i$ . By combining the equation from Miner-Palmgren and the S-N curve give the following equation for the accumulated damage (DNV 2019a):

$$D_{fat} = \frac{1}{a} \sum_{i=1}^k n_i (\Delta\sigma)^m \quad (36)$$

In order to calculate the fatigue damage, it has to be determined how to apply the stress ranges for each of the blocks from the histogram. One of the options is to use the maximum value for each of the blocks. Another option is to use each of the cycles individually and therefore not using a histogram.

When accounting for design criteria it is important to reduce the risk for fatigue failure. Using a Design Fatigue Factor (DFF). The DFF is used in order to add a safety factor to the fatigue life



---

of a design (DNV 2021). The equation for the fatigue design criterion can be expressed as:

$$D_{fat} * DFF < 1 \quad (37)$$

Due to fatigue damage being accumulated as a result from cyclic loading. These stress and strain cycles are dependent on the previous cycles. Miner-Palmgren summation does not account for the stress memory effect. The stress memory effect can lead to a bias creating an uncertainty when it comes to the estimation of the fatigue damage. One of the options that can be applied to account for the bias is to add a relative Miner-Palmgren sum, related to offshore structures are a  $D < 0.5$  proposed (Almar-Næss 1985). On the other side, a DFF are often applied when using the Miner-Palmgren summation that adds a safety factor to the system reducing  $D < 1$ . This means that the Miner-Palmgren summation both measure the damage, and acts as a safety measure when it comes to the design life of the structure.

---

## 5 SIMA RIFLEX

The SIMA workbenche is provided by SINTEF and is used in order to carry out simulations and analysis for floating systems and marine operations. The program is made to support the entire process from defining the simulation to the documentation of results. SIMA workbench is divided into several types of programs in order to carry out different types of tasks. Some of these are; SIMO, VIVANA and RIFLEX. SIMO is a program used in simulation of motion as well as station-keeping behavior for different types of systems (SINTEF 2024g). The VIVANA program is used to carry out vortex induced vibration analysis for slender structures. The VIVANA program has to be paired with the RIFLEX program in order to carry out a VIV analysis. This is because some of the RIFLEX modules are needed to utilize VIVANA (SINTEF 2024c).The RIFLEX program is used to carry out static and dynamic analysis of slender structures.

The RIFLEX program was developed in order to carry out analysis of flexible marine riser systems. The program is also well suited for other types of slender structures, such as mooring lines, pipelines and rigid risers. The RIFLEX program uses the principle of a nonlinear finite element formulation. Some of the key features of the RIFLEX program are; flexible modeling for simple and complex systems. Nonlinear time domain simulation used to analyse system motion and forces. The program also gives the ability to use nonlinear cross section properties (SINTEF 2024f).

The RIFLEX program is often used to compute the static and dynamic forces and motions acting on a structure. The characteristics are computed using different types of analysis. The conditions used in the static and dynamic analysis are presented below (SINTEF 2024f).

### **The static analysis is based on:**

- Equilibrium configuration
- Current velocity and direction
- Parameter variations of tension or position parameters

### **The Dynamic analysis is based on:**

- Eigenvalue analysis, natural frequencies and mode shapes
- Response as a result of harmonic motion and wave excitation
- Response due to irregular wave and motion excitation

### **5.1 Structure of RIFLEX program**

The RIFLEX program is a system that is based on four modules. These modules are used to communicate with a file system. These modules are shown in figure (23) below. A description of the different modules will be carried out below the figure.

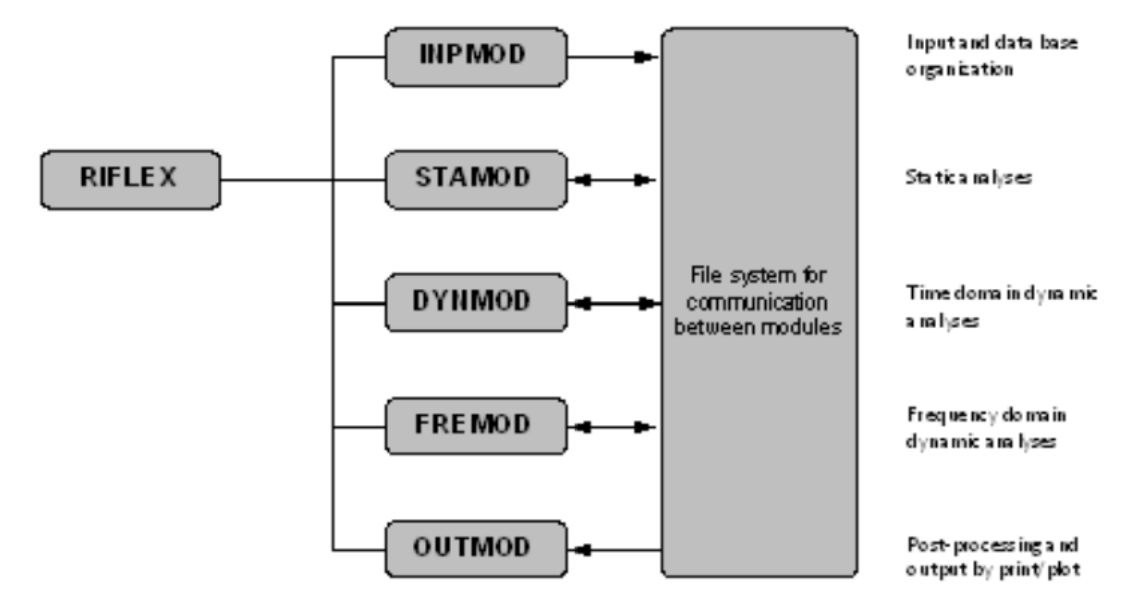


Figure 23: Structure of the RIFLEX program system (SINTEF 2024b)

### INPMOD module

The INPMOD module is used to read input data that is given to the program. The module then organizes a data base. This data base is used to carry out other analyses. As the INPMOD analysis creates a data base it only has to be run once. Thus several analysis can be carried out in different modules without rerunning the INPMOD (SINTEF 2024f).

### STAMOD module

The STAMOD module is used to perform different types of static analyses. The results from the analysis in the STAMOD module can be used directly in parameter studies. They can also be used to define the initial configuration of a system that is to be used in a succeeding dynamic analysis. Key data used in finite element analysis is generated in the STAMOD module. Examples of other attributes generated in the module are the element mesh and the stress free configuration. The module uses the system data from the INPMOD module to generate the the STAMOD data (SINTEF 2024f).

### DYNMOD module

The DYNMOD module is used in time domain dynamic analysis. These analyses are based on the final static configuration found from the STAMOD module. The environment data applied in the model as well as the data used to define the motions that are applied as forced displacements in the analysis. The DYNMOD module can be used to perform several dynamic analyses. This can be achieved without having to rerun the INPMOD and STAMOD module. The response time series are created during the analysis. These time series are stored in the OUTMOD module to be used for postprocessing. By running the module, natural frequencies and modeshapes can be calculated. This is in addition to the dynamic response (SINTEF 2024f).

### OUTMOD module

The OUTMOD module is used to perform postprocessing. The postprossesing is carried out from results generated from running static and dynamic analysis in the STAMOD and DYNMOD modules. In order to further investigate the data time series, they can be exported from the module. This is done by exporting the time series as a standardized file format. These types of files are then used in other programs to extract further post processed data (SINTEF 2024f).

---

## 5.2 Riser system modeling in RIFLEX

In order to create a system in SIMA RIFLEX, the program must know what the system is. This can be done by starting the system definition with defining the system topology. This is done by introducing lines, super nodes and support vessels. The next step in defining the system is adding details to lines and other components. There are two ways to define a system in SIMA RIFLEX, defining the arbitrary system or a standard system. A system that is specified with a general topology is known as an arbitrary riser (AR) system in the RIFLEX program. The system can also be specified by using common configurations. This is done by creating systems with well defined standard systems (SINTEF 2024b). The two ways to carry out system definition is presented in a step by step figure, where figure (24) is presented below.

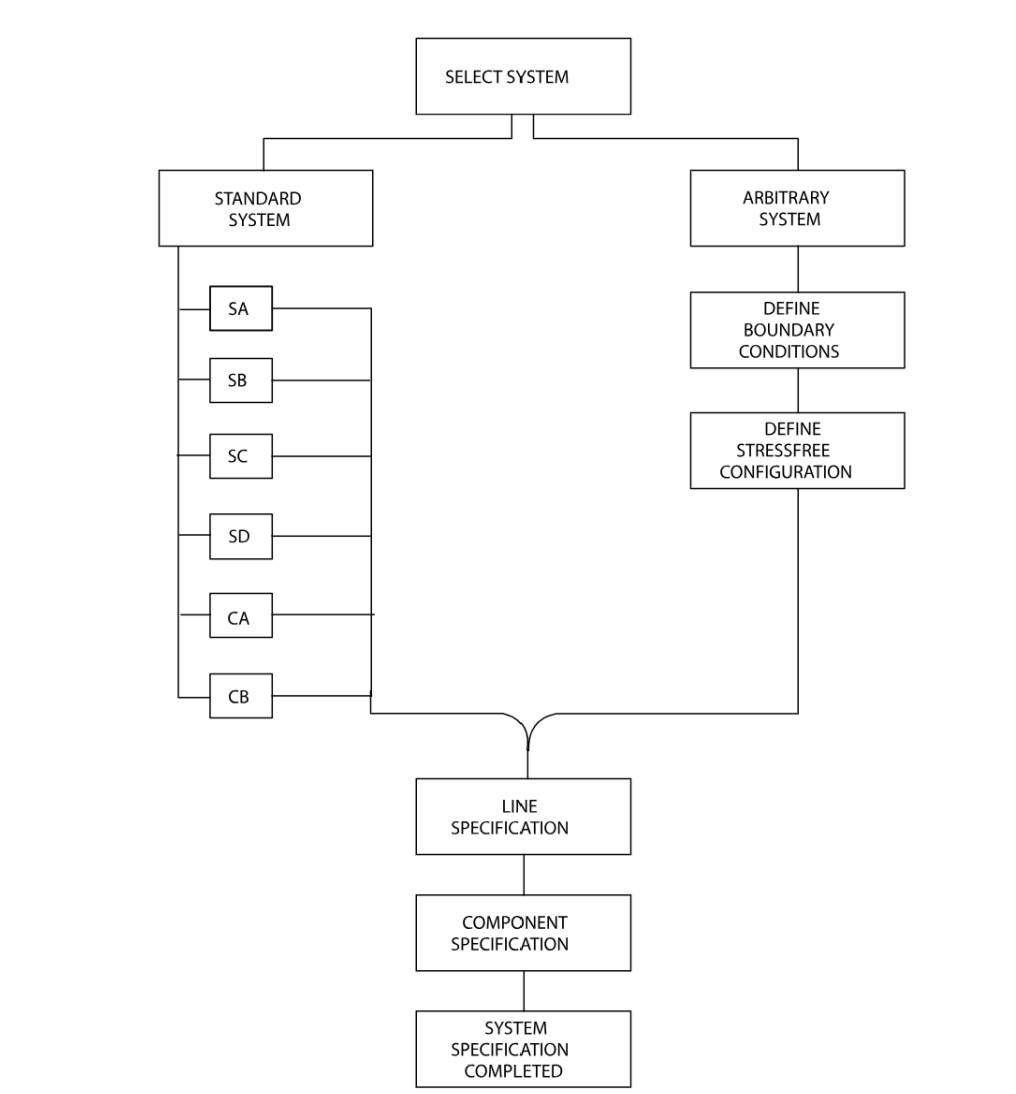


Figure 24: System definition in INPMOD (SINTEF 2024b).

## 5.3 Main components in riser system modeling in RIFLEX

A Supernode can be classified as either free, fixed or prescribed. The classification of the supernode depends on the boundary condition modelling. The definition of a free supernode is a supernode that is free in all degrees of freedom. Supernodes that are classified as fixed can be used to model supports at fixed structures an example of this is the seafloor connections between the system and the seabed. A supernode is classified as fixed if one or several degrees of freedom are set to fixed.

In an arbitrary system, it is possible to specify the status of the supernode as free or fixed for all degrees of freedom. This can be done for each of the supernodes. In standard systems, it is assumed that all degrees of freedom of fixed supernodes are fixed. Prescribed supernodes are often used in cases where the system is subjected to forced dynamic forces. The prescribed supernode is therefore often used to model the connection between the system and a floating support vessel (SINTEF 2024b).

A line is classified in the SIMA RIFLEX program as a linear structural element that stretches between two supernodes. The line is identified by prescribing the line a line type number. When a line is defined it can be used several times in the system. This means that the system is built up by using one or several line types. This is a useful tool in the case of a system that has several lines of the same type. This can for example be the case when modeling an anchoring system. In order to carry out an analysis on a line, it must be divided into smaller sections. This is done by creating line segments and elements. The segments can be described as a line section that has the same cross section properties and the same element length. The element is used as the finite element unit. This is represented in the figure (25) below.

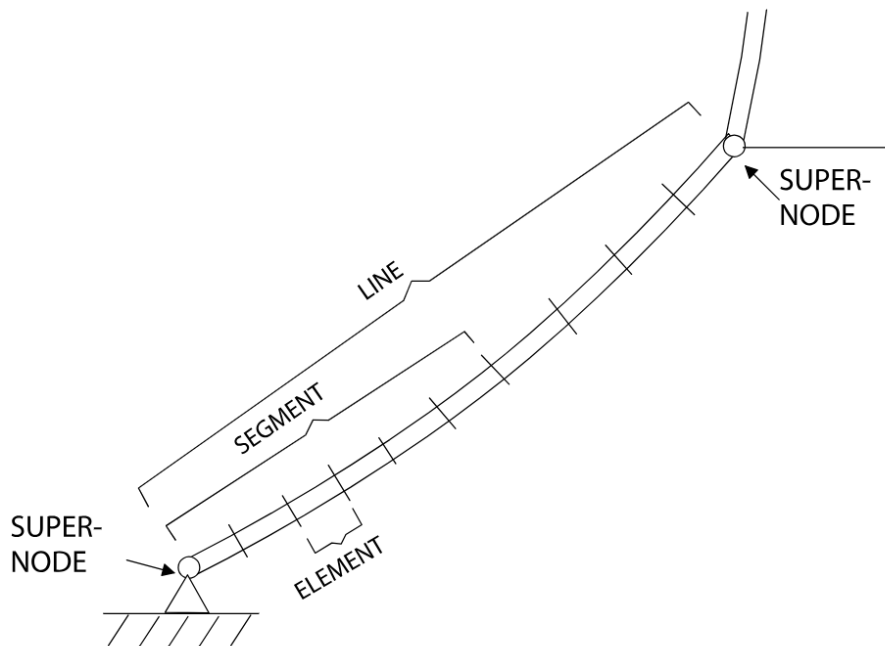


Figure 25: Description of a line in RIFLEX (SINTEF 2024b)

The components used in modeling represent the elementary description that describes the mechanical properties of the system. A component can be identified by its component type number. The components that can be applied in this RIFLEX version can be divided into three groups; cross sectional, nodal and special components (SINTEF 2024b).

The cross sectional components are given as stiffness properties that are divided in terms of axial, bending and torsional stiffness. The components are given with a specific component type. Some of the common types of components are; a pipe cross section (CRS0), an axisymmetric cross section (CRS1), a bisymmetric (CRS2). Cross sections that are used in advanced modeling of floating or partly submerged structures are known as bi-symmetric (CRS5) and a general non-symmetric cross section (CRS7). The CRS5 cross section is only used when modeling an arbitrary system (SINTEF 2024b).

The Nodal components are described as either a body (BODY) or a ball joint connector (CONB). The body is used in modelling of components such as submerged buoys and clumped weights. The ball joint connectors are used in modelling of hinges and swivels. (SINTEF 2024b).

The Special components that is used in modelling can be divided in two groups. One of the

---

groups is described as rollers that is used in description of elastic contact forces between lines. The components also describes tensioner components that is used in modelling of tensioner mechanisms. In order to use both the nodal and special components, the mass, volume and hydrodynamic coefficients must be defined (SINTEF 2024b).

---

## 6 Design codes

In order to design a riser system, the system must be sufficiently safe. In order to determine what is sufficiently safe, there must be regulations for what is safe. The design codes for riser systems are created by authorities and classification societies. Depending on where the riser system is to be deployed, has an effect on what design code that is applied. Some of the most prominent design codes used in design of riser systems are developed by Det norske veritas (DNV) and API.

The main focus when developing a design code is to make the failure probability inside a respectable value. If a riser system is designed according to the design codes should it be able to withstand the environmental, functional and any accidental load effect that the riser system could be subjected to during it's operational lifetime. This is often achieved by adding safety factors when calculating the utilization of the system. The design codes can present design principles that are assumed to be beneficial to follow. An example of this is the DNV standard DNV-ST-F201. The design principles presented in this standard is presented below (DNV 2021).

Design principle of riser system presented by DNV-ST-F201 (DNV 2021):

- The riser system shall satisfy functional and operational requirements that are given in the design basis.
- The riser system is designed such that an unintended event does not turn into an accident that is significantly greater than the original event.
- Permit simple and reliable installation, as well as retrieval, and being robust looking at the respect to use.
- Provide a design that gives sufficient access to carry out; inspection, maintenance, replacement and repair.
- Design of structural details and use of materials shall have the objective to minimise effect of corrosion, erosion and wear.
- Riser mechanical components are as far as practicable designed with a 'fail safe'. Consideration shall be taken in the design in order to achieve possible early detection of failure or redundancy for essential components, that are not designed according to this principle.
- The design should facilitate monitoring of behaviour such as tension, stresses, fatigue cracks, wear, corrosion etc.

### 6.1 DNV-ST-F201

DNV-ST-F201 is the design code created by DNV for riser systems. The objective of the standard is to create a uniform and consistent framework that can be used in the concept development, design, construction, operation and abandonment of riser systems. This is to ensure that the riser system is developed in accordance with international recognized standards, methodology and specifications. The standard provides the requirements for reliability and safety that is in order to limit the hazards related to a riser system. The DNV-ST-F201 standard will also act as a reference document between the buyer and the purchaser (DNV 2021).

The DNV ST-F201 present a design approach for an arbitrary riser system. The design approach is presented in a flow diagram that can be seen in figure (26) below.

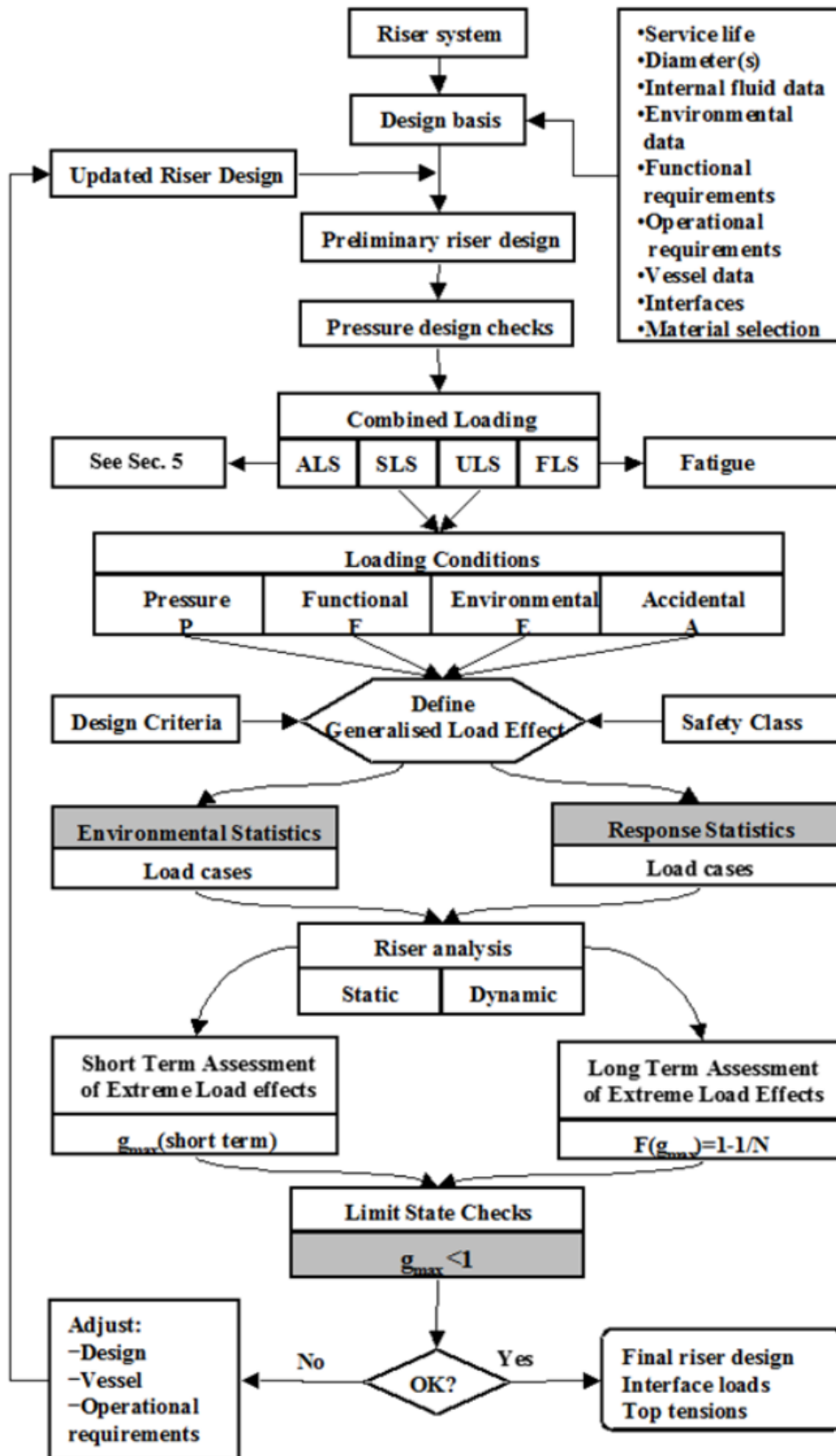


Figure 26: The design approach of a riser system described by DNV ST-F201 (DNV 2021)



---

### 6.1.1 Load and resistance factor design (LRFD)

The principle that is used in the LRFD method is to make sure that the factorised design load effects are not able to exceed the factored design resistance for any of the limit states. The LRFD method divide the load effects acting on the riser system. The load effects are divided into pressure load, functional loads, environmental loads and accidental loads. The reason the load effects are divided is to cope with the uncertainty in the load effects. The safety factor of the environmental load effects is often larger then the pressure and functional load effect. This is due to the uncertainty in the environmental loads typically being higher than the other load effects (DNV 2021).

The main point of the LRFD method is to verify that the design loads don't exceed the design resistance. The general LRFD safety format can be expressed by the following expression (DNV 2021).

$$g(S_P; \gamma_F * S_F; \gamma_E * S_E; \gamma_A * S_A; R_K; \gamma_{SC}; \gamma_m; \gamma_c; t) \leq 1 \quad (38)$$

Where:

- $g$ : Generalised load effect
- $S_P$ : Pressure loads
- $S_F$ : Functional load effects
- $S_E$ : Environmental load effects
- $S_A$ : Accidental load effects
- $\gamma_F$ : Functional load effect factor
- $\gamma_E$ : Environmental load effect factor
- $\gamma_A$ : Accidental loads effect factor
- $R_F$ : The generalised resistance
- $\gamma_{SC}$ : Consequence of failure of the safety class methodology resistance factor
- $\gamma_m$ : Material and resistance uncertainties resistance factor
- $\gamma_c$ : Special condition resistance factor
- $t$ : Time

#### Load effects

In order to obtain the design load effects, the load effects are multiplied with the load effect factors. In DNV-ST-F201 are some of the common load effects summarised in figure (27). The load effect factors are presented with respect to the different limit states of the riser system. The load effect factors are presented in figure (28) (DNV 2021).

<i>F</i> -loads	<i>E</i> -loads	<i>P</i> -loads <sup>7)</sup>
Weight and buoyancy <sup>6)</sup> of riser, tubing, coatings <sup>6)</sup> , marine growth <sup>2)</sup> , anodes, buoyancy modules, contents and attachments. Weight of internal fluid. Applied tension for top-tension risers. Installation induced residual loads or pre-stressing. Pre-load of connectors. Applied displacements and guidance loads, including active positioning of support floater. Thermal loads. Soil pressure on buried risers. Differential settlements. Loads from drilling operations. Construction loads and loads caused by tools.	Waves. Internal waves and other effects due to differences in water density. Current. Earthquake <sup>4)</sup> . Ice <sup>3)</sup> . Platform motions induced by wind, waves and current, i.e.: – mean offset including steady wave drift, wind and current forces – wave frequency motions – low frequency motions – Vortex induced motions (VIM).	External hydrostatic pressure. Internal fluid pressure: hydrostatic, static and dynamic <sup>5)</sup> contributions, as relevant. Water levels.

Figure 27: Typical load types (DNV 2021)

<i>Limit state</i>	<i>F</i> -load effect	<i>E</i> -load effect	<i>A</i> -load effect
	$\gamma_F$ <sup>1)</sup>	$\gamma_E$ <sup>2)</sup>	$\gamma_A$
ULS	1.1	1.3	NA
FLS	1.0	1.0	NA
SLS and ALS	1.0	1.0	1.0
NOTES:			
1) If the functional load effect reduces the combined load effects, $\gamma_F$ shall be taken as 1/1.1.			
2) If the environmental load effect reduces the combined load effects, $\gamma_E$ shall be taken as 1/1.3.			

Figure 28: Load effect factors (DNV 2021)

### Resistance factor

The DNV-ST-F201 standard states resistance factors for safety classes, material and accidental loads. The resistance factors are a tool to account for the uncertainties of the riser system. The resistance factors that are used in the LRFD are stated in the figures below (DNV 2021).

<i>Low</i>	<i>Medium</i>	<i>High</i>
1.04	1.14	1.26

Figure 29: Safety class resistance factor (DNV 2021)

<i>ULS and ALS</i>	<i>SLS and FLS</i>
1.15	1.0

Figure 30: Safety class resistance factor (DNV 2021)

<i>Prob. of occurrence</i>	<i>Safety class low</i>	<i>Safety class medium</i>	<i>Safety class high</i>
$>10^{-2}$	Accidental loads may be regarded similar to environmental loads and may be evaluated similar to ULS design check.		
$10^{-2} - 10^{-3}$	To be evaluated on a case by case basis.		
$10^{-3} - 10^{-4}$	$\gamma_c = 1.0$	$\gamma_c = 1.0$	$\gamma_c = 1.0$
$10^{-4} - 10^{-5}$		$\gamma_c = 0.9$	$\gamma_c = 0.9$
$10^{-5} - 10^{-6}$	Accidental loads or events		$\gamma_c = 0.8$
$<10^{-6}$	may be disregarded.		

Figure 31: Accidental load resistance factor (DNV 2021)

### 6.1.2 Limit states

The DNV-ST-F201 standard divide the limit states of a riser system into four categories. These categories are known as:

#### Serviceability Limit State (SLS)

The SLS criteria is used to determine the acceptable limitation of the riser system in normal operation. These limitations requires that the riser must be able to remain in service and operate properly. This limit state corresponds to criteria limiting or governing the normal operation of the riser system. In the case of exceeding the SLS criteria, this shall not lead to failure. The accidental limit states criteria shall be made in association with the exceeding of the SLS criteria (DNV 2021).

#### Ultimate Limit State (ULS)

ULS criteria requires that the riser system must remain intact and avoid rupture. In the case of an ULS load case, it is not required that the riser system must be able to operate. This limit state provides design checks with focus on the load controlled conditions. For the operating condition this limit state corresponds the riser system's ability to the applied loads with a  $10^{-2}$  annual exceedence probability (DNV 2021).

#### Accidental Limit State (ALS)

ALS is an ULS that is caused by an accidental load or an accidental event. These types of loads are defined as loads that the riser system can be subjected to during abnormal environmental conditions, technical failure or incorrect operation. The ALS events are described as discrete events that has an annual probability of less then  $10^{-2}$ . This means that the events that are used in ALS criteria is expected to occur once in a period longer than 100 years. Depending on the annual probability (DNV 2021).

#### Fatigue Limit State (FLS)

FLS is an ultimate limit state that is based on accumulated excessive fatigue crack growth and accumulated damage as a result of cyclic loading of the riser system. The FLS criteria is used ensure that the riser system is safe against fatigue over the lifetime of the system. The methods used in fatigue assessment can be divided into two. These are methods using the S-N curve and methods that are based on calculations of fatigue crack propagation. The S-N curve methods are often used in the design phase to carry out the fatigue life assessment. The fatigue crack propagation methods can be used to establish the inspection criteria that is used in both the fabrication of the system and the in-service inspections. The fatigue crack propagation is also used to estimate the fatigue crack growth of the riser system (DNV 2021).

The design code DNV-ST-F201 supersedes the design code DNV-OS-F201. In the previous design code, a list was created comprised of typical reasons why limit states are met. The list also describe how the failure of the system will happen. This is presented in figure (32) below.

<b>Table 5-1 Typical limit states for the riser system</b>		
<i>Limit State Category</i>	<i>Limit State</i>	<i>Failure definition/ Comments</i>
SLS	Clearance	No contact between e.g. riser-riser, riser-mooring line, riser-hull, surface tree-floater deck, subsea tree-seabed, surface jumper- floater deck.
	Excessive angular response	Large angular deflections that are beyond the specified operational limits, e.g. inclination of flex joint or ball joint.
	Excessive top displacement	Large relative top displacements between riser and floater that are beyond the specified operational limits for top tensioned risers, e.g. stroke of telescope joint, slick joint and tensioner, coiled tubing, surface equipment and drill floor. Note that systems can be designed for exceeding displacement limits if the structural integrity is maintained.
	Mechanical function	Mechanical function of a connector during make-up/break-out.
ULS	Bursting	Membrane rupture of the pipe wall due to internal overpressure only.
	Hoop buckling (collapse)	Gross plastic deformation (crushing) and/or buckling (collapse) of the pipe cross section caused by external overpressure only.
	Propagating buckling	Propagating hoop buckling initiated by hoop buckling.
	Gross plastic deformation and local buckling	Gross plastic deformation (rupture/crushing) of the pipe cross-section in combination with any local buckling of pipe wall (wrinkling) due to bending moment, axial force and internal overpressure.
	Gross plastic deformation, local buckling and hoop buckling	Gross plastic deformation and hoop buckling of the pipe cross section and/or local buckling of the pipe wall due to the combined effect of external overpressure, effective tension and bending moment.
	Unstable fracture and gross plastic deformation	Unstable crack growth or rest ligament rupture or cross section rupture of a cracked component.
	Liquid tightness	Leakage in the riser system including pipe and components.
ALS	Global buckling	Overall column buckling (Euler buckling) due to axial compression (negative effective tension).
	Same as ULS and SLS	Failure caused by accidental loads directly, or by normal loads after accidental events (damage conditions).
FLS	Fatigue failure	Excessive Miner fatigue damage or fatigue crack growth mainly due to environmental cyclic loading, directly or indirectly. Limiting size of fatigue cracks may be wall thickness (leakage) or critical crack size (unstable fracture/gross plastic deformation).

Figure 32: Typical limit states for a riser system (DNV 2001)

### 6.1.3 Serviceability Limit State

In the SLS condition, the riser system shall be able to operate. This means that the riser system remains in service and operate in a normal fashion. DNV (2021) states five failure modes that should be considered. These are listed below.

- Excessive angular response: Large angular deflections that are larger than the operational limit of the system.
- Excessive top displacement: Large top displacements between the floater and the riser that are larger than the operational limit.
- Clearance: There is no contact between riser and other systems such as other risers, mooring lines or floaters.
- Mechanical function: A mechanical function of a connector during make-up or break-up operation.
- Excessive riser bend displacement: An excessive riser bend as a result of pipeline walking, subsidence or thermal expansion.

From DNV-ST-F201 there are also presented some design control. These shall be carried out in order to ensure that the riser design is safe.

#### Ovalisation

A Riser system shall not be subjected to excessive ovalisation. The ovalisation of the riser shall be documented. The flattening as a result of bending, combined with the out-of-roundness tolerance from fabrication shall be limited to 3.0% (DNV 2021).

---


$$f_0 = \frac{D_{max} - D_{min}}{D_0} \leq 0.03 \quad (39)$$

The parameters in the ovalisation criteria can be summarized by the following:

- $D_{max}$ : is maximum diameter
- $D_{min}$ : is minimum diameter
- $D_0$ : is intended diameter
- $f_0$ : is out of roundness of pipe

### Riser Stroke

In the design of a top tension riser will there be a tensioner that pulls at the top part of the riser in order to maintain constant tension and limit bending. The travel of the tensioner is called the riser stroke. The riser stroke is important in the design of riser components such as tensioner and draw works. The riser systems shall be designed in order to have sufficient stroke such that damage to the riser, components and other equipment are avoided (DNV 2021).

#### 6.1.4 Ultimate Limit State

The riser system shall be designed with focus on the failure modes of the system. The ULS criteria uses design checks that have focus on load controlled conditions. DNV-ST-F201 states seven failure modes that should be considered. These are listed below (DNV 2021).

- Bursting: As a result of membrane rupture in the pipe wall because of internal overpressure.
- Hoop buckling: Due to gross plastic deformation or buckling in the pipe cross-section as a result of external overpressure.
- Gross plastic deformation and local buckling: As a result of gross plastic deformation in the pipe cross-section combined with any local buckling of pipe wall as a result of bending moment, axial force and internal overpressure.
- Gross plastic deformation, local buckling and hoop buckling: Due to gross plastic deformation and hoop buckling in the pipe cross-section or a local buckling of the pipe wall as a result of the combined effect of external overpressure, effective tension and bending moment.
- Unstable fracture and gross plastic deformation: As a result of either a unstable crack growth, a rest ligament rupture or a cross section rupture of a cracked component.
- Liquid tightness: Due to leakage from the riser system like pipes and other components.
- Global buckling: As a result of overall column buckling from axial compression.

### Pressure containment

In the case of a pipe section subjected to net overpressure, there must be regulation in order to have pressure containment. In order to avoid bursting due to overpressure, the cross section of the riser system must satisfy the following equation (DNV 2021):

$$(p_{li} - p_e) \leq \frac{p_b(t)}{\gamma_m \gamma_{SC}} \quad (40)$$

$p_b$  represent the burst resistance of the riser system. The burst resistance can be represented by the equation below.

---


$$p_b(t) = \frac{2}{\sqrt{3}} \frac{2t}{D-t} \min\left(f_y, \frac{f_u}{1.15}\right) \quad (41)$$

The parameters used in in the equations above can be describe by the following:

- $p_{li}$ : Local incidental pressure
- $p_e$ : External pressure
- $p_b$ : Burst resistance
- $\gamma_m$ : Material resistance factor
- $\gamma_{SC}$ : Safety class resistance factor
- D: Riser diameter
- t: Wall thickness
- $f_y$ : Minimum yield strength
- $f_u$ : Minimum tensile strength

### Local buckling

Riser members subjected to an external overpressure can be subjected to local buckling. In order to create a safe design, it is set to be designed to satisfy the following conditions (DNV 2021):

$$(p_e - p_{min}) \leq \frac{p_c(t)}{\gamma_m \gamma_{SC}} \quad (42)$$

$p_{min}$  represent the minimum internal pressure of the riser system. The minimum internal pressure is defined as the least favorable internal pressure combined with the static head of the internal fluid.

The resistance against hoop buckling is represented by the following equation:

$$(p_c(t) - p_{el}(t))(p_c^2(t) - p_p^2(t)) = p_c(t)p_{el}(t)p_p(t)f_0 \frac{D}{t} \quad (43)$$

Elastic collapse pressure as a result of instability of the riser system is represented by the equation below:

$$p_{el}(t) = \frac{2E \frac{t^3}{D}}{1 - \nu^2} \quad (44)$$

The plastic collapse pressure of the riser system is represented in following equation.

$$p_p(t) = 2 \frac{t}{D} f_y \alpha_{fab} \quad (45)$$

The parameters used to define the local buckling criteria can be summarized in the following list:

- $p_{min}$ : Minimum internal pressure
- $p_e$ : External pressure
- $p_{el}$ : Elastic collapse pressure

- $p_p$ : Plastic collapse pressure
- $p_c$ : The resistance for external pressure
- E: Young's modulus
- $\nu$ : Poisson ratio
- $\alpha_{fab}$ : Fabrication safety factor

### Combined Loading Criteria

The combined loading criteria takes into account the different loads acting on the riser system. The pipe members are subjected to; bending moment, effective tension and net internal overpressure, and the riser system shall be designed to satisfy the following equation (DNV 2021):

$$(\gamma_{SC} * \gamma_m) \left( \left( \frac{|M_d|}{\alpha_c M_k} \right) \sqrt{1 - \left( \frac{p_i - p_e}{p_b(t)} \right)^2} + \frac{T_{ed}^2}{\alpha_c T_k} \right) + \left( \frac{p_i - p_e}{p_d(t)} \right)^2 \leq 1 \quad (46)$$

The pipe members subjected to bending moment, effective tension and net external overpressure are designed to satisfy the following equation (DNV 2021):

$$(\gamma_{SC} * \gamma_m)^2 \left( \left( \frac{|M_d|}{\alpha_c M_k} \right) + \frac{T_{ed}^2}{\alpha_c T_k} \right)^2 + \left( \frac{p_e - p_{min}}{p_c(t)} \right)^2 (\gamma_{SC} * \gamma_m)^2 \leq 1 \quad (47)$$

The plastic bending moment resistance of the riser system is represented by the following equation:

$$M_k = f_y (D - t_2)^2 t_2 \quad (48)$$

The plastic axial force resistance in the riser system is expressed as:

$$T_k = f_y \alpha_c \pi (D - t_2) t_2 \quad (49)$$

The parameters used in the combined loading criteria for internal and external overpressure can be summarized in the following list:

- $M_d$ : Design bending moment
- $T_{ed}$ : Design effective tension
- $p_i$ : Local internal design pressure
- $p_e$ : Local external pressure
- $p_b$ : Burst resistance pressure
- $p_c$ : Collapse pressure
- $p_d$ : Design pressure at reference point
- $p_{min}$ : Minimum local internal pressure
- $M_k$ : Plastic bending moment resistance
- $T_k$ : Plastic axial force resistance
- $\alpha_c$ : Strain hardening and wall thinning parameter
- $t_2$ : The wall thickness used for the combined loading criteria

---

### 6.1.5 Accidental Limit State

ALS is a limit state intended to take care of accidental loads or events. Accidental loads are described as loads that the riser system is subjected due to; incorrect operation, abnormal conditions or technical failure. Accidental loads typically result from unplanned occurrences. These events are assumed to have an annual probability of less than  $10^{-2}$ . The following design checks are often applied (DNV 2021):

- The resistance against a direct accidental load
- The ultimate resistance and consequence assessment as a result of exceedence of a SLS criteria
- The post ALS event resistance against the environmental loads

Some of the most common accidental loads can be represented by the following list (DNV 2021):

- Fires or explosions
- Impact or collisions from impact of dropped objects
- Environmental events outside the ULS area
- Hook or snag loads
- Failure in support systems
- Exceedence of the incidental internal overpressure

### 6.1.6 Fatigue Limit State

The riser system shall have sufficient safety against fatigue. This safety is supposed to cover the service life of the system. The fatigue assessment methods can be categorised into methods based on S-N curves and methods based on fatigue crack propagation calculations. The cyclic loading acting on the riser system during the service life of the riser shall be taken into account in the fatigue calculation (DNV 2021).

#### Fatigue assessment using S-N curves

Using the S-N curve methods to do the fatigue assessment is often done during the design for the fatigue life assessment. Some of the aspects to consider when using the S-N curve methods are (DNV 2021):

- The assessment of short-term distribution of nominal stress range
- The selection of a S-N curve that fits the system
- The thickness correction factor
- Choosing the stress concentration factor (SCF)
- Determine the accumulated fatigue damage  $D_{fat}$

The fatigue criterion used in the S-N curve methods can be represented by the equation below (DNV 2021):

$$D_{fat} * DFF \leq 1.0 \quad (50)$$

The parameters in the equation can be described by the following:



- $D_{fat}$ : Accumulated fatigue damage
- DFF: Design fatigue factor

The DFF is divided into safety classes. The safety classes are low, medium and high. The factors used are 3.0, 6.0 and 10.0.

### Fatigue assessment by crack propagation calculations

The crack growth analysis can be used to calculate the fatigue life of a riser system in a case when a S-N curve suited to the system is lacking. The fatigue crack growth life is designed and inspected in order to satisfy the following equation (DNV 2021):

$$\frac{N_{tot}}{N_{cg}} * DFF \leq 1.0 \quad (51)$$

The parameters in the crack growth propagation calculation are described by as the following:

- $N_{tot}$ : Total number of applied stress cycles during service or to in service inspection
- $N_{cg}$ : Number of stress cycles necessary to increase the defect from the initial to the critical defect size
- DFF: Design fatigue factor

## 6.2 Limit states in API STD 2RD

The design code API STD 2RD uses the working stress design (WSD) method to determine if the riser system is inside the design code's different limit states. The WSD method uses a central safety factor that is applied for each of the limit states. The main difference between the LRFD and the WSD method is that the WSD method only uses a single safety factor for each of the different limit states. Compared to several safety factors in the LRFD method, that can be seen in the combined loading criteria in DNV-ST-F201. The design criteria presented in the API STD 2RD design code can be divided into four categories (API 2020):

- Internal pressure
- External pressure
- Combined loads
- Fatigue

### 6.2.1 Internal Pressure

The internal pressure criteria in API STD 2RD states that the casing pressure in the pipe that is equal to the pressure caused by a the following cases; tubing leak, extreme pressure in a drilling riser, hydrostatic test pressure, incidental pressure or design pressure shall not exceed the following criteria. It can be seen in the following equation that the burst pressure of the pipe is determined by the material and the cross section of the pipe (API 2020):

$$p_i - p_e \leq F_D p_b \quad (52)$$

$$p_b = k(S + U) \ln\left(\frac{D}{D - 2t}\right) \quad (53)$$

The parameters used in the internal pressure criteria are explained in the list below:

- 
- $p_e$  represent the external pressure acting on the pipe
  - $p_i$  is the internal pressure in the pipe
  - $F_D$  is the design factor dependent on load case
  - $p_b$  represent the minimum burst calculated for the pipe cross section
  - $k$  is a parameter that accounts for uncertainties in mechanical properties as well as in the wall thickness
  - $S$  represent the minimum yield strength from pipe material
  - $U$  is the minimum ultimate strength from pipe material
  - $D$  is defined as the outside diameter of the pipe
  - $t$  represent the wall thickness

The design factors used in the internal pressure criteria is determined by what load case the riser configuration is subjected to. The different design factors for the load cases can be seen in table (4) below:

Case	FD
Drilling riser with extreme pressure	0.81
Hydrostatic test	0.9
Incidental pressure	0.67
Design pressure	0.6

Table 2: Design factor FD for different load cases (API 2020)

### 6.2.2 External Pressure

The external pressure criteria is a criteria that is used in cases where the external pressure of the pipe exceed the internal pressure. This criteria can for example be used in the case of pipe or riser installations with the pipe being in an empty condition. The reason for the external pressure criteria is to avoid a collapse of the pipe (API 2020).

$$p_e - p_i \leq F_D p_c \quad (54)$$

$$p_c = \frac{P_y p_{el}}{\sqrt{P_y^2 + p_{el}^2}} \quad (55)$$

$$P_y = 2S\left(\frac{t}{D}\right) \quad (56)$$

$$p_{el} = \frac{2E(t/D)^3}{1 - \nu^2} \quad (57)$$

The factors of the external pressure criteria are explained in the following list:

- $p_e$ : External pressure acting on the pipe
- $p_i$ : Internal pressure in the pipe
- $p_c$ : Minimum collapse pressure of the pipe

- $F_D$ : Design factor for different load cases
- $p_{el}$ : Elastic collapse pressure of the pipe
- $P_y$ : Yield collapse pressure of the pipe
- E: Young's modulus of pipe material
- $\nu$ : Poisson's ratio of pipe material

The design factors for the external pressure criteria is determined from the limit states and the type of pipe. The values of the design factor is stated in the table below:

Case	FD
SLS, ULS cold expanded pipe (e.g. DSAW)	0.6
SLS, ULS seamless or ERW pipe	0.7
ALS	1

Table 3: Design factor FD for different limit states (API 2020)

### 6.2.3 Combined loads

The combined loads criteria is a criteria that takes in several types of loads. Such as the axial, pressure and bending loads that are categorised by the different limit states such as SLS, ULS and ALS. This is due to the pipe being subjected to environmental, accidental and temporary loads as a part of the installation and operation. In the API STD 2RD, the combined load criteria is divided for cases with internal and external over pressure. The equations of the load criteria is stated below (API 2020):

#### External overpressure

$$\frac{T}{T_y} + \frac{M}{M_y} \leq \sqrt{F_D^2 - \left(\frac{p_e - p_i}{p_b}\right)^2} \quad (58)$$

#### Internal overpressure

$$\frac{T}{T_y} + \frac{M}{M_y} \leq \sqrt{F_D^2 - \left(\frac{p_i - p_e}{p_c}\right)^2} \quad (59)$$

The factors from the combined loads criteria are presented below:

- T represent the effective tension the system is subjected to
- $T_y$  is the yield effective tension calculated from material and cross section
- M represent the bending moment the system is subjected to
- $M_y$  is the yield bending moment calculated from material and pipe cross section
- $p_e$  is the same as for the pressure criteria
- $p_i$ : is the same as for the pressure criteria
- $p_b$ : is the same as for the pressure criteria
- $p_c$ : is the same as for the pressure criteria
- $F_D$  is a design factor

---

The design factors for the combined loads criteria are determined by the limit states that the system is subjected to. In table (4), the load factors of the combined loads criteria are presented.

Case	FD
SLS, ULS internal and external overpressure	0.8
ALS external overpressure for	0.9
ALS otherwise	1

Table 4: Design factor FD for different limit states (API 2020)

#### 6.2.4 Fatigue

In the API STD 2RD design code, the fatigue design criteria is determined by using the S-N curve approach or the fracture mechanics approach. Using the S-N curve approach, fatigue damage of the system is calculated from the accumulated damage of the system. The damage acting on the system using the S-N curve approach is described using the following equation (API 2020):

$$Damage = \sum_{i=1}^k \frac{n_i}{N_i} \quad (60)$$

The parameters of the damage calculation are described below.

- $N_i$  is the number of cycles to failure at constant stress range
- $n_i$  is the constant stress range in each fatigue stress block

In order to increase the safety of the system in certain limit states, limits are set to how much damage the system is allowed to be subjected to. The damage factors from the fatigue criteria is stated in table (5) below:

Case	Damage must be less than
During service life	0.1
During single ULS event	0.1
During single ALS event	1

Table 5: Damage that is allowed for different limit states (API 2020)

When comparing the safety factor for fatigue damage from the API STD 2RD with the safety class of the DNV-ST-F201, can it be seen that the high safety class from DNV and the maximum damage for the system in the ULS and SLS from API gives the same maximum damage for the system. This leads to a required fatigue life of 10 times the design lifetime.

---

## 7 Design basis

In this chapter, the design input used in the different analysis will be discussed. The design chosen for analysis is a SLWR operating at a deep water condition of 1500 meters, and has a semi-submersible platform as it's floater. The riser is set to operate in the North sea, and will therefor be subjected to harsh North sea weather conditions, as a part of the ULS and ALS check for the system. There will also be carried out a fatigue analysis of the riser design. The riser is design in order to satisfy both the ULS, ALS and the fatigue criteria set by the design codes. The analysis is carried out using the data program SIMA RIFLEX, as this is a software often used for analysis of riser systems.

The standards and design codes used in the analysis is stated below.

- DNV-ST-F201: Dynamic Risers
- DNV-RP-C203: Fatigue Design of Offshore Steel Structures
- DNV-RP-C205: Environmental Conditions and Environmental Loads
- DNV-RP-F204: Riser fatigue
- NORSOK N-003: Actions and Actions Effects
- API Specification 5L: Specification for a Line Pipe
- API RP 2SK: Design and Analysis of Stationkeeping Systems for Floating Offshore Structures

### 7.1 Environmental data

As a part of the environmental data description, there will be focus on the environmental conditions that contribute to forces on the riser system. Some of the most important environmental loads are a result of waves, currents and water depth. The wave and current data is therefore important when it comes to designing a riser system.

#### 7.1.1 Wave conditions

##### ULS and ALS wave conditions

Since wind driven surface waves is a major contributor to the dynamic loads acting on a riser system, it is important when ULS or ALS analysis are carried out. As a part of the USL analysis, a combination of the 100 year wave and the 10 year current is applied in this study. DNV-ST-F201 states that the combinations of characteristic environmental loads can use the 100 year wave in combination with the 10 year current to represent the 100 year return period condition (DNV 2021).

Since the riser system is designed to operate in the North sea, the JONSWAP spectrum will be applied. This spectrum is used to model the irregular waves that the system is subjected to. The significant wave height and the spectral peak period is used as input parameters in the RIFLEX program. As a part of the ULS analysis, the 100 year wave is applied. The NORSOK standard N003 presents typical 100 year  $H_s$  and  $T_p$  values based on the NORA10 data for parts of the North sea as seen in figure (33) below (NORSOK-Standard 2018):

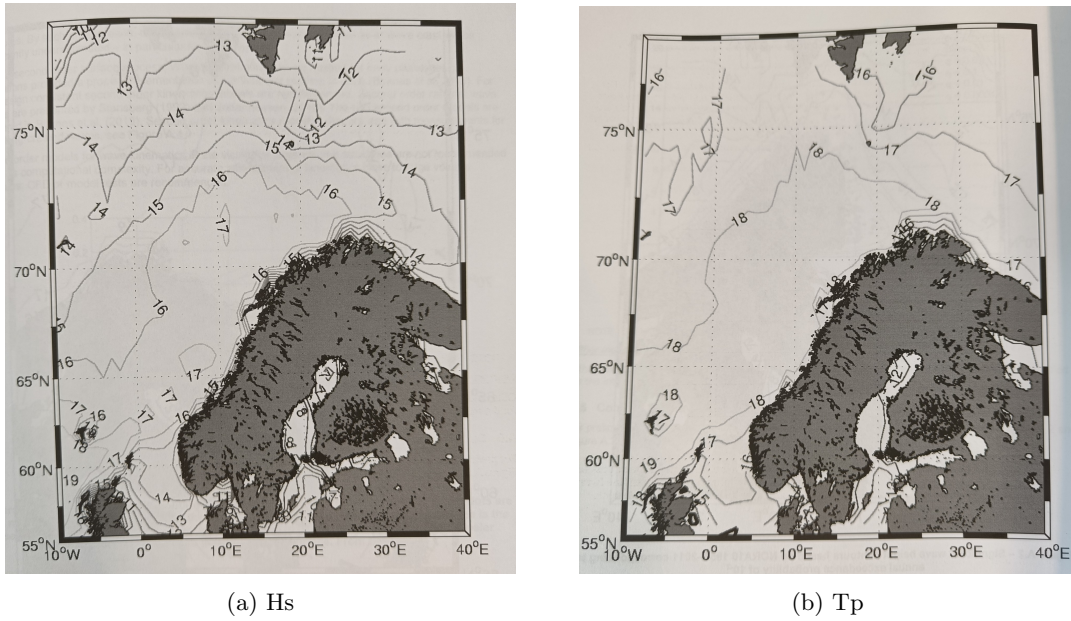


Figure 33: 100 year Hs and Tp sea state of the North sea based on the NORA10 data (NORSOK-Standard 2018)

D.N. Karunakaran and Baarholm (2013) states that a typical 100 year wave sea state is  $H_s = 17$  meters and  $T_p = 18.8$  seconds. Karunakara et al. (2005) presets that the 100 year wave sea state for the North sea could be represented by  $H_s = 15$  meters and  $T_p = 16$  seconds. As a result of this, these ULS sea states will be analysed. It will be investigated which of the different sea states create the largest forces in the riser configuration. The sea states considered to be used in the dynamic analysis are stated below:

- **Sea state 1**
- $H_s = 17.0$  meters
- $T_p = 18.8$  seconds
- **Sea state 2**
- $H_s = 15.0$  meters
- $T_p = 16.0$  seconds

### Fatigue wave condition

The fatigue analysis based on wave and floater motions is based on a combination of characteristic wave heights and periods. These combinations are often obtained from a wave scatter diagram (DNV 2019b). As a part of this study, a wave omni-directional scatter diagram from Haltenbanken will be used. The scatter diagram being used is presented in figure (34) below:

H <sub>s</sub> [m]	Spectral peak period (T <sub>p</sub> ) - [s]																				Sum	
	2-3	3-4	4-5	5-6	6-7	7-8	8-9	9-10	10-11	11-12	12-13	13-14	14-15	15-16	16-17	17-18	18-19	19-20	20-21	21-22		22-23
0.0-0.5		13	43	51	38	80	102	43	30	8	2	2										410
0.5-1.0	2	257	1261	2590	3848	3370	2920	2154	1166	539	348	148	51	44	21	21	5	11	3			18759
1.0-1.5		82	2161	4475	6502	9344	10092	7125	4675	2826	1467	777	338	216	125	79	34	23	2	5		50348
1.5-2.0			503	3649	5534	6631	9187	8685	6492	4549	2985	1538	674	366	257	128	74	16	15	10	3	51297
2.0-2.5			48	974	4325	4913	5954	6600	6170	4525	3330	2064	926	439	256	110	57	30	11	18		40749
2.5-3.0				193	1744	3780	4625	4844	5310	4638	3169	2061	1010	566	308	138	51	39	11	7		32493
3.0-3.5				21	508	2202	3674	3749	4077	4031	2933	1895	1169	551	315	113	57	21	10	5		25331
3.5-4.0			2	79	767	2672	3302	3179	3074	2492	1762	1067	531	311	110	62	18	2	7			19436
4.0-4.5					13	185	1316	2579	2710	2433	1982	1502	911	507	331	141	61	23	7	2		14702
4.5-5.0						34	472	1611	2325	1933	1503	1087	752	425	234	111	34	5	2			10530
5.0-5.5					5	138	831	1792	1798	1205	859	549	290	182	90	30	2	2				7772
5.5-6.0							39	366	1169	1475	1092	661	413	246	151	84	31	5	3			5734
6.0-6.5							13	118	670	1444	1192	638	415	220	144	66	28	2		2		4951
6.5-7.0							2	20	325	841	993	543	313	170	103	66	16	2				3393
7.0-7.5								5	93	433	757	580	213	116	74	49	11	2				2334
7.5-8.0									21	192	416	531	198	74	51	46	13					1543
8.0-8.5									3	56	211	338	170	59	31	26	13					908
8.5-9.0										16	90	187	136	49	34	16	11					541
9.0-9.5										7	56	156	130	38	38	18	8					449
9.5-10.0										2	16	49	69	31	18	8	11					205
10.0-10.5												33	57	26	23	10	3					152
10.5-11.0											3	2	25	16	13	8	2					69
11.0-11.5												2	5	11	3	2						23
11.5-12.0												2	7	10	11	3	2					34
12.0-12.5													2	2	5	2						10
12.5-13.0														2	2	3						7
13.0-13.5															2	5	3					10
13.5-14.0																	2					2
14.0-14.5																	2					2
14.5-15.0																2	2					3
SUM	2	352	4015	11956	22590	31313	41205	42031	40207	34820	26243	17413	9600	5005	3046	1457	620	198	67	54	3	292197

Figure 34: Omni-directional scatter diagram from Haltenbanken (Johnsen 2020)

### 7.1.2 Design current

The design current profile is a description of the current velocity for different water depths. The current velocity vary over the different water depth, where the largest velocity often is situated at the surface. The current profile used in this ULS analysis has a 10 year return period. D.N. Karunakaran and Baarholm (2013) states that a typical 10 year current profile for the Norwegian Sea is described in table (6). This is the design current that will be used in the ULS analysis.

Design current	
Water Depth (m)	Velocity (m/s)
0	1.65
50	1.26
100	1.25
200	1.09
300	0.83
400	0.74
500	0.73
600	0.60
800	0.60
1000	0.55
1200	0.55
1497	0.46
1500	0.00

Table 6: Design current D.N. Karunakaran and Baarholm 2013

### 7.1.3 Floater motions and offset

A semi-submersible platform is used as the floater in this study, due to it having relatively large floater motions. A floater with relatively large floater motions was chosen, due to the SLWR systems better capabilities to absorb floater motions, and therefore being more reliable against

---

fatigue compared to the SCR configuration. The floater is described as a support vessel in the SIMA RIFLEX program. A response amplitude operator (RAO) of the floater is applied in order to describe the floater motion during the simulation. The RAO is obtained from an example file in the SIMA RIFLEX program. The RAO file used in the analysis is presented in Appendix D. The connection between the riser system and the floater is modeled with the use of supernodes.

The forced floater motion are described as the displacements in the riser system as a result of the motion of the floater. The floater offset will also contribute to static and dynamic loads in the riser system. Some of the main load contributions from the floater are stated below (DNV 2021):

#### **Static offset**

Static offset of the floater occur as a result of the mean offset created by wave, current and wind load acting on the floater (DNV 2021).

#### **Wave frequency motions**

Wave frequency motions is a result of first order wave induced motions. These types of motions are described by utilizing a motion transfer function. This motion transfer function is often represented by a RAO for the given floater. The wave frequency motions will typically operate in a period range of 3-25 seconds (DNV 2021).

#### **Low frequency motions**

Low frequency motions acting on the floater can be described as motions created by wind gusts as well as second order wave forces. The low frequency motions act as the response for frequencies close to the surge, sway and yaw eigenperiods. It is common for the low frequency motions to act in a period range from 30-300 seconds (DNV 2021). This type of motion will therefore occur for longer periods compared to the wave frequency motions.

As a part of the ULS analysis, an offset of the floater position will be investigated. In DNV-ST-F201 it is stated that the riser system shall be tested with the floater in two offset positions. These offsets are known as the far and near offset. API RP 2SK states that the ULS condition is assumed that the mooring of the system is intact. In the ALS condition, it is assumed that one of the mooring lines fail as a result of a 10000 year return storm (API 2024). Felisita et al. (2017) present that the offsets used for the extreme response analysis for a SLWR configuration connected to a semi-submersible floater as 8% of the water depth in the ULS condition, and 10% of the water depth in the ALS condition. The ULS offset used in this study was therefore set as 8% of the water depth in the far and near condition. The ALS offset was set to 10% of the water depth in the two conditions.

The wave and current are set such that they act parallel with the riser configuration. This is done in order to create the worst case loading for the near and far offset. several different current and wave direction combinations was implemented to find the worst combination (DNV 2021). The offsets used in the study is summarised in table (7) below:

<b>Condition</b>	<b>Distance from mean position</b>
ULS mean	0 m
ULS near	120 m
ULS far	-120 m
ALS near	150 m
ALS far	-150 m

Table 7: Summary of the offset conditions used in the extreme response analysis

#### **7.1.4 Riser soil interaction**

An important design parameter when designing compliant riser system such as the SLWR is the interaction between the riser and the soil at the seabed. This is especially important for the TDP of the riser, as this point will be subjected to large bending moments. This point can also be



subjected to fatigue. In the SIMA RIFLEX program, the riser soil interaction are modelled as linear springs. The horizontal contact is modelled in the axial and lateral direction. These springs act as the friction between the riser and the seabed, and sliding will occur if the axial or lateral spring forces reaches the friction force value (SINTEF 2024d). Q. Bai and Y. Bai (2014) presents friction coefficients that can be used for pipes in the North Sea as these are presented in figure (35). Karunakara et al. (2005) presents values for riser soil interaction for a SCR in the North sea. These soil parameters will be used for this study. The spring stiffness and friction parameters used in the analysis is presented in table (8) below.

Soil Type	Lateral Coefficient of Friction		Axial Coefficient of Friction	
	Minimum	Maximum	Minimum	Maximum
Noncohesive soils (sand)	0.5	0.9	0.55	1.2
Cohesive soils (clay)	0.3	0.75	0.3	1.0

Figure 35: Friction coefficient for different types of seafloor soil (Q. Bai and Y. Bai 2014)

Riser soil interaction	Values
Horizontal lateral/axial soil stiffness	10 kN/m <sup>2</sup>
Vertical soil stiffness	600 kN/m <sup>2</sup>
Lateral friction coefficient	0.5
Axial friction coefficient	0.5

Table 8: Riser soil interaction (D.N. Karunakaran and Baarholm 2013)

### 7.1.5 Hydrodynamic parameters

Morison equation is used in the SIMA RIFLEX program to calculate the hydrodynamic loads acting on the riser configuration. The equation utilizes relative velocity and acceleration as well as geometry of the structure to calculate loads. The drag coefficient ( $C_D$ ) and mass coefficient ( $C_M$ ) is an important parameter in the Morison equation. These parameters has to be determined empirically due to being dependent on several parameters such as Reynolds number, Keulegan-Carpenter number and the surface roughness ratio (Faltinsen 1990).

The added mass coefficient  $C_A$  is defined in DNV-ST-F201 as  $C_A = C_M - 1$  (DNV 2021). It is also stated that the formulation of the Morison equation for slender structure also can be applied for equivalent circular pipe models. These equivalent circular models can be used for sections that have equally spaced buoyancy elements (DNV 2021). Felisita et al. (2017) presents that the hydrodynamic coefficient of a SLWR system can be described as  $C_D = 1.1$  and  $C_A = 1.0$ . This is the same coefficients that D.N. Karunakaran and Baarholm (2013) uses for the SCR section of a hybrid riser. In this study these coefficients will be used for the entire riser configuration. Summary of hydrodynamic coefficients is stated in table (9) below:

Hydrodynamic coefficient	value
$C_D$	1.1
$C_A$	1.0

Table 9: Hydrodynamic coefficient used for the riser configuration (Felisita et al. 2017) (D.N. Karunakaran and Baarholm 2013)

---

## 7.2 Riser configuration

The riser configuration that is to be analysed in this study is of the type SLWR. The configuration consists of steel pipes creating the riser, and buoyancy modules creating the hog and sag bend in the configuration. The the top end of the riser is modelled as pinned with a flexible joint at the hang-off point. The riser is a production riser, as a result of this is the safety factor of fatigue life set to 10, as recommended in the DNV-ST-F201 (DNV 2021). It is assumed that the design life of a SLWR is set to 25 years. This means that the riser configuration must have a fatigue life of 250 years from the fatigue analysis.

### 7.2.1 Riser material and cross section

The riser configuration cross section is made from steel pipes. The API 5L X65 low carbon steel is chosen as riser material (API 2018). According to Speight (2014) is the diameter of a production riser in the range of 6 to 30 inches. On the other hand states Q. Bai and Y. Bai (2012) that the diameter of a production riser is in the range of 3 to 12 inches. As a result of this was a diameter of 10 inches chosen for this study. The wall thickness of the riser system is set to 25 mm. This is calculated using DNV-ST-F201 criteria for pressure containment. The internal pressure at the seabed connection is set to 65 MPa. From this it was calculated that the minimum required wall thickness for a straight pipe without allowances and tolerances was 19.78 mm in this condition. The specified pipe wall thickness is calculated using the following equation (DNV 2021):

$$t_{nom} = t_1 + t_{fab} + t_{corr} \quad (61)$$

Where  $t_{nom}$  is the design wall thickness of the riser system.  $t_1$  represent the minimum required wall thickness in terms of burst criterion. The  $t_{corr}$  parameter is the corrosion parameter of the riser system. Bahadori (2017) presents that the corrosion allowance for a pipe system can be divided into corrosion classes. Corrosion class B was chosen with an average corrosion rate per year. The corrosion rate was set to 0.1 mm per year. As a result of the design life of 25 years was the  $t_{corr}$  set to 2.5 mm. The fabrication tolerance was set to 10 % leading to a  $t_{fab}$  value of 2.5 mm. This means that  $t_{nom}$  should be larger than 24,78 mm, and therefore was the wall thickness of 25 mm chosen. A summary of the riser material and cross section properties are presented in table (10) below:

Riser parameters	Dimension
Internal riser diameter	254 mm
Wall thickness	25 mm
Material density	7850 $kg/m^3$
Yield strength	450 MPa
Tensile strength	530 MPa
Poisson ratio	0.3
Safety class	High

Table 10: Riser material and cross section properties

### 7.2.2 Buoyancy modules

In order to create the SLWR configuration, buoyancy modules are needed to create the hog and sag bend of the riser in the water column. This is achieved with placing buoyancy modules on the riser to make parts of the riser net buoyant. The density of the buoyancy material is set to 500  $kg/m^3$  this is due to Felisita et al. (2017) and Ruan et al. (2021) using a density of subsequently 500  $kg/m^3$  and 485  $kg/m^3$ . It is also to be assumed that equipment is needed to clamp the modules

to the riser, contributing with some self weight. The total density of the buoyancy modules are therefore set to  $500 \text{ kg}/\text{m}^3$ . For the base case, buoyancy modules that are 1 meter long and 1.3 meters in diameter will be used. The modules are placed with a pitch of 3 meters. The buoyant section of the riser is set to be 550 meters long. A summary of the buoyancy module parameters are stated in table (11) below:

Buoyancy parameters	Dimension
Length	1.0 m
Diameter	1.3 m
Density	$500 \text{ kg}/\text{m}^3$
Mass per unit length	$600.0 \text{ kg}/\text{m}$
Buoyancy per unit length	$1.199 \text{ m}^2$
Buoyancy module pitch	3 m
Distance of buoyancy section	550 m

Table 11: Buoyancy module parameters

In SIMA RILEX, the buoyancy modules are modelled by using external wrapping. The external wrapping gives the opportunity to model the mass, buoyancy and size of the modules. The hydrodynamic coefficients used for the buoyancy modules are the same as the ones used for the rest of the riser configuration.

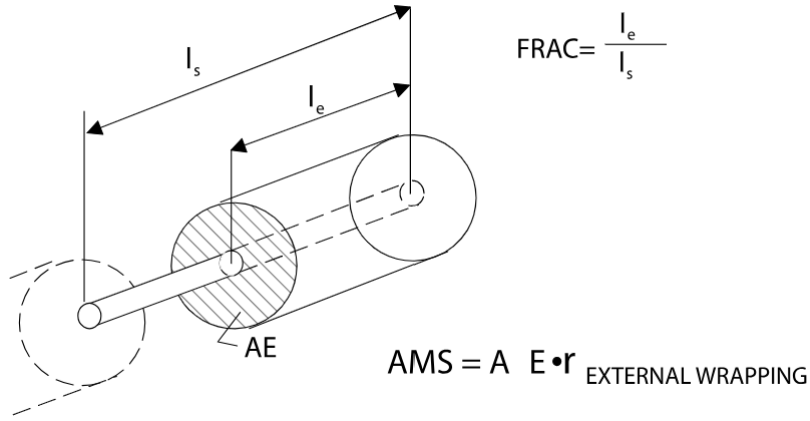


Figure 36: External wrapping in SIMA RIFLEX (SINTEF 2024a)

### 7.2.3 Riser coating

The coating used on risers has several purposes. The coating is set to protect the riser from corrosion as well as act as protection in the case of clashing. Karunakara et al. (2005) states that some of the common coating materials used for risers in the oil and gas industry consist of:

- Multilayer polypropylene
- Polyethylene
- Polyurethane
- Rubber coating

With this in mind will a coating with a density of  $900 \text{ kg}/\text{m}^3$  be applied over the entire riser configuration. A coating thickness of 50 millimeters will be applied for the entire riser configuration.

---

### 7.2.4 Internal fluid

In order to calculate the forces and loads acting on the riser system, the internal fluid is an important parameter. As a part of this study, it is assumed that the density of the internal fluid is  $800 \text{ kg/m}^3$ . This is due to the analysis being carried out on a production riser. It is therefore found that the density of crude oil being between  $0.75$  and  $0.95 \text{ g/ml}$  (API 2022). The internal pressure of the riser configuration is set to  $650 \text{ MPa}$  at the bottom termination point.

### 7.2.5 Riser hang off modeling

In SIMA RIFLEX, the riser hang-off is modelled as a pinned joint with a flex joint. The result of this is that the top end of riser configuration can only transfer axial forces. Karunakara et al. (2005) stated that the flex joint stiffness will not have an influence on the response when the riser configuration is subjected to extreme loading. The flex joint stiffness will however effect the fatigue life of the riser near the flex joint. Fatigue issues created by the flex joint stiffness can be addressed by modelling a 5 to 10 meter long taper section. In SIMA RIFLEX, the flex joint can be modeled as a linear or nonlinear stiffens that is dependent on the angle change of the riser configuration. Felisita et al. (2017) presents a flex joint that is modelled linearly with a stiffness of  $50 \text{ kNm/deg}$ . Hui et al. (2019) presents a nonlinear flex joint that can be seen in figure (37) below.

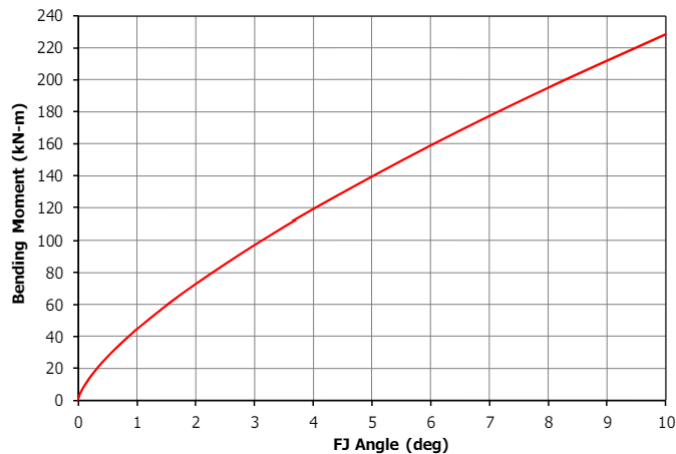


Figure 37: Nonlinear flex joint stiffness plot (Hui et al. 2019)

As a part of this study, a linear flex joint will be applied with a rotational stiffness of  $50 \text{ kNm/deg}$  for the fatigue analysis. As stated by Karunakara et al. (2005), the flex joint will not effect the extreme response loading. Felisita et al. (2017) presents that a flex joint with a lower rotational stiffens can be applied for the limit state analysis. As a result of this, a  $10 \text{ kNm/deg}$  rotational stiffness is applied for the system in extreme response analysis. The flex joint is modeled as a global spring located at the hang-off point. At the riser upper termination, the flex joint will be combined with a taper section. The taper section is set to be 5 meters long with an increased bend stiffness in the range of  $2EI$  to  $1.2EI$  in retaliation to the bending stiffness of the rest of the riser configuration.

---

## 8 Analysis of SLWR in ULS and ALS environmental conditions

As a part of this study, an extreme response analysis of the SLWR will be carried out. The extreme response analysis is used to determine if the riser configuration is inside the acceptance criteria set by the design code DNV-ST-F201. The LRDF combined loading criteria is set as the ULS and ALS acceptance criteria for this study. This means that the utilization of the riser configuration should be less than one. The general formulation of the combined load criteria is presented in the equation below (DNV 2021):

$$g(t) = g(M_d(t), T_{ed}(t), \Delta_p, R_k, \Lambda) \leq 1 \quad (62)$$

The factors in the general formulation of the combined loading criteria is described in the following list:

- $M_d$  represents the design values for bending moment of the system
- $T_{ed}$  is the design value of the effective tension in the system
- $\Delta_p$  can be described as the local pressure differential in the system
- $R_k$  represents the vector of capacities calculated from the cross section of the pipe
- $\Lambda$  represents a vector of safety factors such as the material and safety class factors

The safety factors used in the analysis is stated in the table below.

Load effect and resistance factors	USL	ALS
Functional load effect $\gamma_F$	1.1	1.0
Environmental load effect $\gamma_E$	1.3	1.0
Accidental load effect $\gamma_A$	NA	1.0
Safety class resistance $\gamma_{SC}$	1.26	1.26
Material resistance $\gamma_m$	1.15	1.15
Strain hardening and wall thinning $\alpha_c$	1.2	1.2

Table 12: Safety factors for the combined loading criteria in ULS and ALS conditions (DNV 2021)

### 8.1 Load case selection

#### 8.1.1 Wave and current direction

In the design code DNV-ST-F201, it is stated that the most severe directional combination of wind, waves and current should be applied when carrying out an extreme response analysis. The most severe load case will often occur when the wave, current and floater offset act in the same direction (DNV 2021). As a result of this was a dynamic analysis carried out with the wave and current acting in different combination of  $0^\circ$  and  $180^\circ$ .

The dynamic analysis was carried out with the floater in the mean position. The reason for this analysis is to determine the which of the wave and current combination that shall be used for the extreme response analysis. Figure (38) and (39) present the dynamic bending moment and tension acting on the SLWR configuration for the different load cases.

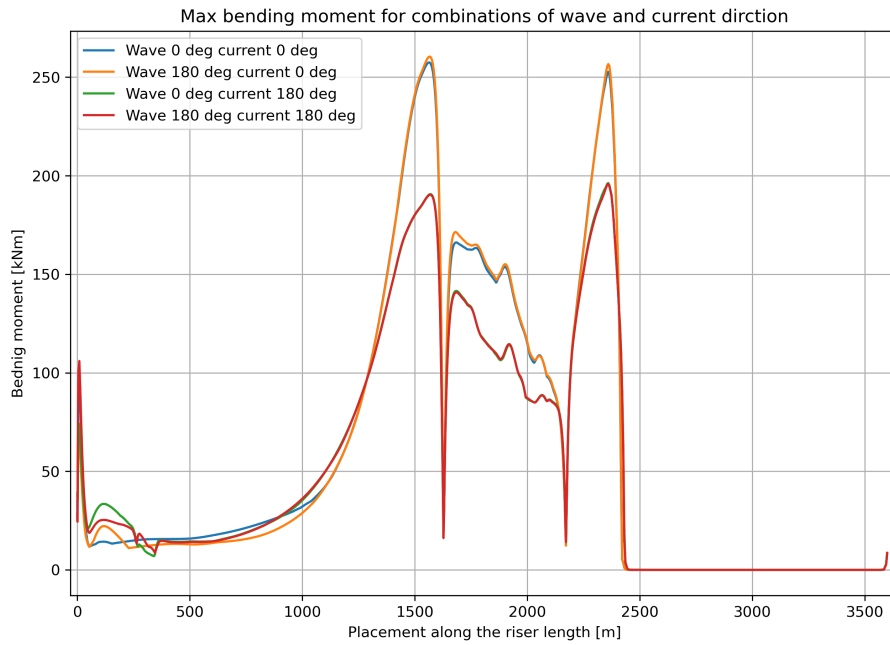


Figure 38: Largest bending moment for different wave and current directions

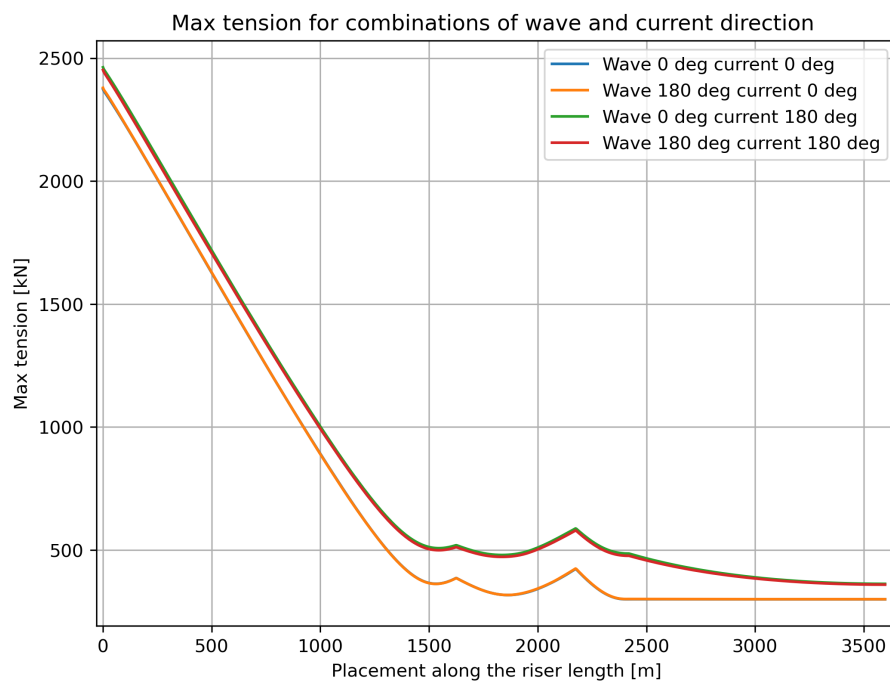


Figure 39: Largest effective tension for different wave and current directions

From the figures, it can be seen that the worst cases of bending moment occur for the load cases with current in the  $0^\circ$  direction. The largest dynamic tension occurs for the load combination of  $180^\circ$  waves and current. From the result of this, the wave and current direction combination of  $0^\circ$  waves and  $0^\circ$  current was chosen. As a result of giving an important bending moment, combined with the statement in DNV-ST-F201 that loads acting in the same direction often create the most severe load case. This direction combination will be used in the extreme response analysis.

---

### 8.1.2 Significant wave height and spectral peak period

As mentioned in chapter 7 can different values of significant wave height and spectral peak period be chosen as the 100 year wave in the North sea. The two sea states mentioned in chapter 7 was therefore used in a dynamic analysis. This was done to see which of the sea states created the worst load case. Figure (40) and (41) present the dynamic bending moment and tension acting on the SLWR for the different sea states.

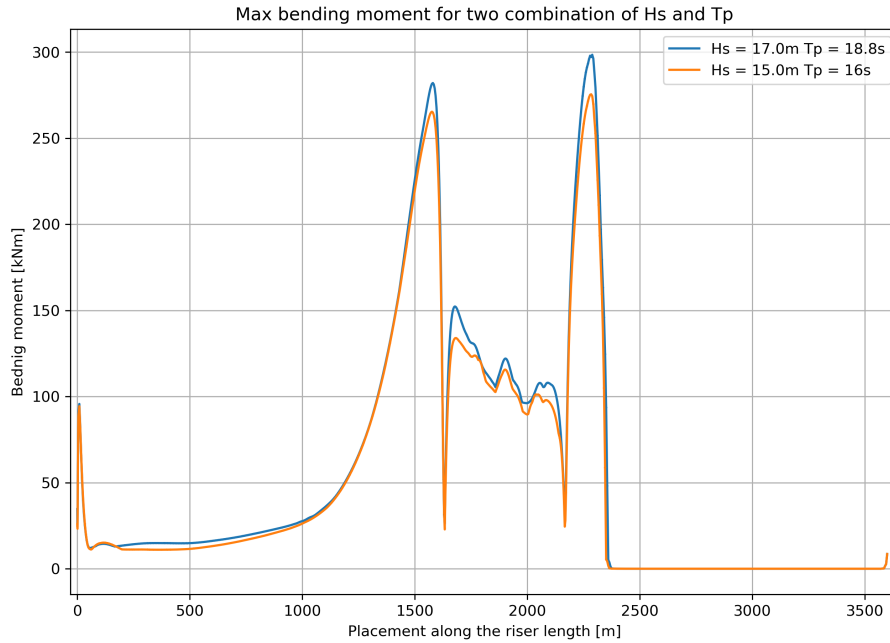


Figure 40: Largest bending moment for different Hs and TP combinations

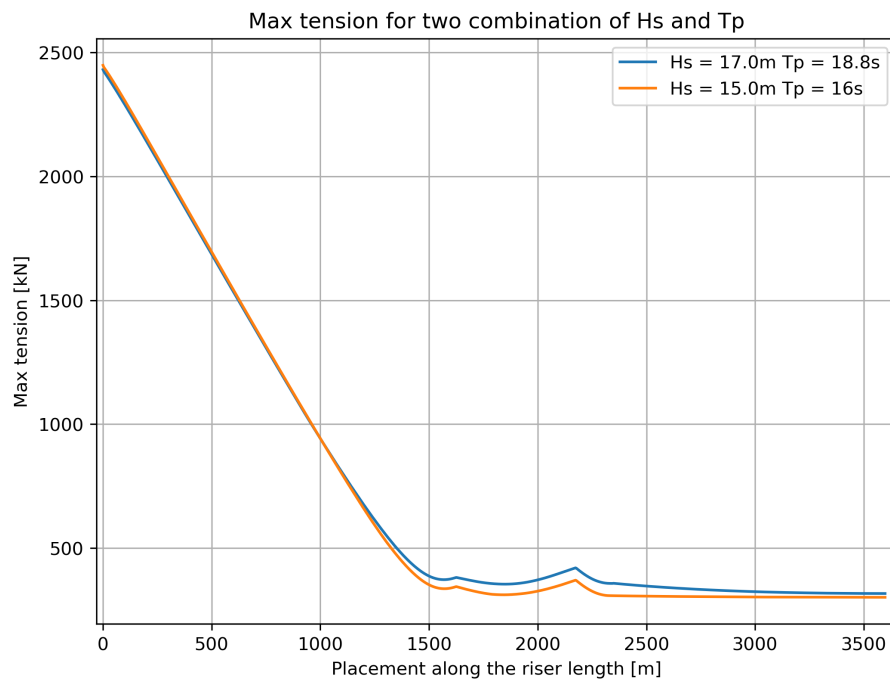


Figure 41: Largest effective tension for different Hs and Tp combinations

Figure (40) shows that the combination 17.0 meter Hs and 18.8 second Tp gives the largest bending

moment in the SLWR configuration. When it comes to the effective tension in the riser it can be seen from figure (41) that these are more similar than for the bending moment. With this in mind, the combination 17.0 meter Hs and 18.8 second Tp will be used in the extreme response analysis.

## 8.2 Static analysis of the SLWR

One of the main reasons to carry out the static analysis of the riser configuration is to find the functional loads acting on the system. This comes from the fact that the design loads in the combined loading criteria is divided into functional and environmental loads. The static analysis was carried out with the ULS and ALS offset of the floater in the far and near case to find the functional loads in these cases. The static SLWR configuration in the mean position as well as the near and far ULS and ALS offsets can be seen in figure (42) below.

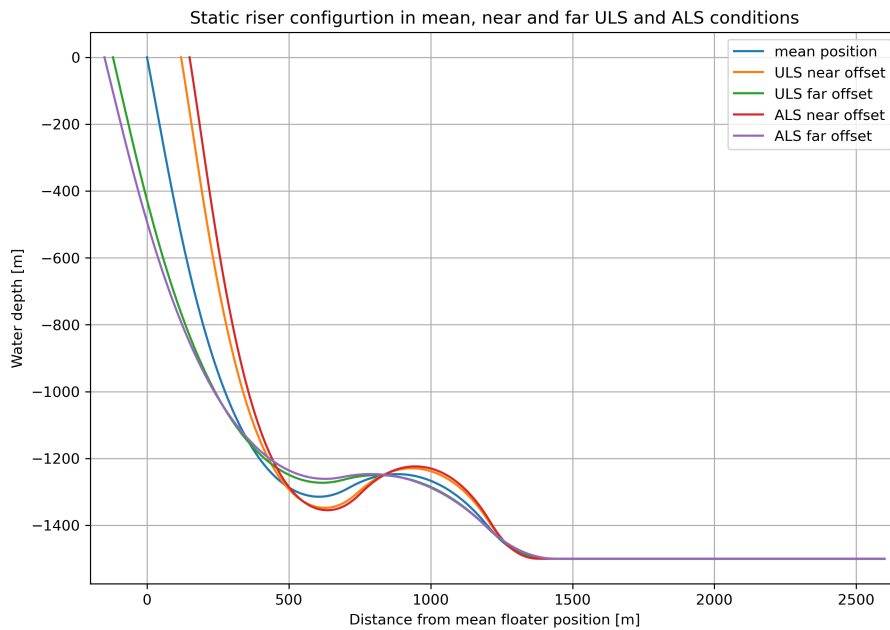


Figure 42: SLWR configuration in the mean, near and far ULS and ALS offset position

The results from the static analysis that are of most interest are the effective tension and the bending moment. In most cases, the effective tension will be at its largest at the connection between the riser and the floater. This is due to the floater carrying the weight of the riser in the water column. The largest bending moments is assumed to be located in one of the bends of the SLWR configuration, either the sag, hog or at the catenary at the TDP. Figure (43) and (44) shows the effective tension and the bending moment in the SLWR configuration for the mean, far and near offset load case.



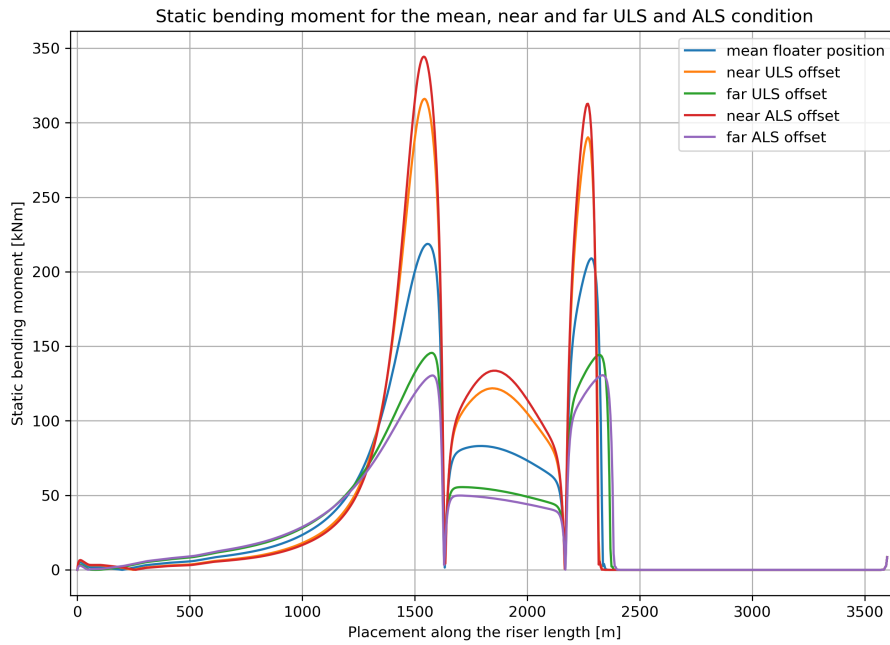


Figure 43: Largest bending moment in the mean, near and far ULS and ALS offsets

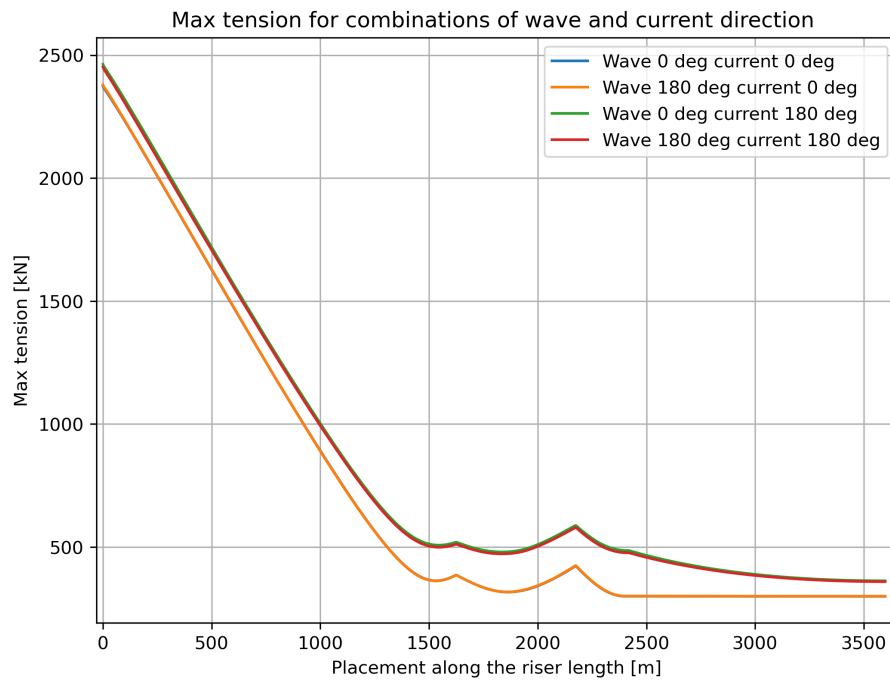


Figure 44: Largest effective tension in the mean, near and far ULS and ALS offsets

The results of the static analysis is summarized in table (13):

Floater position	Maximum effective tension [kN]	Maximum bending moment [kNm]
Mean position	2014	218.7
Near offset ULS	1983	316.0
Far offset ULS	2081	145.6
Near offset ALS	1979	344.3
Far offset ALS	2107	130.4

Table 13: Summary of the results from the static analysis

From these results, it can be seen that the maximum bending moment is located at the sag bend in the near offset position. This is a result of the near offset creating a smaller curvature in the riser configuration, thereby creating larger bending moments. The largest effective tension is located at the hang-off for the far offset. This is logical as the TDP in the static configuration is the closest to the bottom end termination of the riser, thereby being the configuration with the most riser in the water column.

### 8.3 Dynamic analysis of the SLWR

In order to carry out an extreme response analysis, certain tests should be done to ensure that it is the extreme response that is applied for the limit state calculations. DNV-ST-F201 presents that an extreme value is defined as a percentile as a part of the short term extreme response distribution. This distribution can be obtained by running several 3 hour simulation for the same environmental conditions. The most common percentile used in the extreme value distribution for riser is the 90th percentile, but lower percentiles can be applied if there are additional information about similar riser configurations in the same area. The Gumbel distribution is often applied as the model for the extreme value distribution. This can be achieved by running 20 simulations of the 3 hour environmental condition. The Gumbel distribution is then fitted to the extreme value (DNV 2021).

Gemilang and D. Karunakaran (2017) presents that the worst sea state that the SLWR is subjected to can be described by the largest downward velocity located at the hang-off point of the riser. The downward velocity is therefore chosen as the parameter that is used to determine the 90th percentile extreme value.

20 dynamic 3 hour simulations was carried out to determine which of the simulations presents the 90th percentile extreme value. Wave seeds was used to generate random phase angles for each wave frequency component, this gives a different realization of the selected wave spectrum for each of the wave seeds (SINTEF 2024e). The simulations was carried out using 20 different wave seeds. The figures below show the effect of different wave seeds with relation to the vertical displacement of the hang-off point.

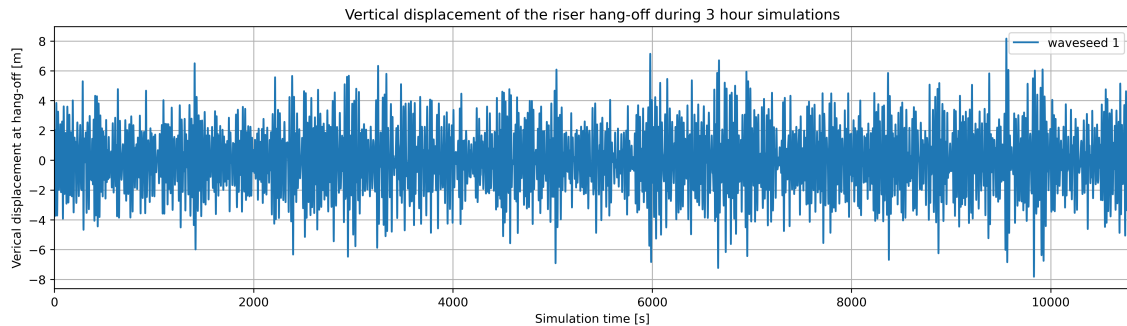


Figure 45: Vertical displacement waveseed 1

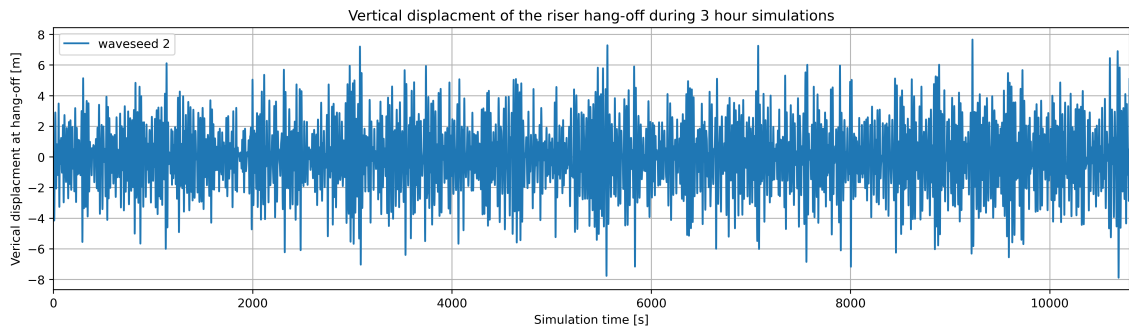


Figure 46: Vertical displacement waveseed 2

The figures (47) and (48) show the effect of the different wave seeds on the dynamic bending moment and the effective tension. This shows the importance of running several simulation of the same environmental conditions.

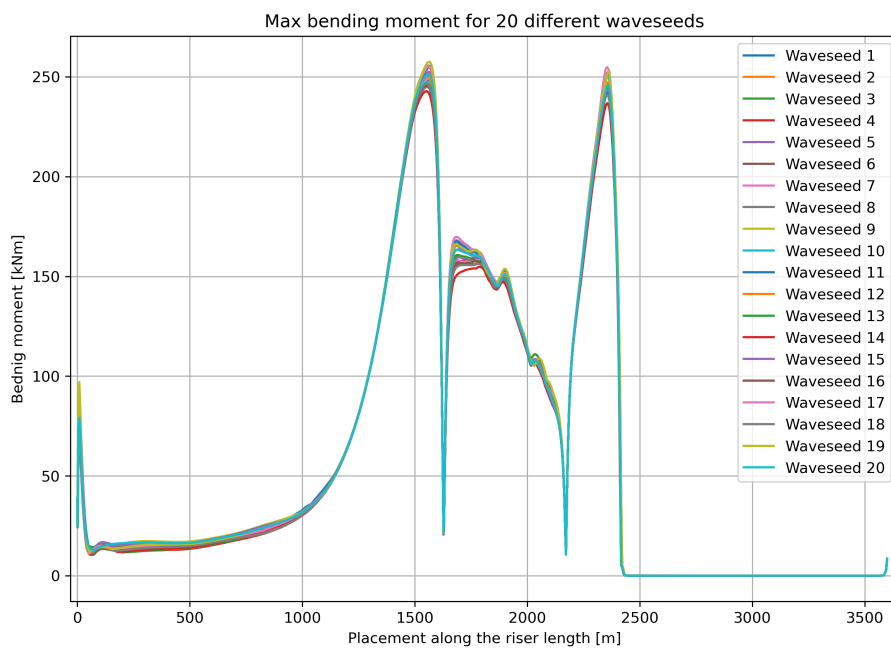


Figure 47: Largest bending moment for 20 different waveseeds

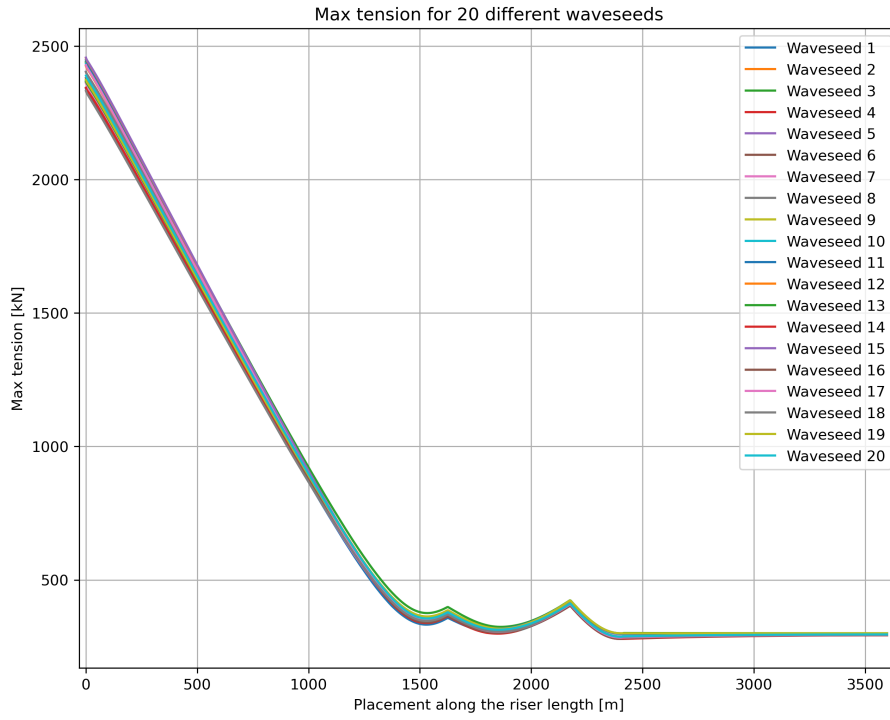


Figure 48: Largest effective tension for 20 different waveseeds

The table below (14) presents the largest downward velocities for the 20 different wave seeds. These velocities are used in the Gumbel distribution to determine the 90th percentile wave seed. This wave seed will be used as the dynamic simulation that is used in the combined loading criteria for the ULS and ALS limit state.

Waveseed number	Downward velocity [m/s]
1	2.699
2	2.773
3	2.6383
4	2.644
5	2.789
6	2.669
7	2.644
8	2.679
9	2.803
10	2.945
11	2.959
12	2.601
13	2.491
14	2.355
15	2.707
16	2.457
17	3.050
18	2.406
19	2.985
20	2.605

Table 14: Maximum downward vertical velocity

Haver (2020) presents that the Gumbel distribution that can be fitted to the 3 hour extreme values. The distribution function is fitted to the largest downward velocity and the 90th percentile is found.

The distribution function is found using the following equation.

$$F(x) = e^{(-e)^{\frac{x-\alpha}{\beta}}} \quad (63)$$

$\alpha$  represents the location parameter and the scale parameter  $\beta$  (Haver 2020). These are calculated from the expected value and the variance of the velocity data of the simulations. In figure (49), the percentile relation to the downward velocity can be seen.

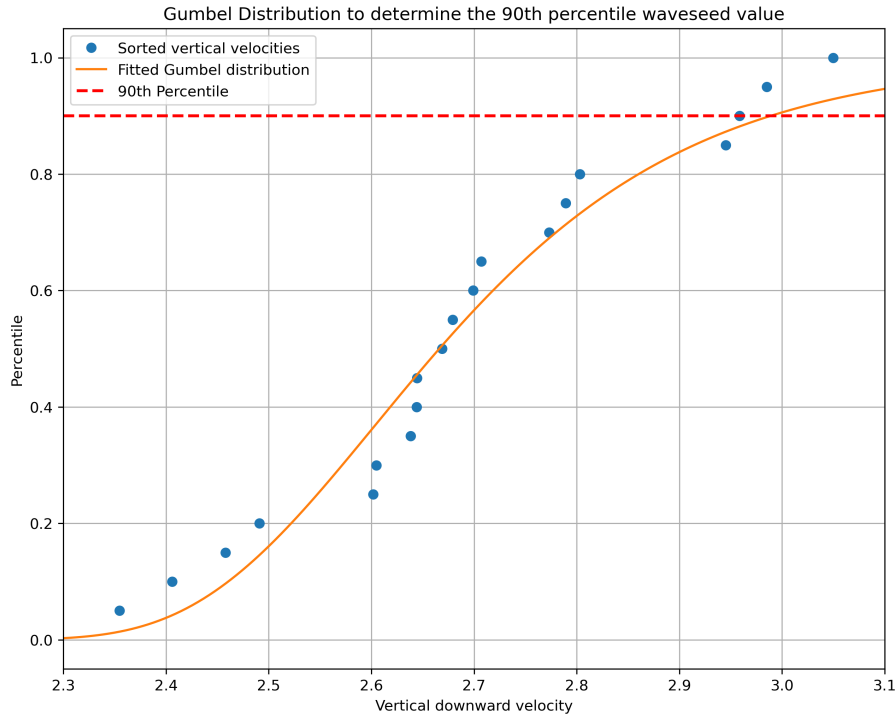


Figure 49: Gumbel distribution presenting the 90th percentile

From this it was found that wave seed number 19 was the closest to the 90th percentile. The dynamic analysis of the SLWR configuration was therefore carried out for this wave seed. The dynamic analysis carried out had a simulation time of 10800 seconds. The ULS and ALS offsets are used as the offsets to determine if the riser configuration is inside the combined loading criteria.

The results from the dynamic analysis that are of the most interest are the dynamic effective tension and bending moment. The difference between the static load and the dynamic load is assumed as the environmental loads. This is used in the calculation of the utilization of the riser. In most cases, the effective tension will be at its largest at the connection between the riser and the floater. This is due to the floater carrying the weight of the riser in the water column. The largest bending moments is assumed to be located in one of the bends of the SLWR configuration, either the sag, hog or at the catenary at the TDP. Figure (50) and (51) shows the dynamic effective tension and bending moment in the SLWR configuration for the mean, far and near offset load cases.

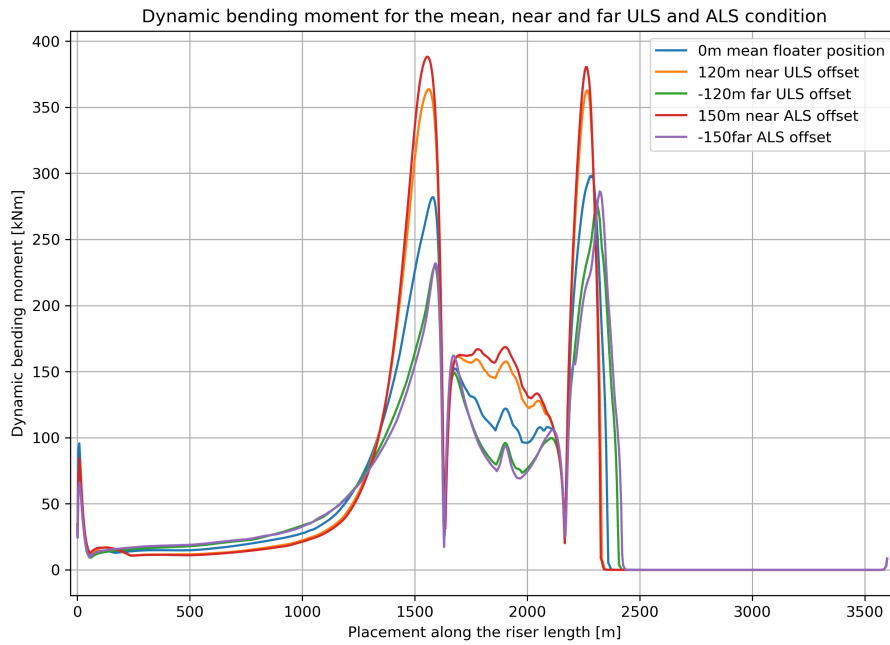


Figure 50: Largest bending moment for waveseed 19 in the mean, near and far ULS and ALS offset position

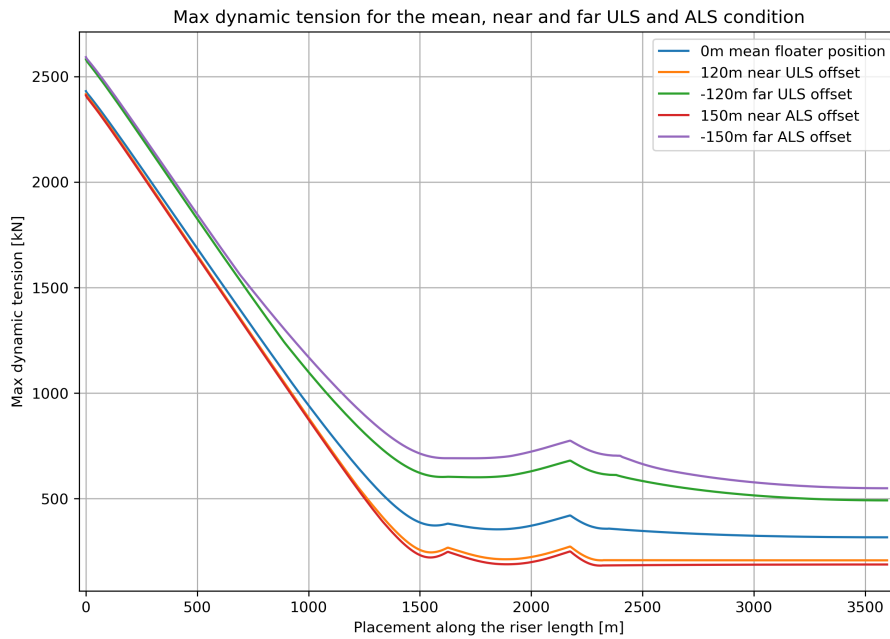


Figure 51: Largest effective tension for waveseed 19 in the mean, near and far ULS and ALS offset position

The most important results from the dynamic analysis is summarized in table (24) below:

Floater position	Maximum effective tension [kN]	Maximum bending moment [kNm]
Mean position	2431	298.5
Near offset ULS	2417	363.6
Far offset ULS	2582	275.5
Near offset ALS	2411	388.3
Far offset ALS	2592	286.4

Table 15: Summary of the results from the dynamic analysis

From these results, it can be seen that the maximum bending moment is located at the sag in the near offset position. The ALS offsets gives the largest moment in the near conditions and the largest effective tension in the far conditions. This is a result of the near offset creating a smaller curvature in the riser configuration, thereby creating larger bending moments. The largest effective tension is located at the hang-off for the far offset. This is a result of the TDP in the static configuration being the closest to the bottom end termination, thereby being the configuration with the most riser in the water column.

## 8.4 Utilization of the SLWR

The utilization of the SLWR configuration was calculated using the combined loading criteria. The combined loading criteria was described in chapter 6 in the description of the ULS criteria. Safety factors used in the analysis was presented earlier in this chapter. In figure (52), the utilization of the riser can be seen.

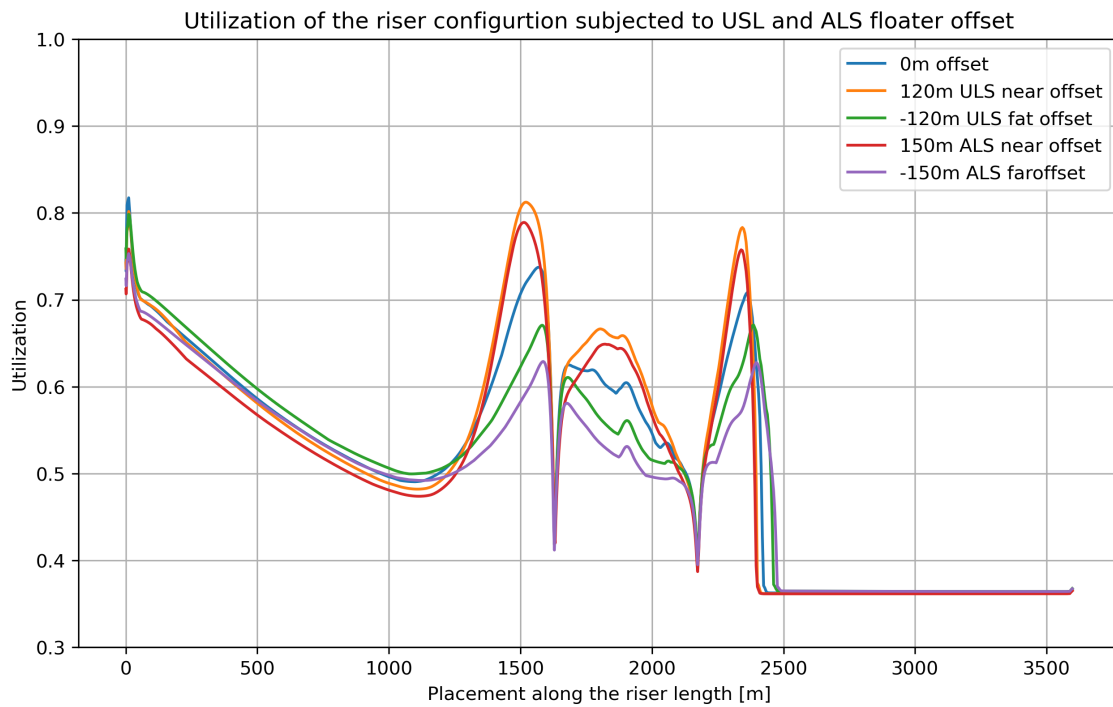


Figure 52: Utilization of the SLWR configuration in the mean, near and far ULS and ALS offset

Floater position	Maximum utilization	Location
Mean position	0.817	Near the hang-off
Near offset ULS	0.812	Sag bend
Far offset ULS	0.798	Near the hang-off
Near offset ALS	0.789	Sag bend
Far offset ALS	0.753	Near the hang-off

Table 16: Largest utilization along the riser configuration

## 8.5 Buckling

Gemilang and D. Karunakaran (2017) presents that downward velocity at the hang-off point of the riser is the main design driver when it comes to buckling at the TDP. The buckling of this riser configuration will not be further investigated as figure (53) shows that the minimum axial force the SLWR is subjected to is in tension.

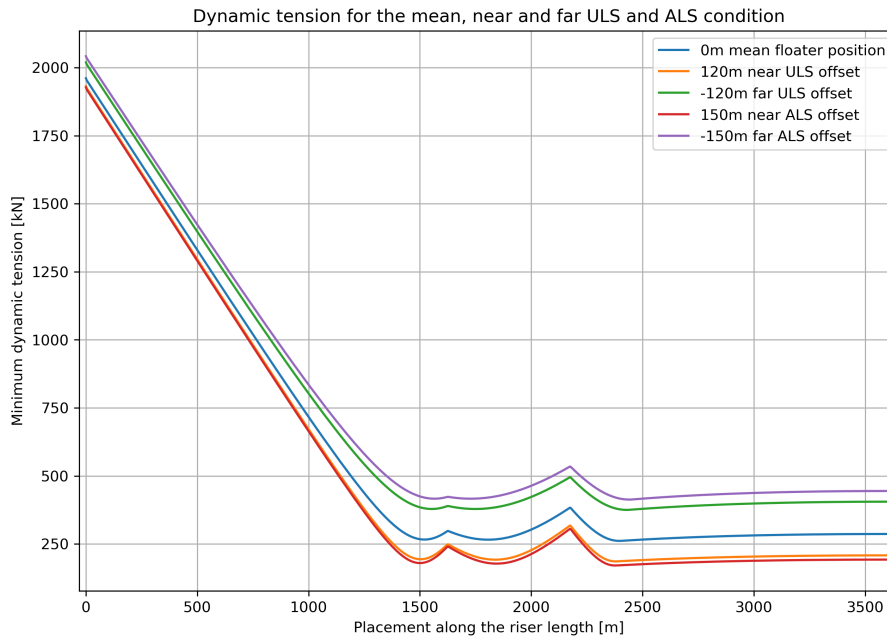


Figure 53: Smallest effective tension for waveseed 19 in the mean, near and far ULS and ALS offset position

## 8.6 Summary of the ULS and ALS limit state analysis

From the static and dynamic analysis, it was found that the the largest utilization of the riser configuration occurred in the mean ULS offset condition. The most important parameter for utilization is found from the utilization graph being the bending moments. This comes from the riser being more capable to carry axial load than bending loads. It was also found that the different safety factors used for the ALS compared to the ULS made it so that utilization of the ALS cases were lower than for the ULS. This was despite the near ALS offset configuration being subjected to larger maximal bending moments.

From the analysis, it was found that the most critical points of the SLWR configuration are near the hang-off, in the sag bend and at the TDP. These are the points that are subjected to the largest utilization in the riser. It was also found that the SLWR configuration satisfies the DNV-ST-F201 combined loading criteria with a maximum utilization of 0.817 near the hang-off for the mean ULS offset condition. As the utilization of the riser system was less than 1.



---

## 9 Fatigue analysis of the SLWR configuration

### 9.1 Introduction

Q. Bai and Y. Bai (2005) presents that for a riser connected to a floater, the fatigue damage can be dividend into four main categories. These categories can be described as:

- 1<sup>st</sup> order and 2<sup>nd</sup> order wave loading as well as the associated floater motion
- VIV from current along the water column
- Vortex-induced hull motions from loop current
- Installation of riser

As a part of this study will the wave fatigue of the SLWR configuration be investigated. A short description of the wave and VIV induced fatigue is presented below.

#### 9.1.1 Wave fatigue

In order to carry out a wave fatigue analysis, the environment of where the riser is located must be described. This is achieved by using a wave scatter diagram that describes the wave environment as a relation between  $H_s$  and  $T_p$ . In order to avoid unwarranted conservatism, the directional probability of wave loading should be applied for at least 8 directions (Q. Bai and Y. Bai 2005).

The wave fatigue can be divided in two categories the 1<sup>st</sup> order wave loading and floater motions induced fatigue and the 2<sup>nd</sup> order floater motion induced fatigue (Q. Bai and Y. Bai 2005). The 1<sup>st</sup> order wave loading and floater motions induced fatigue gets it's cyclic loading from the forced wave frequency. As the 2<sup>nd</sup> order floater motion induced fatigue get it's cyclic loading from low frequency motions. In DNV-RP-F204, it is stated that the wave frequency motions often is the most important wave fatigue component (DNV 2019b).

#### 9.1.2 VIV fatigue

VIV is one of the most important design issues when it comes to riser systems such as the SCR. The main issue with VIV is that it can result in high frequency vibrations as a result of vortex shedding. This can lead to high frequency cyclic loading that can result in fatigue damage (Q. Bai and Y. Bai 2005).

For riser configurations located in deepwater, VIV will be especially important. This is due to the increased length of the riser will lower the natural frequency of the riser. This means that the magnitude of current that is needed to induce VIV is reduced. This combined with the fact that the currents are typically larger for deepwater than for shallower water, and that the possibility of clamping the riser to a structure is far less likely for deepwater. This makes the riser configuration located at deepwater more likely to be subjected to VIV (Q. Bai and Y. Bai 2005).

In order to suppress the VIV motions, spoiler or increased damping can be applied. Faltinsen (1990) presents helical strakes as the most common device to suppress the VIV motions. The main issue with using helical strakes is that marine growth reduces the effect of the strakes and causes increased drag (Faltinsen 1990). An example of helical starkes are presented in figure (54) below.

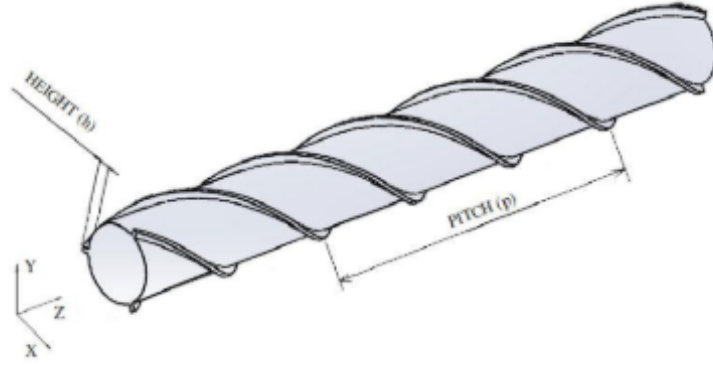


Figure 54: Example of helical strakes on a pipe (Ranjith et al. 2016)

## 9.2 Wave fatigue analysis

### 9.2.1 S-N curve

This study uses the S-N curve method presented in the design code DNV-RP-C203. The S-N curves presented in DNV-RP-C203 are based on the mean-minus-two-standard-deviation curves. These curves are found from relevant experimental data, and the S-N curves can thereby be described with a 97.7% probability of survival of the system (DNV 2019a). The following equations present the parameters used for the S-N curve as a part of the design code DNV-RP-C203.

$$\log N = \log \bar{a} - m * \log(\Delta\sigma) \quad (64)$$

The S-N curve is presented with the following parameters:

- N represents number of cycles subjected to stress range  $\Delta\sigma$  before predicted failure
- $\log \bar{a}$  is the intercept of the design S-N curve represented with a log N-axis by S-N curve
- m is the negative inverse slope of the S-N curve
- $\Delta\sigma$  represent the stress range

$\bar{a}$  and m are described as empirical constants. The stress range is further described by the following equation (DNV 2019b):

$$\Delta\sigma = \Delta\sigma_0 * SCF \left( \frac{t}{t_{ref}} \right)^k \quad (65)$$

The stress range calculated using the following parameters:

- $\Delta\sigma_0$  is the nominal stress range
- SCF represents the stress concentration factor
- $\left( \frac{t}{t_{ref}} \right)^k$  is the thickness correction factor

The design code DNV-RP-C203 presents S-N curves that can be used in the fatigue analysis. The S-N curves presented are divided in two categories, these are S-N curves for air environment and S-N curves for seawater with cathodic protection. From other studies such as (Felisita et al. 2017)

and (Karunakara et al. 2005) is the S-N curve D chosen as a part of the fatigue analysis of their riser configurations. As a result of this is the S-N curve D chosen for the analysis of the SLWR in this study.

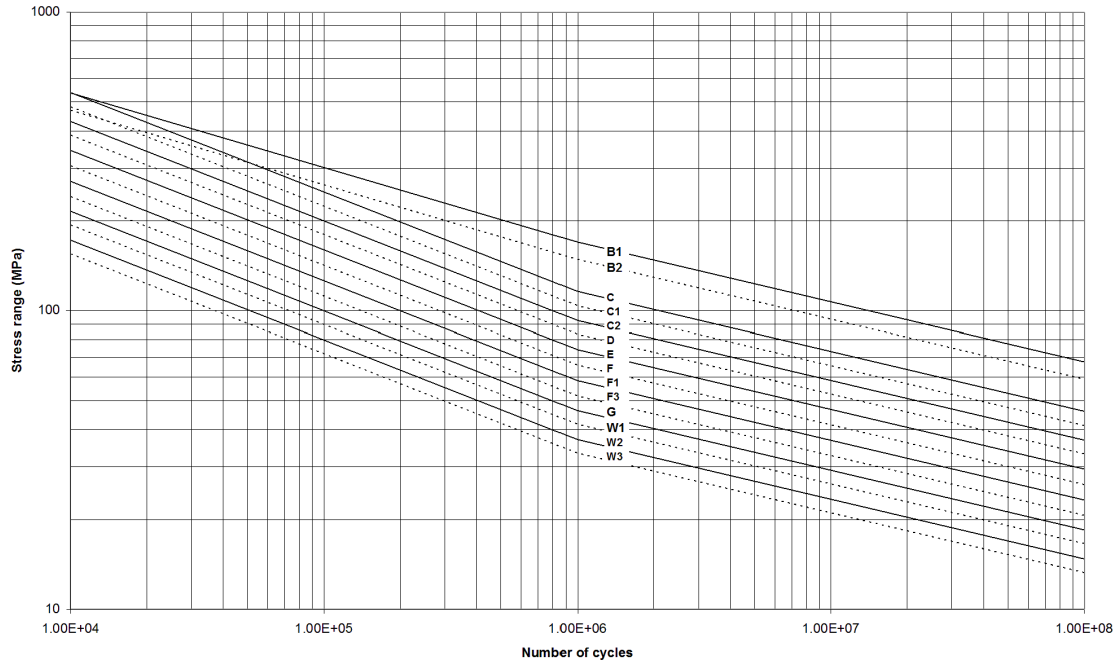


Figure 55: S-N curves presented in the design code DNV-RP-C203

### 9.2.2 Stress concentration factor

The SCF is applied as a part of the fatigue analysis to account for the possibility of stress magnification as a result of imperfect geometry between two adjacent joints. These stress magnifications can occur as a result of the fabrication tolerances of the pipe as well as the installation procedure. One way to determine the SCF is by calculating it by carrying out a detailed finite element analyses. It can also be found by closed form expressions for the actual structural detail. In areas where the stress is increased as a result of local bending from an eccentricity, a stress concentration for the maximum allowable eccentricity should be included (DNV 2019b). Felisita et al. (2017) and D.N. Karunakaran and Baarholm (2013) present the SCF used in the analysis of a SLWR and SCR configuration as 1.251 and 1.2 respectively. The SCF used in the SLWR fatigue analysis is therefore set to 1.2 in this study.

### 9.2.3 Damage

The damage calculation in the design code is based on the assumption of linear cumulative damage. This is achieved by calculating the fatigue life using the S-N curve approach using the Palmgren-Miner rule as an assumption. The accumulated damage can therefore be represented by the following equation (DNV 2019a):

$$D = \sum_{i=1}^k \frac{n_i}{N_i} = \frac{1}{a} \sum_{i=1}^k n_i * (\Delta\sigma)^m \leq \eta = \frac{1}{DFF} \quad (66)$$

The parameters used in calculating the accumulated fatigue damage can be described as the following (DNV 2019a):

- D is the accumulated fatigue damage of the system

- k represents the number of stress blocks
- $n_i$  is the number of stress cycles for a given stress block i
- $N_i$  represents the number of cycles to failure given a constant stress range.
- $\bar{a}$  and m is the same as it is for the S-N curve
- $\eta$  represents the usage factor of the system
- DFF is the design fatigue factor of the system

#### 9.2.4 Wave scatter diagram blocking

The design code DNV-RP-F204 presents how to carry out a global riser fatigue analysis based on waves and floater motions. As stated previously it is assumed that wave frequency motions is often the most important parameter when it comes to wave induced fatigue. (DNV 2019b). The wave data used as a part of the analysis is obtained from a wave scatter diagram. If all the  $H_s$  and  $T_p$  combination of the diagram was to be investigated would that lead to a substantial computational effort. As a result of this, blocking of the scatter diagram is applied. Blocking of a scatter diagram implies that several sea states are analysed as a part of a single block. A sufficient amount of blocks should be used in order to level out the statistical uncertainties that can occur for short term fatigue damage estimates (DNV 2021). A simulation length of 1 hour is often sufficient for each block for standard, well known riser systems located in known environments (DNV 2019b). The blocking carried out for the omni-directional scatter diagram used in this study can be seen in figure (56) below.

$H_s$ [m]	Spectral peak period ( $T_p$ ) - [s]																					
	2-3	3-4	4-5	5-6	6-7	7-8	8-9	9-10	10-11	11-12	12-13	13-14	14-15	15-16	16-17	17-18	18-19	19-20	20-21	21-22	22-23	
0.0-0.5	Block 1			Block 2						Block 3												
0.5-1.0	Block 1			Block 2						Block 3												
1.0-1.5	Block 1			Block 2						Block 3												
1.5-2.0	Block 1			Block 2						Block 3												
2.0-2.5	Block 4			Block 5						Block 6												
2.5-3.0	Block 4			Block 5						Block 6												
3.0-3.5	Block 7			Block 8						Block 9												
3.5-4.0	Block 7			Block 8						Block 9												
4.0-4.5	Block 10			Block 11																		
4.5-5.0	Block 10			Block 11																		
5.0-5.5	Block 12			Block 13																		
5.5-6.0	Block 12			Block 13																		
6.0-6.5	Block 14			Block 15																		
6.5-7.0	Block 14			Block 15																		
7.0-7.5	Block 16			Block 17																		
7.5-8.0	Block 16			Block 17																		
8.0-8.5	Block 16			Block 17																		
8.5-9.0	Block 16			Block 17																		
9.0-9.5	Block 16			Block 17																		
9.5-10.0	Block 16			Block 17																		
10.0-10.5	Block 18			Block 19																		
10.5-11.0	Block 18			Block 19																		
11.0-11.5	Block 18			Block 19																		
11.5-12.0	Block 18			Block 19																		
12.0-12.5	Block 18			Block 19																		
12.5-13.0	Block 18			Block 19																		
13.0-13.5	Block 18			Block 19																		
13.5-14.0	Block 18			Block 19																		
14.0-14.5	Block 18			Block 19																		
14.5-15.0	Block 18			Block 19																		

Figure 56: Blocking used for the fatigue analysis of the SLWR configuration

The scatter diagram was blocked in 18 sea states. The weighted average method was chosen to obtain the  $H_s$  and  $T_p$  for each of the sea state blocks. The following equation was used to calculate the  $H_s$  and  $T_p$  for each of the scatter diagram blocks.

$$H_{s_{Block}} = \frac{\sum_{i=0}^n H_{s_i} * n_i}{N_i} \quad (67)$$

---


$$Tp_{Block} = \frac{\sum_{i=0}^n Tp_i * n_i}{N_i} \quad (68)$$

The parameters in the equations can be described by the following:

- $Hs_{Block}$  is the significant wave height for the block
- $Hs_i$  is a single significant wave height in the block
- $Tp_{Block}$  is the spectral peak period for the block
- $Tp_i$  is a single spectral peak period in the block
- $n_i$  represents the number occurrences for a single sea state
- $N_i$  represents the number of occurrences in the block

The sea states applied in the fatigue analysis of the SLWR configuration is presented in table (17) below:

<b>Block number</b>	<b>Hs</b>	<b>Tp</b>
1	1.259	5.864
2	1.391	9.127
3	1.512	13.585
4	2.430	6.976
5	2.467	9.966
6	2.496	13.598
7	3.426	8.080
8	3.471	10.942
9	3.480	14.547
10	4.428	8.875
11	4.466	13.840
12	5.453	10.664
13	5.474	13.811
14	6.426	12.040
15	6.576	13.665
16	7.441	13.124
17	8.723	14.635
18	10.887	15.283

Table 17: Sea states calculated for the different scatter diagram blocks

The wave scatter diagram used in this analysis is omni-directional. This means that the diagram counts all sea states from every direction. In order to carry out a fatigue analysis of the SLWR configuration, the sea states are applied from 12 sectors. The blocked sea states were applied in all 12 sectors. The SLWR configuration will therefore be analysed for  $18 \times 12 = 216$  sea states. This will not give a perfect representation of the waves acting in any of the sectors, but it is a method presented by Felisita et al. (2017) for the fatigue analysis of another SLWR configuration. Johnsen (2020) presents the probability of waves in a given sector. This will be applied as weighting of the fatigue life from the different sectors. The probability of a wave coming in a set direction is presented in table (18) below.

---

Wave direction [deg]	Probability [%]
0	12.63
30	5.67
60	2.22
90	1.05
120	0.04
150	0.31
180	0.58
210	9.69
240	24.50
270	18.56
300	11.61
330	12.78

Table 18: Probability of waves from different directions (Johnsen 2020)

From the table above, it can be seen that the sector with highest probability of waves is the 240 degree sector. In the SIMA program this sector is applied as a 0 degree wave direction acting on the riser system.

### 9.2.5 Effect of the tapered section

Karunakara et al. (2005) states that rotational stiffness of the flex joint can cause fatigue at the hang-off point of the riser. This low fatigue life near the hang-off can be avoided if a 5-10 meter long taper section is applied. In this section, the effect of the taper section will be investigated. As mentioned in chapter 7 is the hang-off of the SLWR configuration modeled as a pinned joint with a flex joint represented by a global spring with the rotational stiffness of 50 kNm/deg. A taper section is also included in the hang-off with an increased bending stiffness of  $2EI$  to  $1.2EI$  over the length of 5 meters. In order to investigate the effect of the taper section, a fatigue analysis of one sector of wave direction is carried out. One for a system without a taper section and one with the modeled taper section.

The analysis is carried out for wave conditions acting at  $0^\circ$  angle to the riser system. The results from the analysis can be seen in figure (57) below:

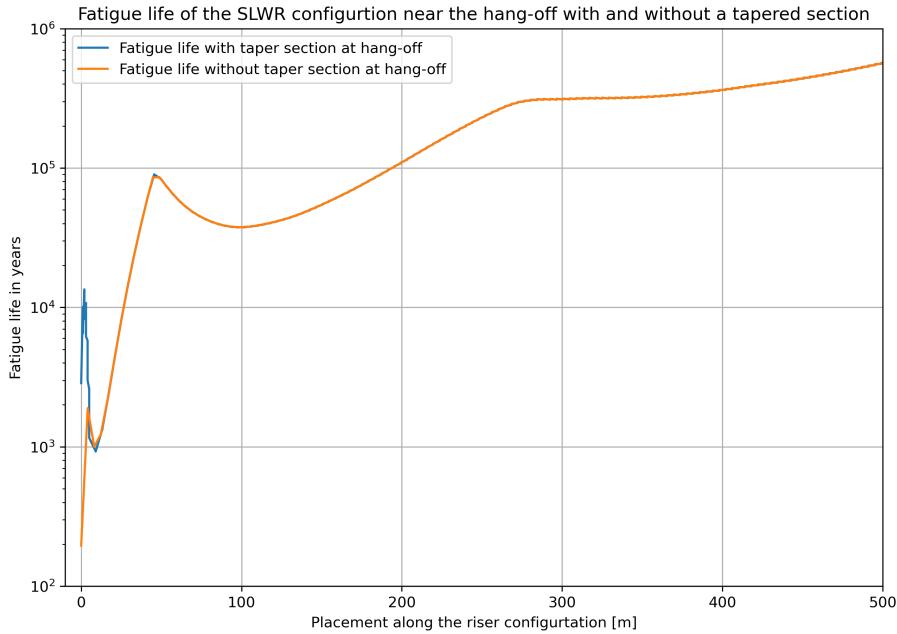


Figure 57: Fatigue life of the SLWR configuration near the hang-off with and without a tapered section

As seen from figure (57) is the fatigue life near the hang-off a lot higher for the model with a taper section compared to the one without. The fatigue life for model without the taper section is 195.6 years. This is lower than the required fatigue life of 250 years for the SLWR configuration. As a result of this, the taper section will be applied in the fatigue analysis of the SLWR configuration.

### 9.2.6 Effect of simulation time

In order to determine the simulation length of the fatigue analysis, simulation times of 500, 1000, 2000, 3600 and 5000 seconds were applied. The simulation was carried out for the 0° wave direction for the 18 sea states calculated from the wave scatter diagram. The effect of the simulation time on the fatigue life near the hang-off and at the TDP is summarized in table (19) below:

Simulation time [s]	Fatigue life near the hang-off	Fatigue life at the TDP
500	898	1246
1000	957	803
2000	1337	1023
3600	1141	1063
5000	1043	1005

Table 19: Fatigue life of the SLWR configuration for different simulation lengths

It can be seen that the simulation time has an effect on the simulated fatigue life of the SLWR configuration. Since the SLWR configuration is a known riser configuration 1 hour simulations are applied for the fatigue analysis as stated in DNV-RP-F204 (DNV 2019b).

## 9.3 Results of the SLWR wave induced fatigue analysis

The fatigue analysis of the SLWR configuration was carried out using the commuter program SIMA. Each sea state was carried out in an 1 hour simulation in SIMA RIFLEX. The data was processed in the VIVANA fatigue analysis task. Where accumulate damage was calculated with respect to

the S-N curve applied for the model. The fatigue life of the riser configuration is presented in figure (58) below:

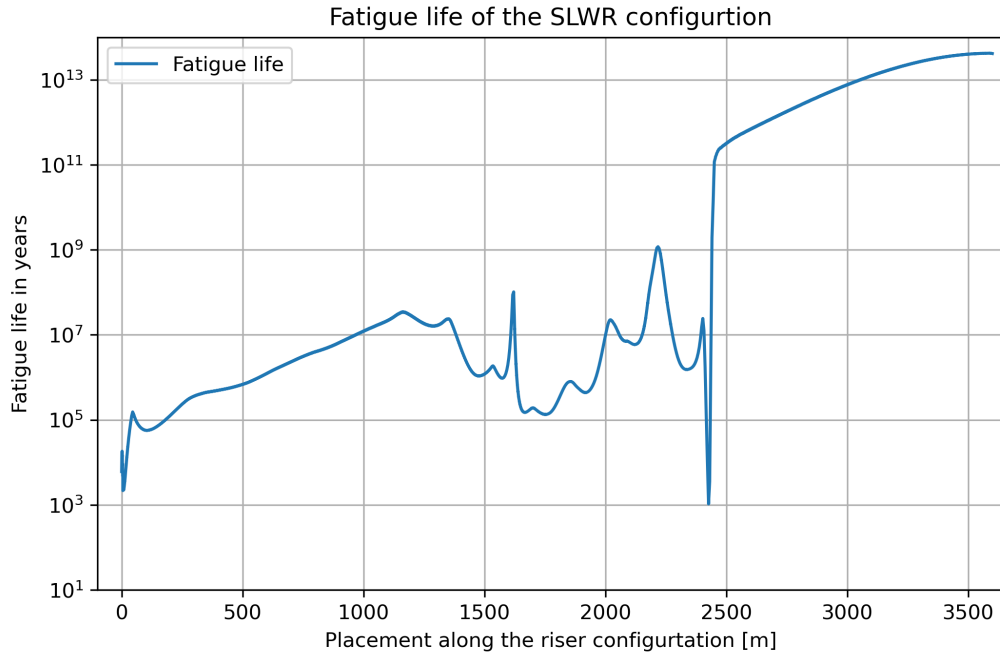


Figure 58: Fatigue life of the SLWR configuration subjected to wave induced fatigue

It can be seen from figure (58) that there are two critical points when it comes to the fatigue life of the SLWR configuration. These are located near the hang-off point and at the TDP of the riser. Table (20) presents the fatigue life in these locations.

Location	Fatigue life years
Near the hang-off point	2173
TDP	1057

Table 20: Important locations with respect to fatigue life

From the fatigue analysis of the SLWR configuration, it is found that the minimum fatigue life, as a result of wave induced fatigue, is 1057 years. This means that the riser configuration has a larger fatigue life than the required fatigue life presented by the design code DNV-ST-F201 of 250 years. This means that the configuration has sufficient resistance against fatigue to have a 25 year design life.



---

## 10 Parametric study of the buoyancy section of the SLWR configuration

A parametric study of the buoyancy section of the SLWR configuration was carried out. The study focuses on the ULS utilization and the fatigue life of the SLWR configuration with different buoyancy sections. The SLWR configuration analysed in the previous chapters is assumed to be the base case in the parametric study. The factors assumed as a part of the parametric study is presented in the list below:

- ULS offset is applied as a part of the utilization calculations.
- Fluid density is set to  $800 \text{ kg/m}^3$
- Coating thickness is set to 50mm with density of  $900 \text{ kg/m}^3$
- Riser hang-off is a pinned joint with a flex-joint with a 50 kNm/deg stiffness for the fatigue analysis
- Mean floater position assumed for fatigue analysis.
- Wave seed number 1 is applied for all analysis
- Fatigue analysis is carried out for the 18 sea state blocks for the 0 degree wave direction
- S-N curve D is applied
- Simulation times are the same as the ones applied in the previous chapters.

### 10.1 SLWR configuration conditions

The parametric analysis was carried out for different buoyancy section lengths and buoyancy module geometries. 5 different SLWR configurations was analysed for the two parameters. The description of the configuration can be seen in table (21) and (22) below:

Buoyancy section case	Buoyancy section length [m]
Length 1	500
Length 2	525
Length 3 (Base case)	550
Length 4	575
Length 5	600

Table 21: Buoyancy section length cases

Buoyancy module case	Mass [kg/m]	Buoyancy [ $m^2$ ]	Diameter [m]
Buoyancy module 1	501.3	1.002	1.2
Buoyancy module 2	549.5	1.099	1.25
Buoyancy module 3 (Base case)	600	1.199	1.3
Buoyancy module 4	651.6	1.303	1.35
Buoyancy module 5	705.6	1.411	1.4

Table 22: Buoyancy module geometry cases

#### 10.1.1 Geometry of the different configurations

The different buoyancy sections and modules have an effect on the SLWR configuration geometry. The variation creates a different wave shape for each of the SLWR configurations. The longer

buoyancy section and the most buoyant modules create a larger more defined wave shape for the riser configuration. The different wave shapes have an effect on the risers ability to sustain dynamic loads as well as fatigue resistance. In the figures (59) and (60) can the shape of the different buoyancy configurations be seen.

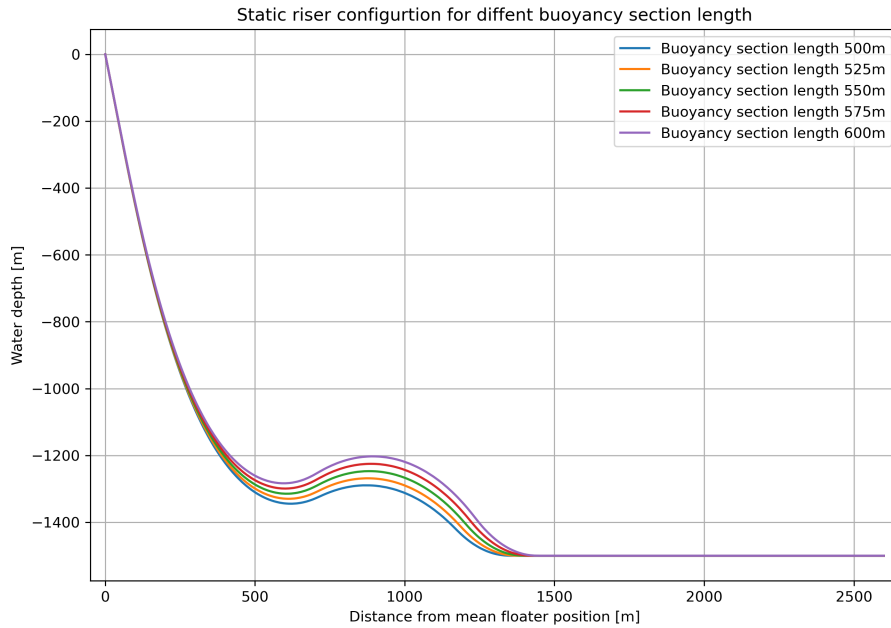


Figure 59: Static configuration for 5 different buoyancy section length

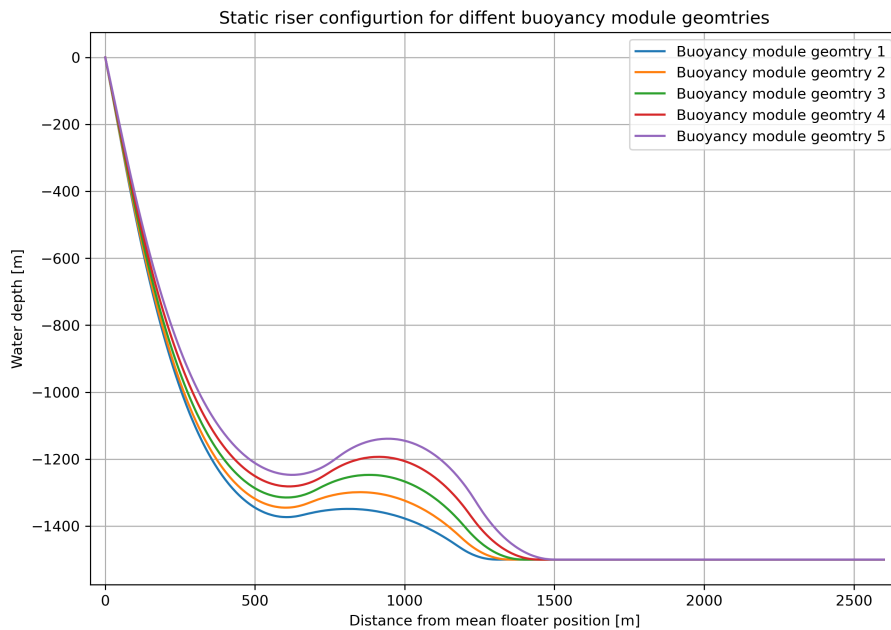


Figure 60: Static configuration for 5 different buoyancy section geometries

### 10.1.2 ULS capabilities

In order to test the ULS capabilities of the different riser configurations, a static and dynamic analysis of the mean, near and far ULS offset was carried out. The ALS offset was left out as the ULS load cases contributed to the largest utilization of the riser configuration in chapter 8. In the

parametric study, only the worst load cases of utilization for each of the parameters investigated will be presented. Two load cases of the buoyancy section length was included due to similar utilization in several areas of the riser configuration. The results from the rest of the load cases can be seen in the Appendix E. The results from the static analysis can be seen in the figures below:

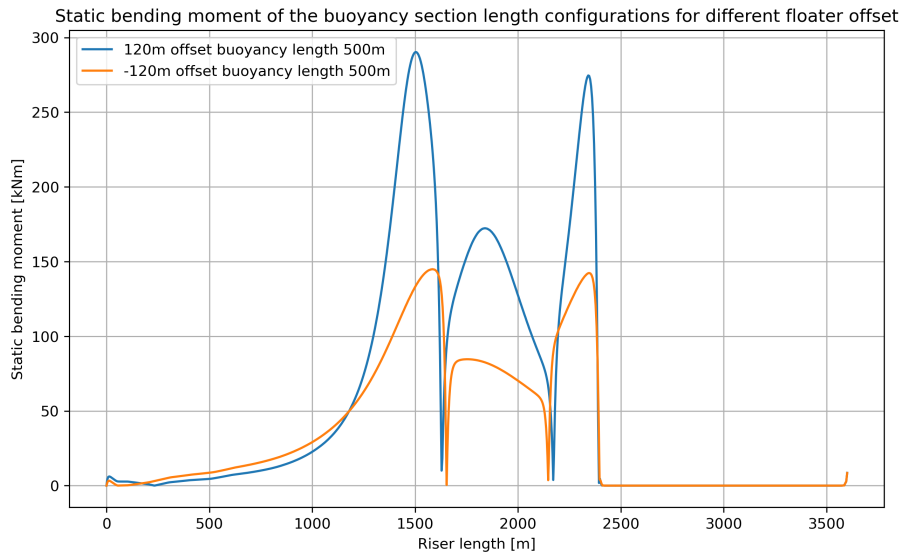


Figure 61: Static bending moment for the worst cases of the 5 different buoyancy section length configurations in the mean, near and far ULS offset

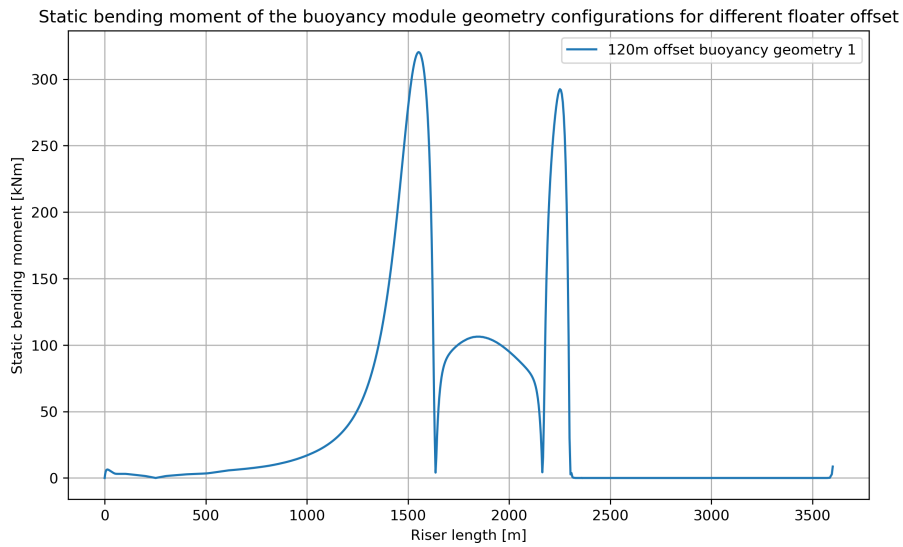


Figure 62: Static bending moment for the worst case of the 5 different buoyancy module geometry configurations in the mean, near and far ULS offset

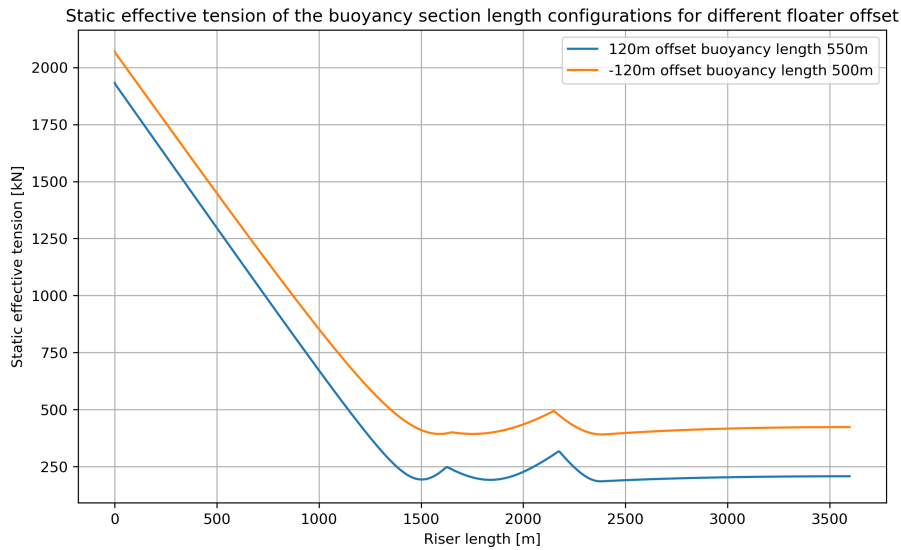


Figure 63: Effective tension for the worst case of the 5 different buoyancy section length configurations in the mean, near and far ULS offset

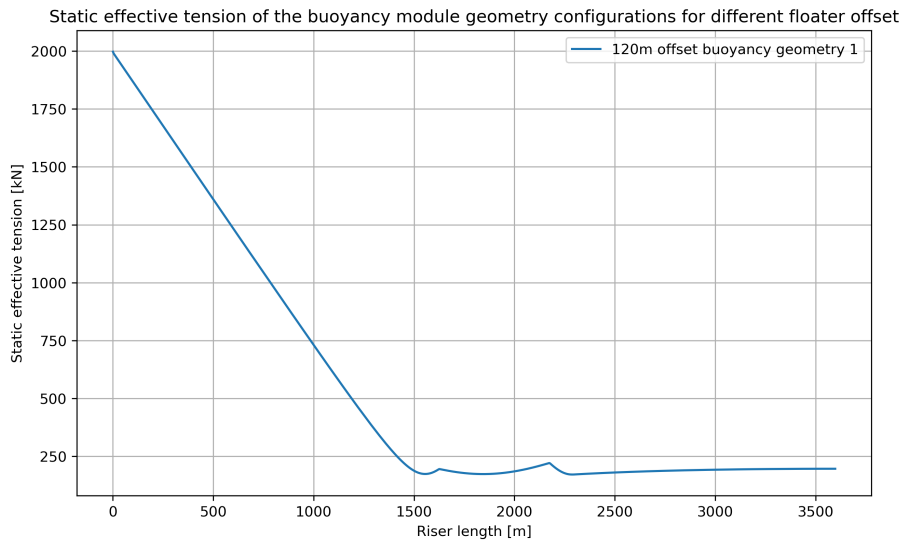


Figure 64: Effective tension for the worst case of the 5 different buoyancy module geometry configurations in the mean, near and far ULS offset

The reason for carrying out the parametric study was to see the effect of changing the buoyancy section of the SLWR configuration. As a result of this, the 90th percentile worst sea state was not investigated for all the different configurations. The dynamic analysis was therefore carried out using wave seed number 1. The results from the dynamic analysis can be seen in the figures below:

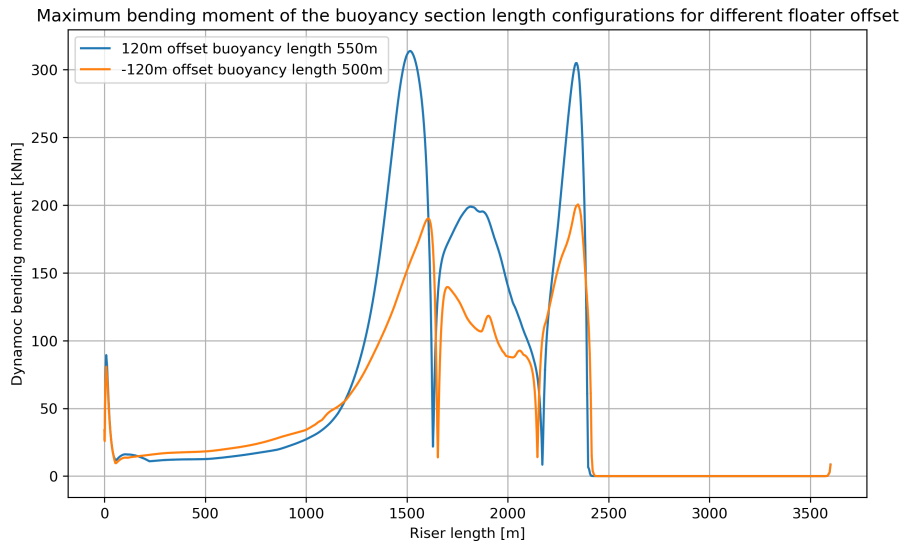


Figure 65: Dynamic bending moment for the worst case of the 5 different buoyancy section length configurations in the mean, near and far ULS offset

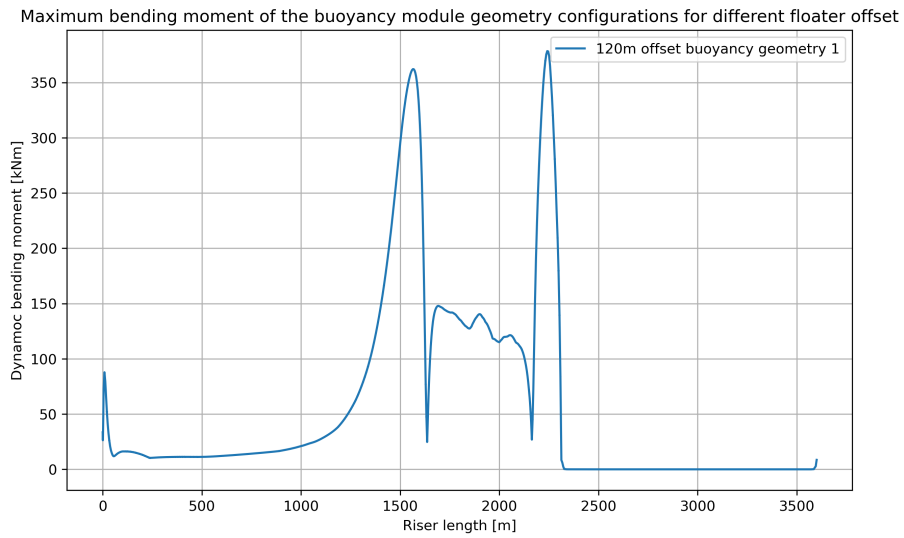


Figure 66: Dynamic bending moment for the worst case of the 5 different buoyancy module geometry configurations in the mean, near and far ULS offset

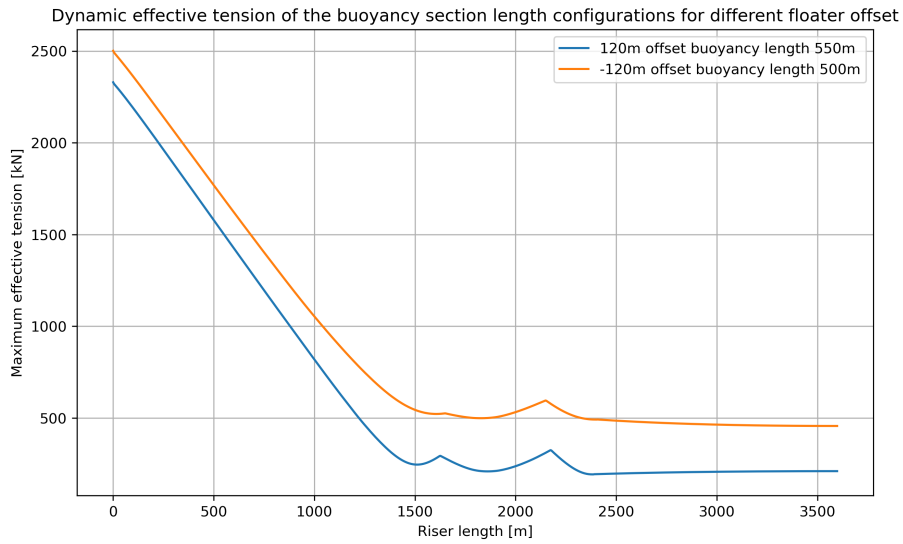


Figure 67: Effective tension for the worst case of the 5 different buoyancy section length configurations in the mean, near and far ULS offset

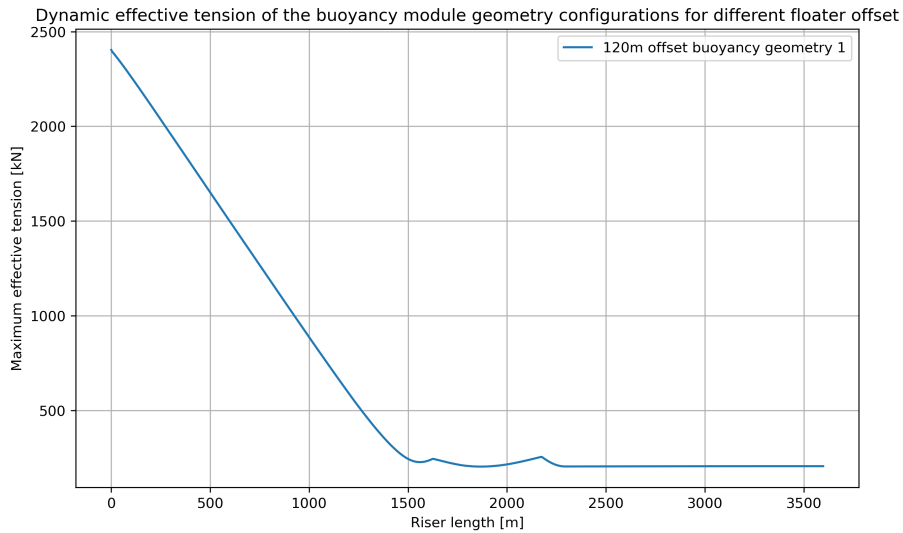


Figure 68: Effective tension for the worst case of the 5 different buoyancy module geometry configurations in the mean, near and far ULS offset

Utilization of the different riser configurations was calculated from these analysis. The utilization of the worst case buoyancy section length and buoyancy module geometry can be seen in the figures below:

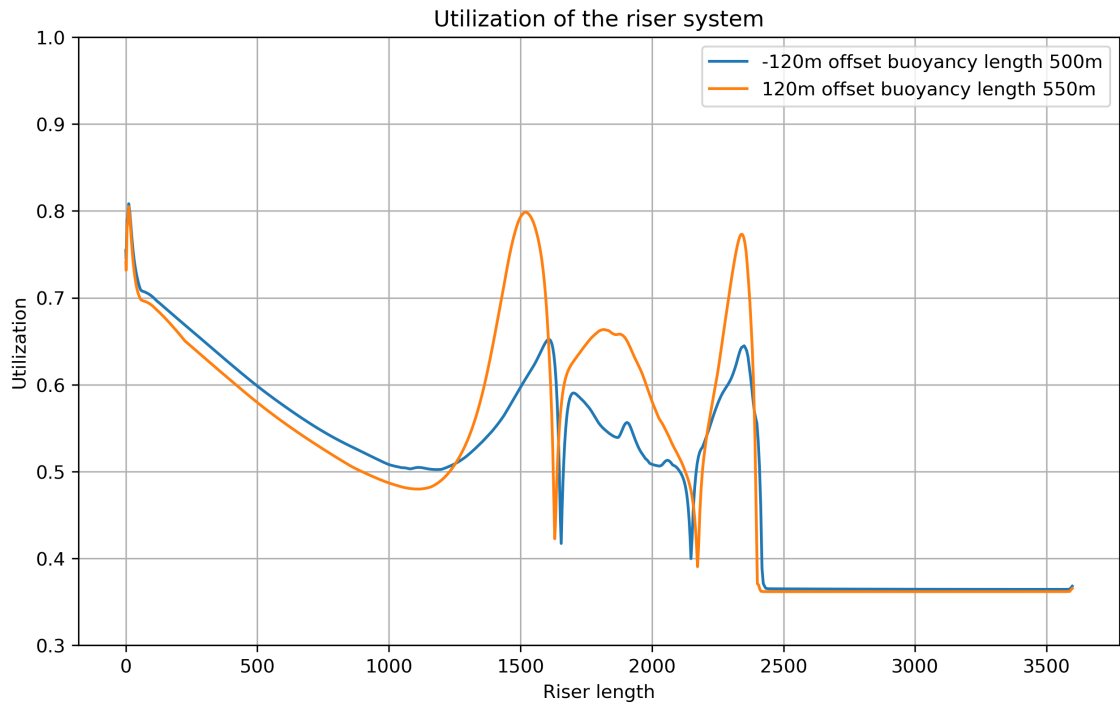


Figure 69: The worst utilization found for the worst case of the 5 different buoyancy section length configurations in the mean, near and far ULS offset

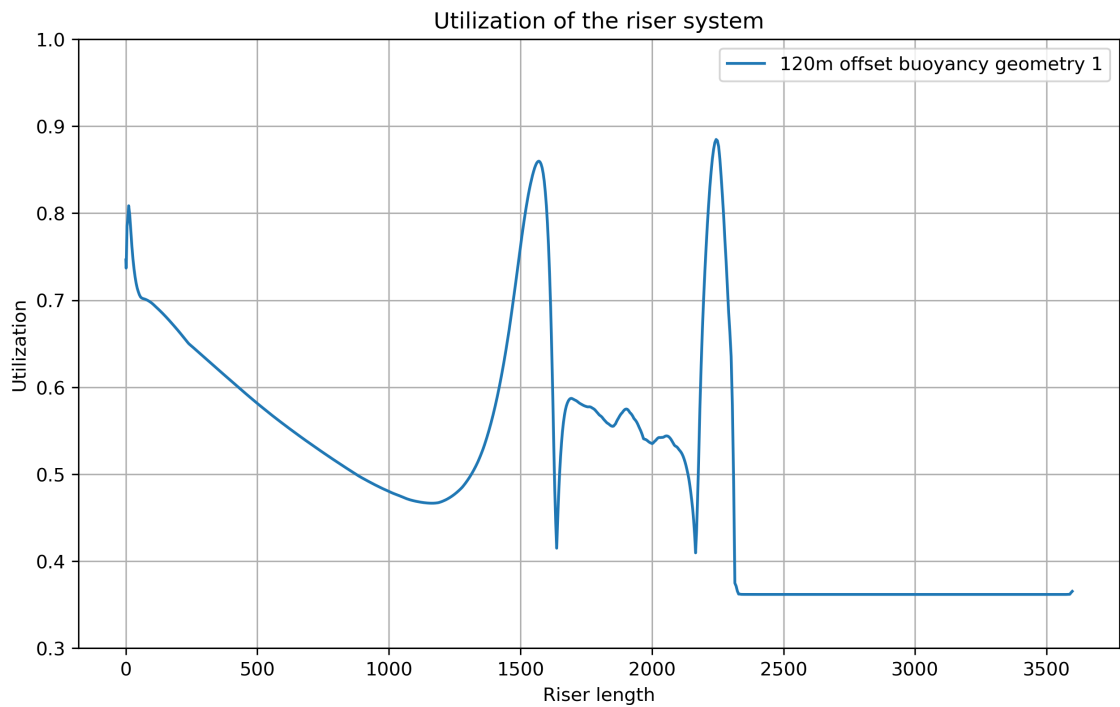


Figure 70: The worst utilization found for the worst case of the 5 different buoyancy section geometries in the mean, near and far ULS offset condition

The largest utilization found from the worst load cases of the parametric configurations in the study is summarized in table (23) below. The table only states the largest utilization found for all buoyancy section length configurations and the buoyancy module geometry load cases.

Buoyancy configuration	Utilization	Location
Buoyancy section length 1 far offset	0.807	Near the hang-off
Buoyancy section length 3 near offset	0.799	Sag bend
Buoyancy module geometry 1 near offset	0.885	TDP

Table 23: Largest utilization along the riser parameter configurations

From the utilization calculations, it was found that the largest utilization of the riser configurations was located at the TDP, for the near offset, for the smallest buoyancy module. It is found that the change in utilization is the largest for the configurations that are dependent on the buoyancy modules. It is also found that changing the buoyancy section length does not effect the utilization of the riser in a large manner. It seems like it just moves the location of the sag bend and the TDP of the riser. One of the most important observationw of this analysis is that all the configurations have an utilization lower than 1, which means that all the configurations satisfies the combined loading criteria from DNV-ST-F201.

### 10.1.3 Fatigue life of different SLWR configurations

A fatigue analysis was carried out for the different riser configurations. The fatigue analysis is carried out for 18 sea states coming in from the 0 degree wave direction. The points of interest found from the fatigue analysis of the base case were fatigue life near the hang-off point and at the TDP of the riser configuration. These will also be points of interest for the different riser configurations.

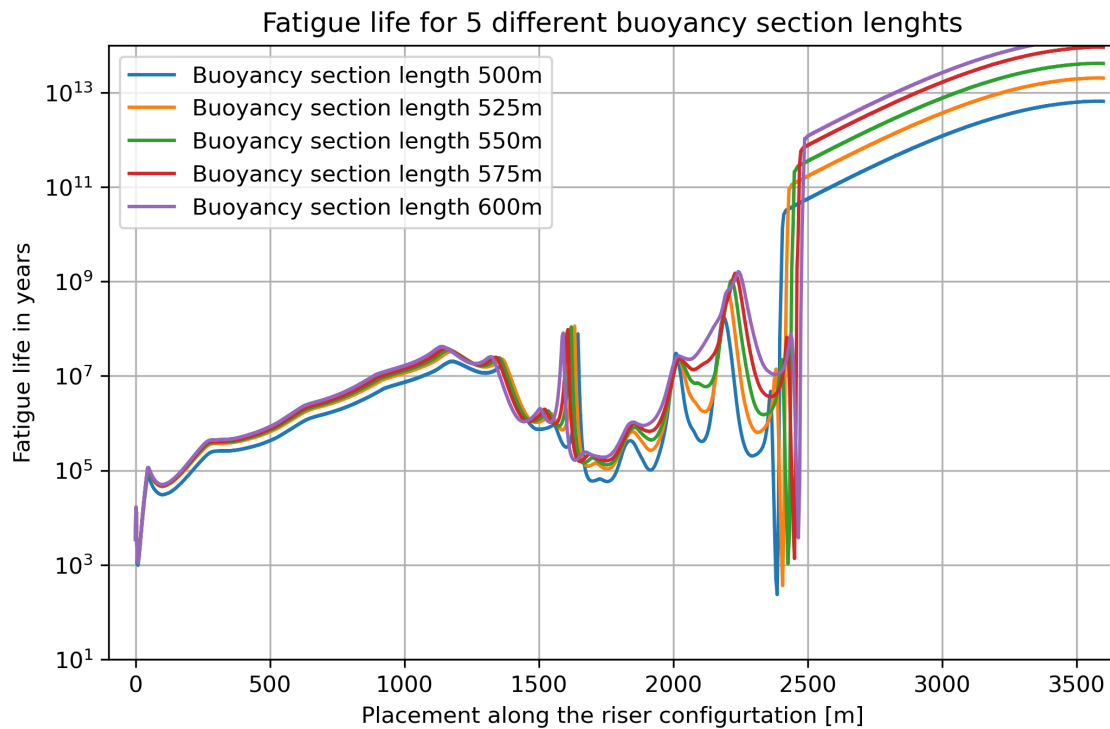


Figure 71: Fatigue life for the 5 different buoyancy section length configurations



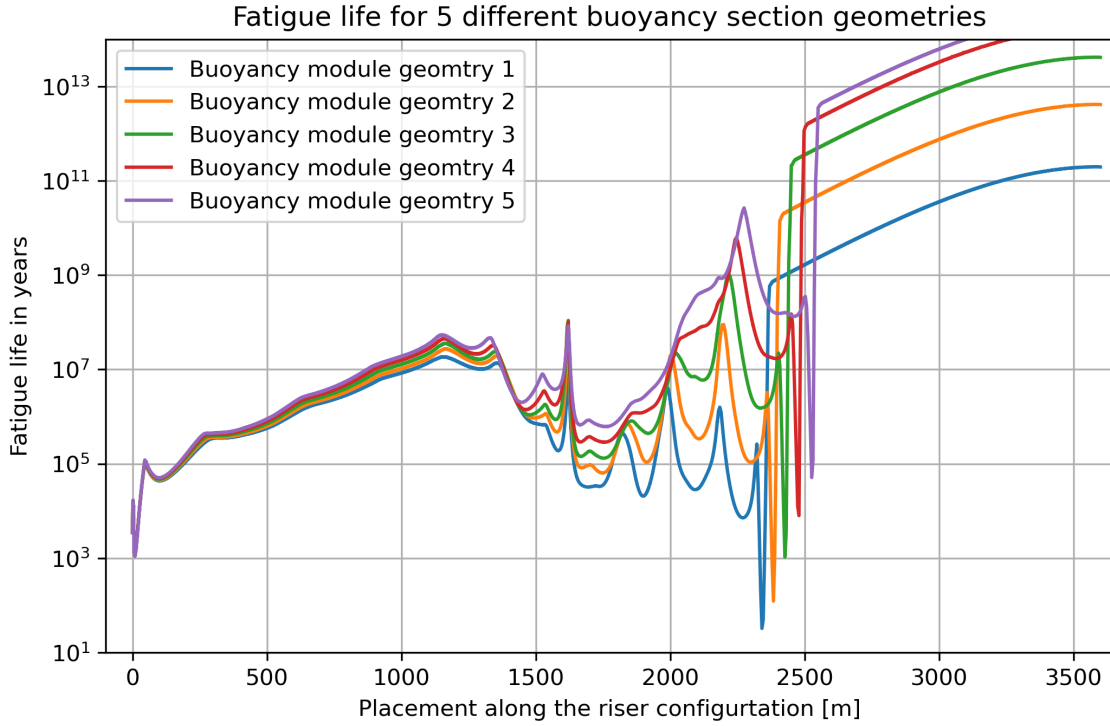


Figure 72: Fatigue life for the 5 different buoyancy module geometry configurations

The shortest fatigue life of the riser configurations, as well as its location is presented in (24) below:

Buoyancy section	Minimum fatigue life [years]	Location
Buoyancy length 1	236.3	TDP
Buoyancy length 2	364.3	TDP
Buoyancy length 3	1061	TDP
Buoyancy length 4	1122	Near hang-off
Buoyancy length 5	1089	Near hang-off
Buoyancy geometry 1	32.6	TDP
Buoyancy geometry 2	123.5	TDP
Buoyancy geometry 3	1061	TDP
Buoyancy geometry 4	1118	Near hang-off
Buoyancy geometry 5	1094	Near hang-off

Table 24: Summary of the results from the dynamic analysis

From figure (71) and (72), it can be seen that the buoyant section of the riser configurations has little effect on the fatigue life near the hang-off point of the riser. The main differences between the configurations are the fatigue life at the TDP. From the figures, it can be seen that the configurations with the least buoyancy also have the lowest fatigue life at the TDP. This shows that in order to have an effective SLWR configuration, the wave section of the configuration must be sufficiently large in order to decouple the floater motions from the seabed.

## 10.2 Summary of the parametric study

Through the parametric study of the SLWR configuration, it was found that the main benefit of the buoyancy section is the fatigue life at the TDP. It was found from the study that the buoyancy section has little effect on the fatigue life near the hang-off point of the riser configuration. As a

---

result of this, the fatigue life near the hang-off point was the most severe fatigue life when it came to fatigue for the configurations with the largest buoyancy in the buoyancy sections.

From the dynamic analysis of the SLWR configurations, it was found that the different buoyancy sections lengths have little effect on the riser utilization. This can be seen from the results presented in Appendix E. From the figures representing the maximum bending moments of the riser configurations it can be seen that the moments in the sag bend and at the TDP just moves further apart. In relation to the configurations represented by the geometry of the buoyancy module, the utilization in the sag bend and the TDP vary considerably. The most critical sections found in chapter 8 remained the most critical sections for all the different buoyancy configurations. It is also found that all the configurations satisfies the combined load criteria from the design code DNV-ST-F201.

The parametric study shows the importance of a sufficient buoyancy section when modeling a SLWR configuration. With a sufficient buoyancy section, the SLWR configuration is able to accommodate for the issues with low fatigue life at the TDP that is present for the SCR configuration connected to floaters with large heave motions.

---

## 11 Conclusion and further work

### 11.1 Conclusion

As a part of this study, static, dynamic and fatigue analysis have been carried out for a SLWR configuration modeled for 1500 meter of water depth. Where the utilization and fatigue life of the riser was investigated.

In the extreme response analysis, the mean, near and far ULS and ALS offset was investigated. The dynamic analysis was determined by using Gumbel distribution to calculate the 90th percentile worst load case. The worst load case was determined as the highest downward velocity at the hang-off point. From the static and dynamic analysis, the utilization was calculated. From the utilization calculations, it was found that the most critical areas of the SLWR configuration were near the hang-off, at the sag bend and at the TDP. The largest utilization was found in the mean ULS offset with a value of 0.817. With an utilization less than one, the riser configuration satisfies the combined loading criteria given by DNV-ST-F201.

The fatigued analysis of the SLWR configuration focused on wave induced fatigue. The sea state used in the analysis was calculated using the weighted average of  $H_s$  and  $T_p$  values from an omnidirectional scatter diagram. The diagram was blocked into 18 blocks and these was analysed for 12 wave directions. S-N curve D was applied for the analysis. The effect of a taper section was investigated and it was found that having a 5 meter long taper section at the hang-off greatly increased the fatigue life in the hang-off region. From the fatigue analysis, it was found that the most critical points when it comes to fatigue life in the SLWR configuration were near the hang-off point and at the TDP. The lowest fatigue life of the SLWR configuration was 1057 years located at the TDP. Given that the fatigue criteria from DNV-ST-F201 for a system with a 25 year design life and a high safety class result in a required fatigue life of 250 years. From this it is found that the system satisfies the fatigue criteria.

The parametric study was carried out to investigate the effect of changing the buoyancy section of the SLWR configuration. The configurations were defined by either changing the buoyancy section length or by changing the buoyancy module geometry. The parametric study looked at how the different configurations effected the utilization of the riser, as well as the fatigue life of the riser. It was found that changing the buoyancy section length had little effect on the utilization of the riser system. This came mainly down to the largest bending moment of the riser just mowing location. Changing the buoyancy module geometry had more of an effect on the on the utilization especially in the sag bend and at the TDP. The largest utilization found in the parametric study was found in the TDP for smallest buoyancy module geometry in the near ULS offset, with a value of 0.885. From this it was found that all the configuration satisfied the combined loading criteria. In the fatigue analysis of the configurations, it was found that the buoyancy section had a large effect on the fatigue life of the system. The largest effect of the buoyancy section could be seen in the TDP where it could be seen that he fatigue life was drastically reduced when reducing the buoyancy section. Where the fatigue life at the TDP of the smallest buoyancy module geometry was 33 years compared to 1061 years for the base case. It was found that the buoyancy section had little effect on the fatigue life near the hang-off point. From the parametric study, it was found that by modeling a sufficient buoyancy section will remove the issue with wave induced fatigue at the TDP of a SLWR configuration.

---

## 11.2 Further work

This section consist of further work that would be interesting to investigate.

- Carry out a fatigue analysis of the SLWR configuration based on VIV induced fatigue. This will give indication if components such as helical strakes should be utilized for this riser configuration.
- Carry out wave induced fatigue analysis for other locations.
- Making specific calculations of the hydrodynamic coefficients of the buoyancy modules.
- The RAO used in the analysis is an example file of a RAO of a semi-submersible platform. Carry out the analysis for other semi-submersible platform RAOs.
- Carry out a parametric study for other riser parameters.
- Further flex joint modeling.

---

## Bibliography

- Almar-Næss, A. (1985). *Fatigue handbook offshore steel structures*. Tapir.
- API (2018). *Line Pipe API SPECIFICATION 5L FORTY-SIXTH EDITION*. API.
- (2020). *API STD 2RD 2ND ED Dynamic Risers for Floating Production Systems*. API.
- (2022). *ASTM D5002-22 Standard Test Method for Density, Relative Density, and API Gravity of Crude Oils by Digital Density Analyzer*. API.
- (2024). *API RP 2SK 4TH ED Design and Analysis of Stationkeeping Systems for Floating Offshore Structures*. API.
- Arikan, Y. (2024). *3 Things to Consider When Using Tapered Stress Joints on a Tieback*. URL: <https://2hoffshore.com/knowledge/3-things-to-consider-when-using-tapered-stress-joints-on-a-tieback> (visited on 20th Apr. 2024).
- Athisakul, C., K. Klaycham and S. Chucheeprakul (2014). ‘Critical Top Tension for Static Equilibrium Configuration of Steel Catenary Riser’. In: *China Ocean Eng* 28, pp. 829–842. DOI: <https://doi.org/10.1007/s13344-014-0064-x>.
- Bahadori, A. (2017). *Oil and Gas Pipelines and Piping Systems, Design, Construction, Management, and Inspection*. Gulf Professional Publishing.
- Bai, Q. and Y. Bai (2005). *Subsea pipelines and risers*. Elsevier Science.
- (2012). *Subsea Engineering Handbook Second Edition*. Gulf Professional Publisher.
- (2014). *Subsea Pipeline Design, Analysis, and Installation*. Gulf Professional Publishing.
- (2018). *Subsea Engineering Handbook*. Gulf Professional Publishing.
- Berge, S. (2006). *Fatigue and Fracture Design of Marine Structures*. INSTITUTT FOR MARIN TEKNIKK.
- Chakrabarti, S. K. (2005a). *HANDBOOK OF OFFSHORE ENGINEERING Offshore Structure Analysis*. Vol. 1. ELSEVIER.
- (2005b). *HANDBOOK OF OFFSHORE ENGINEERING Offshore Structure Analysis*. Vol. 2. ELSEVIER.
- Cheng, Y., L. Tang and T. Fan (2020). ‘Dynamic analysis of deepwater steel lazy wave riser with internal flow and seabed interaction using a nonlinear finite element method’. In: *Ocean Engineering* 209. DOI: <https://doi.org/10.1016/j.oceaneng.2020.107498>.
- DNV (2001). *DNV-OS-F201 DYNAMIC RISERS*. DNV.
- (2019a). *DNV-RP-C203 Fatigue design of offshore steel structures*. DNV.
- (2019b). *DNV-RP-F204 Riser fatigue*. DNV.
- (2020). *DNV-RP-B204 Welding of subsea production system equipment*. DNV.
- (2021). *DNV-ST-F201 Riser systems*. DNV.
- DrillingFormulas (2024a). *J-Lay Pipeline Installation*. URL: <https://www.drillingformulas.com/j-lay-pipeline-installation/> (visited on 15th Apr. 2024).
- (2024b). *Pipe Line S-Lay Method*. URL: <https://www.drillingformulas.com/pipe-line-s-lay-method/> (visited on 15th Apr. 2024).
- Faltinsen, O. M. (1990). *Sea Loads on Ships and Offshore Structures*. Cambridge University Press.
- Felisita, A. et al. (2017). ‘Review of Steel Lazy Wave Riser Concepts for the North Sea’. In: *Proceedings of the ASME 2015 34th International Conference on Ocean, Offshore and Arctic Engineering OMAE2015*. DOI: 10.1115/1.4034822].
- Fergestad, D. and S.A. Løvteit (2017). *HANDBOOK on DESIGN and OPERATION of FLEXIBLE PIPES*. SINTEF Ocean AS.

- 
- Gavin, H. (2012). ‘Geometric Stiffness Effects in 2D and 3D Frames’. In.
- Gemilang, G.M. and D. Karunakaran (2017). ‘Feasibility Study of Selected Riser Concepts in Deep Water and Harsh Environment’. In: DOI: <https://doi.org/10.1115/OMAE2017-62453>.
- Haver, S. (2020). *METOCEAN MODELLING AND PREDICTION OF EXTREMES*. UiS.
- Hu, X., M. Duan and P. Liu (2012). ‘Risk and Reliability Analysis of Deepwater Reel-Lay Installation: A Scenario Study of Pipeline during the Process of Tensioning’. In: *Natural Resources* 3, pp. 156–163. DOI: 10.4236/nr.2012.33020.
- Hui, G. et al. (2019). ‘EFFECT OF FLEXIBLE JOINT MODELLING METHOD ON DEEP WATER CATENARY RISER HANG-OFF FATIGUE RESPONSE’. In: DOI: <https://doi.org/10.1115/OMAE2019-96826>.
- Johnsen, Ø. (2020). *MariCulture Smart Fishfarm Metocean Design Basis, Haltenbanken II*. URL: <https://www.fiskeridir.no/Akvakultur/Dokumenter/Hoeringer/horing-om-klarering-av-lokalitet-for-akvakultur-i-norskehavet>.
- Karunakara, D. et al. (2005). ‘Weight Optimized SCRs for Deepwater Harsh Environments’. In: DOI: <https://doi.org/10.4043/17224-MS>.
- Karunakaran, D., J.L. Legras and R.L. Jones (2013). ‘Fatigue Enhancement of SCRs: Design Applying Weight Distribution and Optimized Fabrication’. In: DOI: <https://doi.org/10.4043/23945-MS>.
- Karunakaran, D.N. and R. Baarholm (2013). ‘COBRA: An Uncoupled Riser System for Ultradeep Water in Harsh Environment’. In: DOI: <https://doi.org/10.4043/23986-MS>.
- Kim, B. W., H. G. Sung and S. Y. Hong (2017). ‘Coupled Versus Decoupled Analysis for Floating Body and Mooring Lines’. In: DOI: <https://onepetro.org/ISOPEIOPEC/proceedings/ISOPE17/All-ISOPE17/ISOPE-I-17-146/17396>.
- Langen, I. and R. Sigbjørnson (1979). *Dynamisk Analyse av konstruksjoner*. Tapir.
- Larsen, C. M. et al. (2021). *Marine Dynamics*. NTNU.
- Miller, C. A. (2017). ‘Risers Introduction’. In: *In Encyclopedia of Maritime and Offshore Engineering*. DOI: <https://doi.org/10.1002/9781118476406.emoe485>.
- Moan, T. (2003). *Finite element modelling and analysis of marine structures*. NTNU.
- NORSOK-Standard (2018). *NORSOK N-003 Actions and action effects*. Standard Norway.
- Ranjith, E.R., A.S. Sunil and P. Lippin (2016). ‘Analysis of flow over a circular cylinder fitted with helical strakes’. In: *Procedia Technology* 24.
- Ray, K. K. (2001). ‘Crack Growth Measurement’. In: *Encyclopedia of Materials: Science and Technology*.
- Ruan, W. et al. (2021). ‘Study on fatigue damage optimization mechanism of deepwater lazy wave risers based on multiple waveform serial arrangement’. In: *Ocean Engineering* 228. DOI: <https://doi.org/10.1016/j.oceaneng.2021.108926>.
- Sævik, S. (2017). *Lecture Notes in Offshore Pipeline Technology*. NTNU.
- SINTEF (2024a). *1. Data Group C: Component Data*. URL: [https://sima.sintef.no/doc/4.4.0/riflex/userguide/inpmod/component\\_data.html](https://sima.sintef.no/doc/4.4.0/riflex/userguide/inpmod/component_data.html) (visited on 16th May 2024).
- (2024b). *SIMA DOCUMANTATION System Spesification*. URL: [https://sima.sintef.no/doc/4.6.0/riflex/userguide/system\\_specification.html](https://sima.sintef.no/doc/4.6.0/riflex/userguide/system_specification.html) (visited on 7th May 2024).
- (2024c). *SIMA DOCUMENTATION Abstract*. URL: <https://sima.sintef.no/doc/4.6.0/vivana/userguide/mainpage.html> (visited on 7th May 2024).
- (2024d). *SIMA DOCUMENTATION Abstract*. URL: [https://sima.sintef.no/doc/4.4.0/riflex/userguide/inpmod/riser\\_data/seafloor\\_contact.html](https://sima.sintef.no/doc/4.4.0/riflex/userguide/inpmod/riser_data/seafloor_contact.html) (visited on 15th May 2024).
-

- 
- SINTEF (2024e). *SIMA DOCUMENTATION Dynamic Calculation Parameters*. URL: <https://sima.sintef.no/doc/4.6.0/riflex/sima/context/CoupledDynamicCalculationParameters.html> (visited on 12th Mar. 2024).
- (2024f). *SIMA DOCUMENTATION Introduction*. URL: <https://sima.sintef.no/doc/4.6.0/riflex/userguide/introduction.html> (visited on 7th May 2024).
- (2024g). *SIMA DOCUMENTATION SIMO*. URL: <https://sima.sintef.no/doc/4.6.0/simo/index.html> (visited on 7th May 2024).
- (2024h). *SIMA DOCUMENTATION Static Finite Element Analysis*. URL: [https://sima.sintef.no/doc/4.6.0/riflex/theory/static\\_finite\\_element\\_analysis.html](https://sima.sintef.no/doc/4.6.0/riflex/theory/static_finite_element_analysis.html) (visited on 12th Mar. 2024).
- (2024i). *SIMA DOCUMENTATION Eigenvalue Analysis*. URL: [https://sima.sintef.no/doc/4.6.0/riflex/theory/eigenvalue\\_analysis.html](https://sima.sintef.no/doc/4.6.0/riflex/theory/eigenvalue_analysis.html) (visited on 12th Mar. 2024).
- Speight, J.G. (2014). *Handbook of Offshore Oil and Gas Operations*. Gulf Professional Publishing.
- Wægter, J. (2024). *Note 5.1 Stress range histories and Rain Flow counting*. URL: <https://homes.civil.aau.dk/lda/Advanced%20Structural%20Engineering/Stress%20range%20histories%20and%20Rain%20Flowcounting.pdf> (visited on 6th May 2024).

---

## Appendix

### A Programfiles

The analysis is performed using SIMA RIFLEX and the corresponding files is delivered in a folder along with the report. The master poster is also included in the folder.



---

## B Python file used for utilization calculations

```
1
2 import numpy as np
3 import matplotlib.pyplot as plt
4
5 # Parameters:
6
7 # Safety factors
8 Gamma_M = 1.15
9 Gamma_SC = 1.26
10 ULS_Gamma_F = 1.1
11 ULS_Gamma_E = 1.3
12 ALS_Gamma_F = 1.0
13 ALS_Gamma_E = 1.0
14 alpha_c = 1.2
15
16 # X65 strength
17 f_y = 450*10**6
18 f_u = 535*10**6
19
20 # Dimensions
21 D = 0.304
22 t2 = 0.0225
23 p_i = 65*10**6
24 rho = 1025
25 g = 9.81
26
27 # Capacity
28 T_K = f_y*(D-t)*t*np.pi
29 M_K = f_y*t*(D-t)**2
30 p_b = (2/np.sqrt(3))*(2*t/(D-t))*f_y
31
32
33
34 # Make numpy arrays from result file
35 def read_tension_file(file_path):
36     with open(file_path, 'r') as file:
37         lines = file.readlines()
38         column_data = []
39         data = line.strip().split()
40         column_data.append([float(x) for x in data])
41     return np.array(column_data).T
42 if FileNotFoundError:
43     print("File not found.")
44
45
46 # Read position, tension and moment results
47 Dynamic_moment = read_tension_file("C:/Users/danir/OneDrive/Documents/V r 2023/
48 Master/data/ULS and ALS/M_MAX.txt")
49 Dynamic_tension = read_tension_file("C:/Users/danir/OneDrive/Documents/V r 2023/
50 Master/data/ULS and ALS/F_MAX.txt")
51 Static_moment = read_tension_file("C:/Users/danir/OneDrive/Documents/V r 2023/
52 Master/data/ULS and ALS/M_stat.txt")
53 Static_tension = read_tension_file("C:/Users/danir/OneDrive/Documents/V r 2023/
54 Master/data/ULS and ALS/F_stat.txt")
55 XZ = read_tension_file("C:/Users/danir/OneDrive/Documents/V r 2023/Master/data/ULS
56 and ALS/XZ_ULS_ALS.txt")
57
58
59 # Make the arrays on the same form
60 Dyn_selected = Dynamic_moment[:, :2]
61 stat_selected = Static_moment[:, :2]
62 Z = XZ[:, 1:]
63
64 # Calculate functional and environmental loads
65 ULS_fun_ten=np.array([[Static_tension[1]],[Static_tension[3]],[Static_tension[5]]])
66 ALS_fun_ten=np.array([[Static_tension[7]],[Static_tension[9]]])
67
68 ULS_fun_mom=np.array([[stat_selected[1]],[stat_selected[3]],[stat_selected[5]]])
69 ALS_fun_mom=np.array([[stat_selected[7]],[stat_selected[9]]])
70
```

---

```

66 ULS_env_mom=np.array([[Dyn_selected[1]-stat_selected[1]],[Dyn_selected[3]-
    stat_selected[3]],[Dyn_selected[5]-stat_selected[5]])]
67 ALS_env_mom=np.array([[Dyn_selected[7]-stat_selected[7]],[Dyn_selected[9]-
    stat_selected[9]])]
68
69 ULS_env_tension=np.array([[Dynamic_tension[1]-Static_tension[1]],[Dynamic_tension
    [3]-Static_tension[3]],[Dynamic_tension[5]-Static_tension[5]])]
70 ALS_env_tension=np.array([[Dynamic_tension[7]-Static_tension[7]],[Dynamic_tension
    [9]-Static_tension[9]])]
71
72 # Calculate external pressure
73 p_e = rho * g * (-Z[1])
74
75 # Calculate design loads
76 ULS_T_ed = ULS_Gamma_F * ULS_fun_ten + ULS_Gamma_E * ULS_env_tension
77 ULS_M_D = ULS_Gamma_F * ULS_fun_mom + ULS_Gamma_E * ULS_env_mom
78
79 ALS_T_ed = ALS_Gamma_F * ALS_fun_ten + ALS_Gamma_E * ALS_env_tension
80 ALS_M_D = ALS_Gamma_F * ALS_fun_mom + ALS_Gamma_E * ALS_env_mom
81
82 # Calculate utilization
83 ULS_Utilization = (Gamma_M*Gamma_SC)*((ULS_M_D/(alpha_c*M_K))*np.sqrt(1-((p_i-p_e)/
    p_b)**2)+(ULS_T_ed/(alpha_c*T_K)**2)+((p_i-p_e)/p_b)**2
84 ALS_Utilization = (Gamma_M*Gamma_SC)*((ALS_M_D/(alpha_c*M_K))*np.sqrt(1-((p_i-p_e)/
    p_b)**2)+(ALS_T_ed/(alpha_c*T_K)**2)+((p_i-p_e)/p_b)**2
85
86
87 mean_ULS=ULS_Utilization[0]
88 near_ULS=ULS_Utilization[1]
89 far_ULS=ULS_Utilization[2]
90 near_ALS=ALS_Utilization[0]
91 far_ALS=ALS_Utilization[1]
92
93 plt.figure(figsize=(12, 8), dpi=300)
94 plt.plot(Dynamic_tension[0], mean_ULS[0], label='0m offset')
95 plt.plot(Dynamic_tension[0], near_ULS[0], label='120m ULS near offset')
96 plt.plot(Dynamic_tension[0], far_ULS[0], label='-120m ULS fat offset')
97 plt.plot(Dynamic_tension[0], near_ALS[0], label='150m ALS near offset')
98 plt.plot(Dynamic_tension[0], far_ALS[0], label='-150m ALS faroffset')
99 plt.xlabel('Placement along the riser length [m]')
100 plt.ylabel('Utilization')
101 plt.title('Utilization of the riser configurtion subjected to USL and ALS floater
    offset')
102 plt.legend()
103 plt.grid(True)
104 plt.ylim(0,1)
105 plt.show()

```

---

---

## C Python file used for Gumbel distribution of the downward velocity at the hang-off point

```
1 import numpy as np
2 import matplotlib.pyplot as plt
3 from scipy.stats import gumbel_r
4
5 def read_displacement_file(file_path):
6     with open(file_path, 'r') as file:
7         lines = file.readlines()
8         column_data = []
9         for line in lines:
10            data = line.strip().split()
11            column_data.append([float(x) for x in data])
12        return np.array(column_data).T
13    if FileNotFoundError:
14        print("File not found.")
15
16
17
18 Vertical_displacement = read_displacement_file("C:/Users/danih/OneDrive/Documents/
19         V r 2023/Master/data/20_waveseed/displacement.txt")
20
21 # Make array for vertical displacement for different wave seeds
22 Displacement_waveseed_1=Vertical_displacement[1]
23 Displacement_waveseed_2=Vertical_displacement[3]
24 Displacement_waveseed_3=Vertical_displacement[5]
25 Displacement_waveseed_4=Vertical_displacement[7]
26 Displacement_waveseed_5=Vertical_displacement[9]
27 Displacement_waveseed_6=Vertical_displacement[11]
28 Displacement_waveseed_7=Vertical_displacement[13]
29 Displacement_waveseed_8=Vertical_displacement[15]
30 Displacement_waveseed_9=Vertical_displacement[17]
31 Displacement_waveseed_10=Vertical_displacement[19]
32 Displacement_waveseed_11=Vertical_displacement[21]
33 Displacement_waveseed_12=Vertical_displacement[23]
34 Displacement_waveseed_13=Vertical_displacement[25]
35 Displacement_waveseed_14=Vertical_displacement[27]
36 Displacement_waveseed_15=Vertical_displacement[29]
37 Displacement_waveseed_16=Vertical_displacement[31]
38 Displacement_waveseed_17=Vertical_displacement[33]
39 Displacement_waveseed_18=Vertical_displacement[35]
40 Displacement_waveseed_19=Vertical_displacement[37]
41 Displacement_waveseed_20=Vertical_displacement[39]
42
43 # Calculate velocities
44 def calculate_velocities(displacements, time_intervals):
45     displacement_differences = np.diff(displacements, axis=0)
46
47     velocities = displacement_differences / time_intervals
48
49     return velocities
50
51 time_interval = 0.1
52
53 # Make array for velocity for the different wave seeds
54 velocities_1 = calculate_velocities(Displacement_waveseed_1, time_interval)
55 velocities_2 = calculate_velocities(Displacement_waveseed_2, time_interval)
56 velocities_3 = calculate_velocities(Displacement_waveseed_3, time_interval)
57 velocities_4 = calculate_velocities(Displacement_waveseed_4, time_interval)
58 velocities_5 = calculate_velocities(Displacement_waveseed_5, time_interval)
59 velocities_6 = calculate_velocities(Displacement_waveseed_6, time_interval)
60 velocities_7 = calculate_velocities(Displacement_waveseed_7, time_interval)
61 velocities_8 = calculate_velocities(Displacement_waveseed_8, time_interval)
62 velocities_9 = calculate_velocities(Displacement_waveseed_9, time_interval)
63 velocities_10 = calculate_velocities(Displacement_waveseed_10, time_interval)
64 velocities_11 = calculate_velocities(Displacement_waveseed_11, time_interval)
65 velocities_12 = calculate_velocities(Displacement_waveseed_12, time_interval)
66 velocities_13 = calculate_velocities(Displacement_waveseed_13, time_interval)
67 velocities_14 = calculate_velocities(Displacement_waveseed_14, time_interval)
68 velocities_15 = calculate_velocities(Displacement_waveseed_15, time_interval)
```

```

69 velocities_16 = calculate_velocities(Displacement_waveseed_16, time_interval)
70 velocities_17 = calculate_velocities(Displacement_waveseed_17, time_interval)
71 velocities_18 = calculate_velocities(Displacement_waveseed_18, time_interval)
72 velocities_19 = calculate_velocities(Displacement_waveseed_19, time_interval)
73 velocities_20 = calculate_velocities(Displacement_waveseed_20, time_interval)
74
75
76
77
78 x=np.linspace(0.1, 10800,107999)
79 x2=np.linspace(0, 10800,108000)
80
81
82 plt.figure(figsize=(16, 4), dpi=400)
83 plt.plot(x2, Displacement_waveseed_1, label='waveseed 1')
84 plt.xlabel('Simulation time [s]')
85 plt.ylabel('Vertical displacement at hang-off [m]')
86 plt.title('Vertical displacement of the riser hang-off during 3 hour simulations')
87 plt.legend()
88 plt.grid(True)
89 plt.xlim(0, 10800)
90 plt.show()
91
92 plt.figure(figsize=(16, 4), dpi=400)
93 plt.plot(x2, Displacement_waveseed_2, label='waveseed 2')
94 plt.xlabel('Simulation time [s]')
95 plt.ylabel('Vertical displacement at hang-off [m]')
96 plt.title('Vertical displacement of the riser hang-off during 3 hour simulations')
97 plt.legend()
98 plt.grid(True)
99 plt.xlim(0,10800)
100 plt.show()
101
102
103 # Make array of minimum velocities of different wave seeds
104 Min_velocity_values = np.array([np.min(velocities_1),np.min(velocities_2),
105                                np.min(velocities_3),np.min(velocities_4),
106                                np.min(velocities_5),np.min(velocities_6),
107                                np.min(velocities_7),np.min(velocities_8),
108                                np.min(velocities_9),np.min(velocities_10),
109                                np.min(velocities_11),np.min(velocities_12),
110                                np.min(velocities_13),np.min(velocities_14),
111                                np.min(velocities_15),np.min(velocities_16),
112                                np.min(velocities_17),np.min(velocities_18),
113                                np.min(velocities_19),np.min(velocities_20)])
114
115
116
117 velocity=abs(Min_velocity_values)
118
119 # Sort minimum velocities
120 sorted_values = np.sort(velocity)
121 print(sorted_values)
122
123 # Calculate probabilities
124 n = len(sorted_values)
125 empirical_probabilities = np.arange(1, n+1) / (n+1)
126
127 # Transform probabilities with inverse CDF
128 gumbel_quantiles = gumbel_r.ppf(empirical_probabilities)
129
130 # Calculate percentiles
131 percentiles = empirical_probabilities * 100
132
133 data=abs(Min_velocity_values)
134
135 # Gumbel distribution fitted to velocities
136 params = gumbel_r.fit(data)
137
138 # Find location and scale parameters
139 loc, scale = params
140
141 # Generate range of values for the fitted CDF

```

---

```

142 x = np.linspace(min(data) - 1, max(data) + 1, 1000)
143
144 # Calculate the fitted CDF values
145 fitted_cdf = gumbel_r.cdf(x, loc=loc, scale=scale)
146
147 # Calculate the empirical CDF
148 sorted_data = np.sort(data)
149 empirical_cdf = np.arange(1, len(sorted_data)+1) / len(sorted_data)
150
151 percentile_90 = np.percentile(sorted_data, 10)
152 # Plot the empirical CDF and the fitted Gumbel CDF
153
154 plt.figure(figsize=(10, 8), dpi=300)
155 plt.plot(sorted_data, empirical_cdf, marker='o', linestyle='none', label='Sorted
    vertical velocities')
156 plt.plot(x, fitted_cdf, label='Fitted Gumbel distribution')
157 plt.axhline(0.9, color='r', linestyle='--', linewidth=2, label='90th Percentile')
158 plt.title('Gumbel Distribution to determine the 90th percentile waveseed value')
159 plt.xlabel('Vertical downward velocity')
160 plt.ylabel('Percentile')
161 plt.legend()
162 plt.grid(True)
163 plt.xlim(2.3, 3.1)
164 plt.show()

```

---

## D Python program used to calculate the fatigue life from several wave sectors

```
1 import numpy as np
2 import matplotlib.pyplot as plt
3
4 def read_fatigue_file(file_path):
5     with open(file_path, 'r') as file:
6         lines = file.readlines()
7         column_data = []
8         for line in lines:
9             data = line.strip().split()
10            column_data.append([float(x) for x in data])
11        return np.array(column_data).T
12    if FileNotFoundError:
13        print("File not found.")
14
15
16 # Read fatigue life of riser from different wave directions
17 Fatigue_life = read_fatigue_file("C:/Users/danlh/OneDrive/Documents/V r 2023/
18     Master/data/Fatigue/Fatigue life.txt")
19
20 # MAke arrays for different wave directions
21 Fatigue_life_0_degree=Fatigue_life[13]
22 Fatigue_life_30_degree=Fatigue_life[15]
23 Fatigue_life_60_degree=Fatigue_life[3]
24 Fatigue_life_90_degree=Fatigue_life[1]
25 Fatigue_life_120_degree=Fatigue_life[7]
26 Fatigue_life_150_degree=Fatigue_life[5]
27 Fatigue_life_180_degree=Fatigue_life[9]
28 Fatigue_life_210_degree=Fatigue_life[11]
29 Fatigue_life_240_degree=Fatigue_life[17]
30 Fatigue_life_270_degree=Fatigue_life[19]
31 Fatigue_life_300_degree=Fatigue_life[21]
32 Fatigue_life_330_degree=Fatigue_life[23]
33
34 Placement_on_riser=Fatigue_life[0]
35
36 Sector_probability=np.array([24.50,18.56, 11.61, 12.78, 12.63, 5.67, 2.21, 1.05,
37     0.40, 0.31, 0.58, 9.69])/100
38
39 # Calculate the total fatigue life of the system
40 Total_fatigue_life= Fatigue_life_0_degree*Sector_probability[0]+
41     Fatigue_life_30_degree*Sector_probability[1]+Fatigue_life_60_degree*
42     Sector_probability[2]+Fatigue_life_90_degree*Sector_probability[3]+
43     Fatigue_life_120_degree*Sector_probability[4]+Fatigue_life_150_degree*
44     Sector_probability[5]+Fatigue_life_180_degree*Sector_probability[6]+
45     Fatigue_life_210_degree*Sector_probability[7]+Fatigue_life_240_degree*
46     Sector_probability[8]+Fatigue_life_270_degree*Sector_probability[9]+
47     Fatigue_life_300_degree*Sector_probability[10]+Fatigue_life_330_degree*
48     Sector_probability[11]
49
50 #Find lowest fatigue life
51 print(min(Total_fatigue_life))
52
53 # Plot the total fatigue life of the system
54 plt.figure(figsize=(8, 5), dpi=300)
55 plt.plot(Placement_on_riser, Total_fatigue_life, label='Fatigue life')
56 plt.yscale('log')
57 plt.xlabel('Placement along the riser configuration [m]')
58 plt.ylabel('Fatigue life in years')
59 plt.title('Fatigue life of the SLWR configuration')
60 plt.legend()
61 plt.xlim(-100, 3650)
62 plt.ylim(10**1, 10**14)
63 plt.grid(True)
64 plt.show()
65
66 # Investigate effect of taper section at the hang-off point
67 Fatigue_taper_section = read_fatigue_file("C:/Users/danlh/OneDrive/Documents/V r
68     2023/Master/data/Fatigue/taper.txt")
69 Fatigue_no_taper_section = read_fatigue_file("C:/Users/danlh/OneDrive/Documents/
```

---

```
V r 2023/Master/data/Fatigue/no taper.txt")
59
60
61 plt.figure(figsize=(10, 7), dpi=300)
62 plt.plot(Fatigue_taper_section[0], Fatigue_taper_section[1], label='Fatigue life
with taper section at hang-off')
63 plt.plot(Fatigue_no_taper_section[0], Fatigue_no_taper_section[1], label='Fatigue
life without taper section at hang-off')
64 plt.yscale('log')
65 plt.xlabel('Placement along the riser configuratation [m]')
66 plt.ylabel('Fatigue life in years')
67 plt.title('Fatigue life of the SLWR configurtion near the hang-off with and without
a tapered section')
68 plt.legend()
69 plt.xlim(-10, 500)
70 plt.ylim(10**2, 10**6)
71 plt.grid(True)
72 plt.show()
```

---

## E RAO file used in the SIMA RIFEX program

```
1 *****
2 INPMOD IDENTIFICATION TEXT 4.0
3 *****
4
5
6
7 -----
8 UNIT NAMES SPECIFICATION
9 -----
10 'ut ul um uf grav gcons
11 s m Mg kN / 1.000000
12 *****
13 SUPPORT VESSEL IDENTIFICATION
14 *****
15
16 'idhftr
17 VESSEL
18 -----
19 HFTRANSFER REFERENCE POSITION
20 -----
21 'zg
22 0.000000
23 -----
24 HFTRANSFER CONTROL DATA
25 -----
26 'ndhftr nwhftr isymhf itypin
27 4 19 2 2
28 -----
29 WAVE DIRECTIONS
30 -----
31 'ihead head
32 1 0.000000
33 2 30.000000
34 3 60.000000
35 4 90.000000
36 -----
37 WAVE FREQUENCIES
38 -----
39 'ifreq whftr
40 1 0.200000
41 2 0.262000
42 3 0.273000
43 4 0.279000
44 5 0.286000
45 6 0.299000
46 7 0.314000
47 8 0.349000
48 9 0.393000
49 10 0.449000
50 11 0.483000
51 12 0.524000
52 13 0.571000
53 14 0.628000
54 15 0.698000
55 16 0.785000
56 17 0.900000
57 18 1.000000
58 19 1.200000
59 -----
60 HFTRANSFER FUNCTION SURGE
61 -----
62 'idir ifreq amplitude phase[deg]
63 1 1 1.034000 -90.0059970
64 1 2 0.888000 -90.0360030
65 1 3 0.870000 -90.0309980
66 1 4 0.860000 -90.0319980
67 1 5 0.849000 -90.0339970
68 1 6 0.830000 -90.0380020
69 1 7 0.808000 -90.0449980
70 1 8 0.754000 -90.0660020
71 1 9 0.680000 -90.0999980
```



```

72 1 10 0.5710000 -90.1539990
73 1 11 0.4970000 -90.1890030
74 1 12 0.4020000 -90.1620030
75 1 13 0.2880000 -90.1269990
76 1 14 0.1480000 -89.7040020
77 1 15 1.2000000e-02 69.2549970
78 1 16 0.1640000 85.7509990
79 1 17 0.2380000 83.8270030
80 1 18 0.0000000 0.0000000
81 1 19 0.0000000 0.0000000
82 2 1 0.8950000 -90.0059970
83 2 2 0.7690000 -90.0390010
84 2 3 0.7530000 -90.0339970
85 2 4 0.7450000 -90.0350040
86 2 5 0.7360000 -90.0360030
87 2 6 0.7190000 -90.0410000
88 2 7 0.7000000 -90.0479970
89 2 8 0.6540000 -90.0700000
90 2 9 0.5900000 -90.1070020
91 2 10 0.4980000 -90.1670000
92 2 11 0.4360000 -90.2099990
93 2 12 0.3590000 -90.2210010
94 2 13 0.2680000 -90.2570040
95 2 14 0.1610000 -90.2040020
96 2 15 5.0000001e-02 -89.0189970
97 2 16 3.7000000e-02 85.3310010
98 2 17 4.6999998e-02 87.1530000
99 2 18 0.0000000 0.0000000
100 2 19 0.0000000 0.0000000
101 3 1 0.5170000 -90.0029980
102 3 2 0.4440000 -90.0550000
103 3 3 0.4350000 -90.0429990
104 3 4 0.4300000 -90.0429990
105 3 5 0.4250000 -90.0439990
106 3 6 0.4150000 -90.0490040
107 3 7 0.4040000 -90.0569990
108 3 8 0.3780000 -90.0810010
109 3 9 0.3410000 -90.1220020
110 3 10 0.2880000 -90.1930010
111 3 11 0.2530000 -90.2460020
112 3 12 0.2080000 -90.3050000
113 3 13 0.1560000 -90.3929980
114 3 14 9.6000001e-02 -90.4769970
115 3 15 3.2000002e-02 -90.1169970
116 3 16 1.7999999e-02 86.5210040
117 3 17 2.3000000e-02 88.2720030
118 3 18 0.0000000 0.0000000
119 3 19 0.0000000 0.0000000
120 4 1 0.0000000 0.0000000
121 4 2 0.0000000 -180.0000000
122 4 3 0.0000000 -180.0000000
123 4 4 0.0000000 -180.0000000
124 4 5 0.0000000 -180.0000000
125 4 6 0.0000000 -180.0000000
126 4 7 0.0000000 0.0000000
127 4 8 0.0000000 0.0000000
128 4 9 0.0000000 0.0000000
129 4 10 0.0000000 0.0000000
130 4 11 0.0000000 0.0000000
131 4 12 0.0000000 0.0000000
132 4 13 0.0000000 0.0000000
133 4 14 0.0000000 0.0000000
134 4 15 0.0000000 0.0000000
135 4 16 0.0000000 0.0000000
136 4 17 0.0000000 0.0000000
137 4 18 0.0000000 0.0000000
138 4 19 0.0000000 0.0000000
139 -----
140 HFTRANSFER FUNCTION SWAY
141 -----
142 'idir ifreq amplitude phase[deg]
143 1 1 0.0000000 0.0000000
144 1 2 0.0000000 0.0000000

```

145	1	3	0.0000000	0.0000000
146	1	4	0.0000000	0.0000000
147	1	5	0.0000000	0.0000000
148	1	6	0.0000000	0.0000000
149	1	7	0.0000000	0.0000000
150	1	8	0.0000000	0.0000000
151	1	9	0.0000000	0.0000000
152	1	10	0.0000000	0.0000000
153	1	11	0.0000000	0.0000000
154	1	12	0.0000000	0.0000000
155	1	13	0.0000000	0.0000000
156	1	14	0.0000000	0.0000000
157	1	15	0.0000000	0.0000000
158	1	16	0.0000000	0.0000000
159	1	17	0.0000000	0.0000000
160	1	18	0.0000000	0.0000000
161	1	19	0.0000000	0.0000000
162	2	1	0.5110000	-90.0000000
163	2	2	0.4290000	-89.9769970
164	2	3	0.4180000	-89.9700010
165	2	4	0.4130000	-89.9660030
166	2	5	0.4060000	-89.9609990
167	2	6	0.3950000	-89.9469990
168	2	7	0.3820000	-89.9300000
169	2	8	0.3520000	-89.8759990
170	2	9	0.3120000	-89.7730030
171	2	10	0.2560000	-89.5800020
172	2	11	0.2200000	-89.4290010
173	2	12	0.1780000	-88.9980010
174	2	13	0.1290000	-88.6409990
175	2	14	7.59999998e-02	-88.0500030
176	2	15	2.4000000e-02	-85.6340030
177	2	16	1.3000000e-02	83.2080000
178	2	17	1.3000000e-02	83.9469990
179	2	18	0.0000000	0.0000000
180	2	19	0.0000000	0.0000000
181	3	1	0.8840000	-90.0019990
182	3	2	0.7420000	-89.9800030
183	3	3	0.7230000	-89.9730000
184	3	4	0.7140000	-89.9690020
185	3	5	0.7030000	-89.9649960
186	3	6	0.6830000	-89.9509960
187	3	7	0.6610000	-89.9329990
188	3	8	0.6080000	-89.8769990
189	3	9	0.5360000	-89.7659990
190	3	10	0.4370000	-89.5420000
191	3	11	0.3730000	-89.3519970
192	3	12	0.2940000	-88.9580000
193	3	13	0.2060000	-88.4120030
194	3	14	0.1090000	-87.1269990
195	3	15	1.4000000e-02	-71.2740020
196	3	16	5.29999999e-02	86.0609970
197	3	17	4.6000000e-02	87.8079990
198	3	18	0.0000000	0.0000000
199	3	19	0.0000000	0.0000000
200	4	1	1.0210000	-90.0039980
201	4	2	0.8560000	-89.9850010
202	4	3	0.8350000	-89.9789960
203	4	4	0.8230000	-89.9759980
204	4	5	0.8110000	-89.9710010
205	4	6	0.7880000	-89.9580000
206	4	7	0.7620000	-89.9410020
207	4	8	0.7000000	-89.8850020
208	4	9	0.6160000	-89.7720030
209	4	10	0.4970000	-89.5360030
210	4	11	0.4200000	-89.3229980
211	4	12	0.3210000	-88.9479980
212	4	13	0.2100000	-88.2070010
213	4	14	7.9000004e-02	-85.1169970
214	4	15	6.4000003e-02	83.9670030
215	4	16	0.1900000	87.3529970
216	4	17	0.2390000	85.9560010
217	4	18	0.0000000	0.0000000

```

218 4 19 0.0000000 0.0000000
219 |-----|
220 HFTRANSFER FUNCTION HEAVE
221 |-----|
222 'idir ifreq amplitude phase[deg]
223 1 1 1.1260000 -0.1420000
224 1 2 1.2760000 -150.7059900
225 1 3 0.1280000 -99.5630040
226 1 4 0.1860000 -25.1089990
227 1 5 0.3000000 -10.1750000
228 1 6 0.4180000 -4.6050000
229 1 7 0.4820000 -2.8350000
230 1 8 0.5230000 -1.6790000
231 1 9 0.5030000 -1.3240000
232 1 10 0.4360000 -1.1930000
233 1 11 0.3850000 -1.1510000
234 1 12 0.3220000 -3.8269999
235 1 13 0.2430000 -3.9040000
236 1 14 0.1530000 -3.8020000
237 1 15 6.1999999e-02 -3.1740000
238 1 16 8.9999996e-03 173.4070000
239 1 17 3.4000002e-02 177.4340100
240 1 18 0.0000000 0.0000000
241 1 19 0.0000000 0.0000000
242 2 1 1.1270000 -0.1430000
243 2 2 1.2900000 -150.8470000
244 2 3 0.1300000 -102.4380000
245 2 4 0.1810000 -26.0040000
246 2 5 0.2950000 -10.4070000
247 2 6 0.4140000 -4.6820002
248 2 7 0.4780000 -2.8770001
249 2 8 0.5200000 -1.7040000
250 2 9 0.4990000 -1.3450000
251 2 10 0.4310000 -1.2150000
252 2 11 0.3800000 -1.1750000
253 2 12 0.3190000 -3.2079999
254 2 13 0.2410000 -3.2800000
255 2 14 0.1550000 -3.2770000
256 2 15 7.0000000e-02 -3.2850001
257 2 16 4.9999999e-03 -11.7540000
258 2 17 1.8999999e-02 -177.4190100
259 2 18 0.0000000 0.0000000
260 2 19 0.0000000 0.0000000
261 3 1 1.1280000 -0.1460000
262 3 2 1.3160000 -151.1130100
263 3 3 0.1340000 -107.6550000
264 3 4 0.1720000 -27.8370000
265 3 5 0.2860000 -10.8620000
266 3 6 0.4060000 -4.8280001
267 3 7 0.4710000 -2.9549999
268 3 8 0.5120000 -1.7450000
269 3 9 0.4900000 -1.3720000
270 3 10 0.4200000 -1.2220000
271 3 11 0.3670000 -1.1600000
272 3 12 0.3040000 -1.8350000
273 3 13 0.2230000 -1.7270000
274 3 14 0.1330000 -1.3620000
275 3 15 4.3000001e-02 0.3340000
276 3 16 2.4000000e-02 175.2410000
277 3 17 4.1000001e-02 178.4350000
278 3 18 0.0000000 0.0000000
279 3 19 0.0000000 0.0000000
280 4 1 1.1289999 -0.1480000
281 4 2 1.3279999 -151.2430000
282 4 3 0.1370000 -110.0190000
283 4 4 0.1680000 -28.7610000
284 4 5 0.2820000 -11.0790000
285 4 6 0.4020000 -4.8930001
286 4 7 0.4670000 -2.9879999
287 4 8 0.5080000 -1.7589999
288 4 9 0.4850000 -1.3760000
289 4 10 0.4130000 -1.2040000
290 4 11 0.3580000 -1.1140000

```

```

291 4 12 0.2910000 -1.0880001
292 4 13 0.2060000 -0.7990000
293 4 14 0.1060000 0.2290000
294 4 15 4.0000002e-03 83.6100010
295 4 16 8.6999997e-02 176.0300000
296 4 17 0.1170000 177.5010100
297 4 18 0.0000000 0.0000000
298 4 19 0.0000000 0.0000000

```

```

-----
300 HFTRANSFER FUNCTION ROLL
-----

```

```

302 |idir ifreq amplitude phase[deg]
303 | 1 1 0.0000000 0.0000000
304 | 1 2 0.0000000 0.0000000
305 | 1 3 0.0000000 0.0000000
306 | 1 4 0.0000000 0.0000000
307 | 1 5 0.0000000 0.0000000
308 | 1 6 0.0000000 0.0000000
309 | 1 7 0.0000000 0.0000000
310 | 1 8 0.0000000 0.0000000
311 | 1 9 0.0000000 0.0000000
312 | 1 10 0.0000000 0.0000000
313 | 1 11 0.0000000 0.0000000
314 | 1 12 0.0000000 0.0000000
315 | 1 13 0.0000000 0.0000000
316 | 1 14 0.0000000 0.0000000
317 | 1 15 0.0000000 0.0000000
318 | 1 16 0.0000000 0.0000000
319 | 1 17 0.0000000 0.0000000
320 | 1 18 0.0000000 0.0000000
321 | 1 19 0.0000000 0.0000000
322 | 2 1 0.2980000 -90.2669980
323 | 2 2 0.3000000 -90.3919980
324 | 2 3 0.2980000 -90.4189990
325 | 2 4 0.2960000 -90.4329990
326 | 2 5 0.2940000 -90.4469990
327 | 2 6 0.2890000 -90.4960020
328 | 2 7 0.2830000 -90.5479970
329 | 2 8 0.2660000 -90.6770020
330 | 2 9 0.2400000 -90.8550030
331 | 2 10 0.2030000 -91.0820010
332 | 2 11 0.1790000 -91.2040020
333 | 2 12 0.1510000 -93.0899960
334 | 2 13 0.1170000 -93.3649980
335 | 2 14 7.9999998e-02 -93.4769970
336 | 2 15 4.1999999e-02 -93.1019970
337 | 2 16 1.2000000e-02 -90.7590030
338 | 2 17 3.0000000e-03 80.7990040
339 | 2 18 0.0000000 0.0000000
340 | 2 19 0.0000000 0.0000000
341 | 3 1 0.5100000 -90.2720030
342 | 3 2 0.5150000 -90.4110030
343 | 3 3 0.5110000 -90.4410020
344 | 3 4 0.5080000 -90.4570010
345 | 3 5 0.5050000 -90.4739990
346 | 3 6 0.4970000 -90.5289990
347 | 3 7 0.4870000 -90.5889970
348 | 3 8 0.4590000 -90.7429960
349 | 3 9 0.4180000 -90.9660030
350 | 3 10 0.3590000 -91.2789990
351 | 3 11 0.3210000 -91.4710010
352 | 3 12 0.2790000 -92.4179990
353 | 3 13 0.2260000 -92.7669980
354 | 3 14 0.1670000 -93.1149980
355 | 3 15 0.1050000 -93.3820040
356 | 3 16 4.8000000e-02 -93.4440000
357 | 3 17 8.9999996e-03 -93.3079990
358 | 3 18 0.0000000 0.0000000
359 | 3 19 0.0000000 0.0000000
360 | 4 1 0.5860000 -90.2699970
361 | 4 2 0.5920000 -90.4160000
362 | 4 3 0.5870000 -90.4479980
363 | 4 4 0.5840000 -90.4649960

```

```

364 4 5 0.5800000 -90.4830020
365 4 6 0.5720000 -90.5420000
366 4 7 0.5610000 -90.6070020
367 4 8 0.5290000 -90.7740020
368 4 9 0.4830000 -91.0199970
369 4 10 0.4180000 -91.3769990
370 4 11 0.3770000 -91.6060030
371 4 12 0.3310000 -92.0390010
372 4 13 0.2730000 -92.4039990
373 4 14 0.2070000 -92.8259960
374 4 15 0.1350000 -93.2809980
375 4 16 6.4999998e-02 -93.7740020
376 4 17 1.1000000e-02 -96.1299970
377 4 18 0.0000000 0.0000000
378 4 19 0.0000000 0.0000000

```

```

379 -----
380 HFTRANSFER FUNCTION PITCH
381 -----

```

```

382 'idir ifreq amplitude phase[deg]
383 1 1 0.5200000 87.7310030
384 1 2 0.5590000 91.5410000
385 1 3 0.5630000 90.0820010
386 1 4 0.5610000 89.8349990
387 1 5 0.5590000 89.6689990
388 1 6 0.5520000 89.4700010
389 1 7 0.5430000 89.3320010
390 1 8 0.5130000 89.0999980
391 1 9 0.4670000 88.8229980
392 1 10 0.4000000 88.4479980
393 1 11 0.3560000 88.2170030
394 1 12 0.3020000 85.6470030
395 1 13 0.2410000 85.0630040
396 1 14 0.1710000 84.4830020
397 1 15 9.7999997e-02 84.0080030
398 1 16 3.4000002e-02 83.5459980
399 1 17 6.0000001e-03 -91.6770020
400 1 18 0.0000000 0.0000000
401 1 19 0.0000000 0.0000000
402 2 1 0.4520000 87.4580000
403 2 2 0.4850000 91.8860020
404 2 3 0.4890000 90.1999970
405 2 4 0.4880000 89.9170000
406 2 5 0.4850000 89.7279970
407 2 6 0.4800000 89.5100020
408 2 7 0.4710000 89.3659970
409 2 8 0.4450000 89.1380000
410 2 9 0.4040000 88.8820040
411 2 10 0.3430000 88.5550000
412 2 11 0.3040000 88.3669970
413 2 12 0.2570000 86.4759980
414 2 13 0.2030000 86.1019970
415 2 14 0.1430000 85.8369980
416 2 15 8.2000002e-02 85.9020000
417 2 16 3.2000002e-02 86.7450030
418 2 17 3.0000000e-03 90.2760010
419 2 18 0.0000000 0.0000000
420 2 19 0.0000000 0.0000000
421 3 1 0.2640000 85.9380040
422 3 2 0.2790000 93.7419970
423 3 3 0.2830000 90.7900010
424 3 4 0.2830000 90.3079990
425 3 5 0.2820000 89.9940030
426 3 6 0.2780000 89.6660000
427 3 7 0.2730000 89.4710010
428 3 8 0.2570000 89.2230000
429 3 9 0.2310000 89.0019990
430 3 10 0.1930000 88.7710040
431 3 11 0.1690000 88.6699980
432 3 12 0.1380000 88.0120010
433 3 13 0.1040000 88.0189970
434 3 14 6.4999998e-02 88.4280010
435 3 15 2.6000001e-02 90.6780010
436 3 16 4.9999999e-03 -109.4060000

```

```

437 3 17 1.7000001e-02 -95.3580020
438 3 18 0.0000000 0.0000000
439 3 19 0.0000000 0.0000000
440 4 1 1.7000001e-02 0.1760000
441 4 2 2.2000000e-02 -159.5020000
442 4 3 7.0000002e-03 -168.1759900
443 4 4 4.0000002e-03 -169.3300000
444 4 5 3.0000000e-03 -169.8880000
445 4 6 1.0000000e-03 -169.3560000
446 4 7 1.0000000e-03 0.0000000
447 4 8 0.0000000 0.0000000
448 4 9 0.0000000 0.0000000
449 4 10 0.0000000 0.0000000
450 4 11 0.0000000 0.0000000
451 4 12 0.0000000 0.0000000
452 4 13 0.0000000 0.0000000
453 4 14 0.0000000 0.0000000
454 4 15 0.0000000 0.0000000
455 4 16 0.0000000 0.0000000
456 4 17 0.0000000 0.0000000
457 4 18 0.0000000 0.0000000
458 4 19 0.0000000 0.0000000

```

-----  
HFTRANSFER FUNCTION YAW  
-----

```

461 |-----|
462 |idir ifreq amplitude phase[deg]|
463 | 1 1 0.0000000 0.0000000|
464 | 1 2 0.0000000 0.0000000|
465 | 1 3 0.0000000 0.0000000|
466 | 1 4 0.0000000 0.0000000|
467 | 1 5 0.0000000 0.0000000|
468 | 1 6 0.0000000 0.0000000|
469 | 1 7 0.0000000 0.0000000|
470 | 1 8 0.0000000 0.0000000|
471 | 1 9 0.0000000 0.0000000|
472 | 1 10 0.0000000 0.0000000|
473 | 1 11 0.0000000 0.0000000|
474 | 1 12 0.0000000 0.0000000|
475 | 1 13 0.0000000 0.0000000|
476 | 1 14 0.0000000 0.0000000|
477 | 1 15 0.0000000 0.0000000|
478 | 1 16 0.0000000 0.0000000|
479 | 1 17 0.0000000 0.0000000|
480 | 1 18 0.0000000 0.0000000|
481 | 1 19 0.0000000 0.0000000|
482 | 2 1 7.2999999e-02 178.7039900|
483 | 2 2 6.4000003e-02 178.2410000|
484 | 2 3 6.3000001e-02 178.1369900|
485 | 2 4 6.3000001e-02 178.0860000|
486 | 2 5 6.1999999e-02 178.0300000|
487 | 2 6 6.1000001e-02 177.8370100|
488 | 2 7 5.9999999e-02 177.6260100|
489 | 2 8 5.7000000e-02 177.0939900|
490 | 2 9 5.4000001e-02 176.3750000|
491 | 2 10 4.8999999e-02 175.5610000|
492 | 2 11 4.6000000e-02 175.2240000|
493 | 2 12 4.3000001e-02 174.8820000|
494 | 2 13 3.9999999e-02 174.9579900|
495 | 2 14 3.7999999e-02 175.2640100|
496 | 2 15 3.5999998e-02 175.3170000|
497 | 2 16 3.5000000e-02 173.8560000|
498 | 2 17 3.0999999e-02 169.4780000|
499 | 2 18 0.0000000 0.0000000|
500 | 2 19 0.0000000 0.0000000|
501 | 3 1 7.1999997e-02 178.0200000|
502 | 3 2 6.1000001e-02 177.6349900|
503 | 3 3 5.9000000e-02 177.5340000|
504 | 3 4 5.7999998e-02 177.4810000|
505 | 3 5 5.7000000e-02 177.4230000|
506 | 3 6 5.6000002e-02 177.2059900|
507 | 3 7 5.4000001e-02 176.9520000|
508 | 3 8 4.8000000e-02 176.2079900|
509 | 3 9 3.9999999e-02 174.8620000|

```

---

```
510 3 10 2.8000001e-02 172.0440100
511 3 11 2.0000000e-02 168.8780100
512 3 12 8.9999996e-03 156.5010100
513 3 13 4.9999999e-03 38.2160000
514 3 14 1.7000001e-02 5.2179999
515 3 15 3.0999999e-02 -0.7770000
516 3 16 3.9999999e-02 -4.3360000
517 3 17 3.7999999e-02 -8.4650002
518 3 18 0.0000000 0.0000000
519 3 19 0.0000000 0.0000000
520 4 1 2.0000001e-03 90.0889970
521 4 2 2.0000001e-03 90.2279970
522 4 3 1.0000000e-03 90.2590030
523 4 4 1.0000000e-03 90.2740020
524 4 5 1.0000000e-03 90.2920000
525 4 6 1.0000000e-03 90.3420030
526 4 7 1.0000000e-03 90.3970030
527 4 8 1.0000000e-03 90.5400010
528 4 9 1.0000000e-03 90.7399980
529 4 10 1.0000000e-03 91.0029980
530 4 11 0.0000000 180.0000000
531 4 12 0.0000000 0.0000000
532 4 13 0.0000000 0.0000000
533 4 14 0.0000000 0.0000000
534 4 15 0.0000000 0.0000000
535 4 16 0.0000000 0.0000000
536 4 17 0.0000000 0.0000000
537 4 18 0.0000000 0.0000000
538 4 19 0.0000000 0.0000000
539 '*****
540 END
541 '*****
```

## F Parametric study ULS limit state results

### F.1 Buoyancy module geometry 1

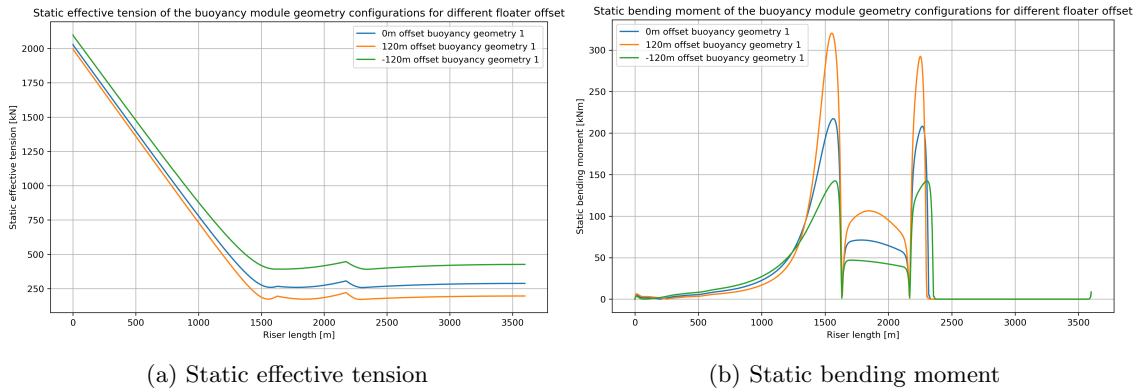


Figure 73: Static results

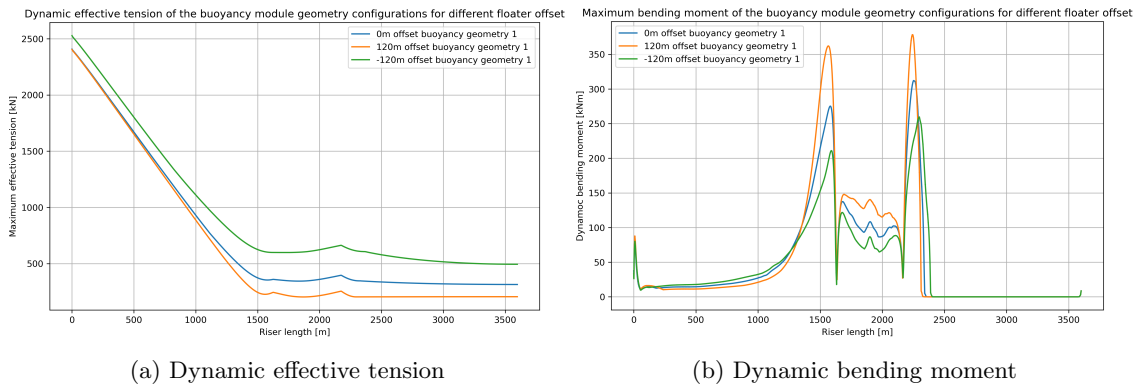


Figure 74: Dynamic results

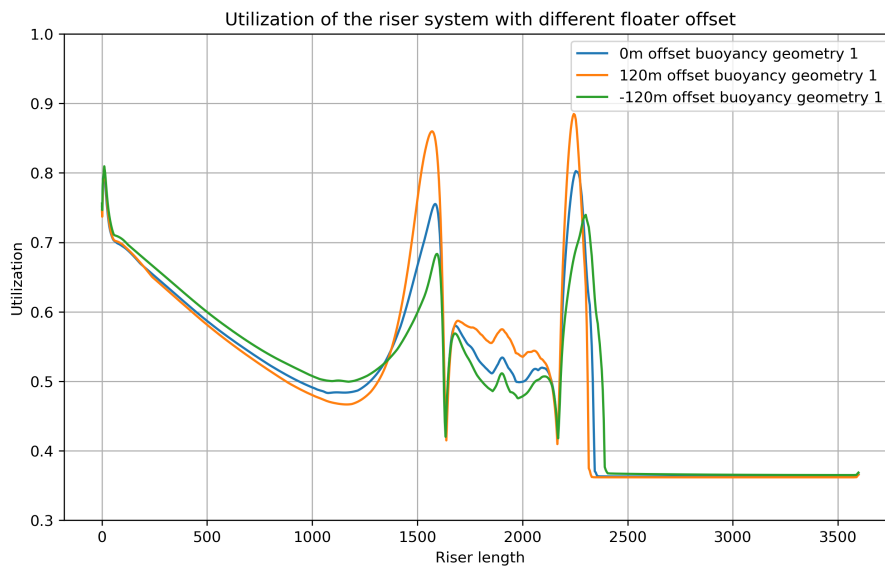


Figure 75: Utilization of buoyancy module geometry for different offsets



---

	<b>Maximum value in riser</b>	<b>Location on the riser</b>
Static bending moment	217.4 kNm	In the sag bend
Static effective tension	2029.3 kN	At the hang-off
Dynamic bending moment	312.0 kNm	At the TDP
Dynamic effective tension	2407.9 kN	At the hang-off
Utilization	0.803	Near the hang-off

Table 25: Summary of the loads and utilization of the mean offset

	<b>Maximum value in riser</b>	<b>Location on the riser</b>
Static bending moment	320.4 kNm	In the sag bend
Static effective tension	1997.5 kN	At the hang-off
Dynamic bending moment	378.4 kNm	At the TDP
Dynamic effective tension	2403.5 kN	At the hang-off
Utilization	0.885	At the TDP

Table 26: Summary of the loads and utilization of the near offset

	<b>Maximum value in riser</b>	<b>Location on the riser</b>
Static bending moment	142.5 kNm	In the sag bend
Static effective tension	2098.8 kN	At the hang-off
Dynamic bending moment	259.6 kNm	At the TDP
Dynamic effective tension	2528.0 kN	At the hang-off
Utilization	0.810	Near the hang-off

Table 27: Summary of the loads and utilization of the far offset

## F.2 Buoyancy module geometry 2

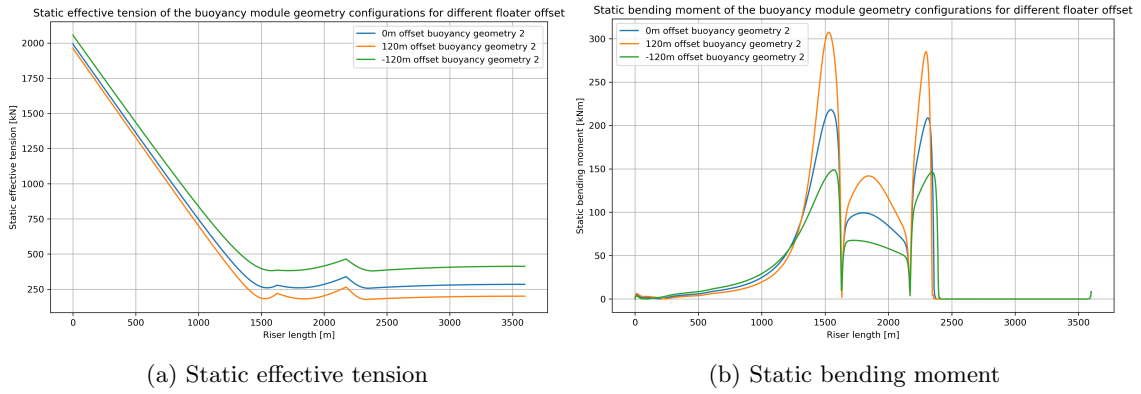


Figure 76: Static results

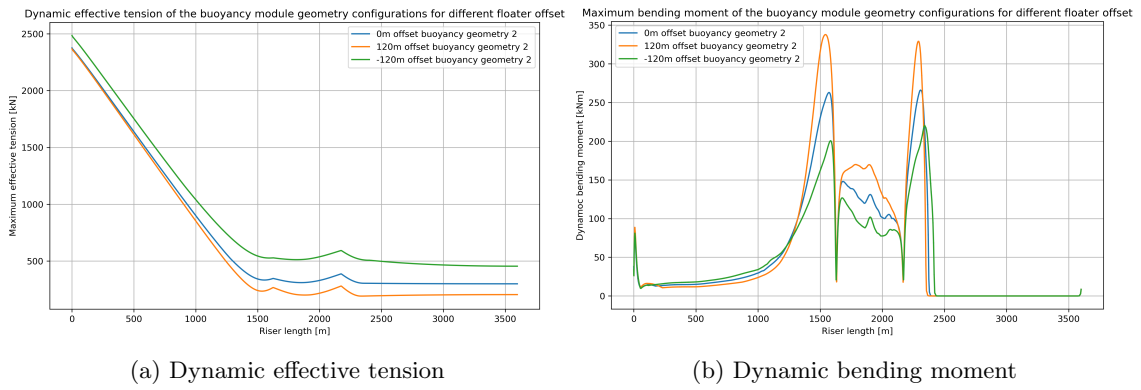


Figure 77: Dynamic results

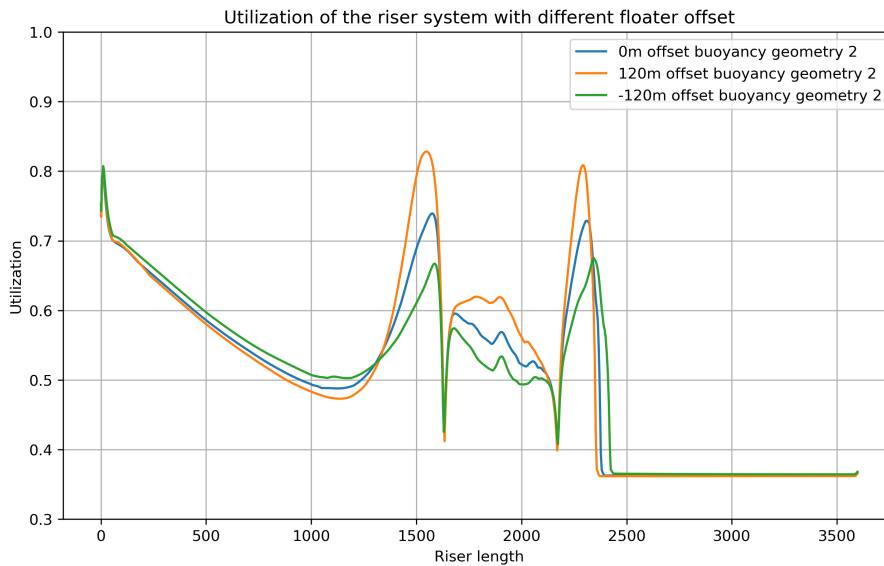


Figure 78: Utilization of buoyancy module geometry for different offsets

---

	<b>Maximum value in riser</b>	<b>Location on the riser</b>
Static bending moment	218.2 kNm	In the sag bend
Static effective tenison	1993.8 kN	At the hang-off
Dynamic bending moment	265.9 kNm	AT the TDP
Dynamic effective tension	2375.9 kN	At the hang-off
Utilization	0.797	Near the hang-off

Table 28: Summary of the loads and utilization of the mean offset

	<b>Maximum value in riser</b>	<b>Location on the riser</b>
Static bending moment	307.4 kNm	In the sag bend
Static effective tenison	1963.9 kN	At the hang-off
Dynamic bending moment	337.7 kNm	At the TDP
Dynamic effective tension	2366.2 kN	At the hang-off
Utilization	0.828	At the TDP

Table 29: Summary of the loads and utilization of the near offset

	<b>Maximum value in riser</b>	<b>Location on the riser</b>
Static bending moment	148.6 kNm	In the sag bend
Static effective tenison	2057.2 kN	At the hang-off
Dynamic bending moment	220.4 kNm	At the TDP
Dynamic effective tension	2485.1kN	At the hang-off
Utilization	0.807	Near the hang-off

Table 30: Summary of the loads and utilization of the far offset

### F.3 Buoyancy module geometry 3

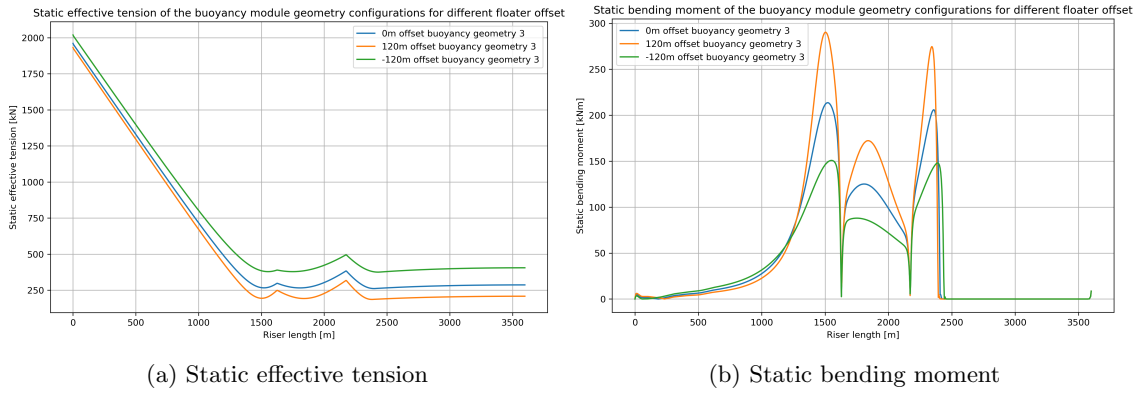


Figure 79: Static results

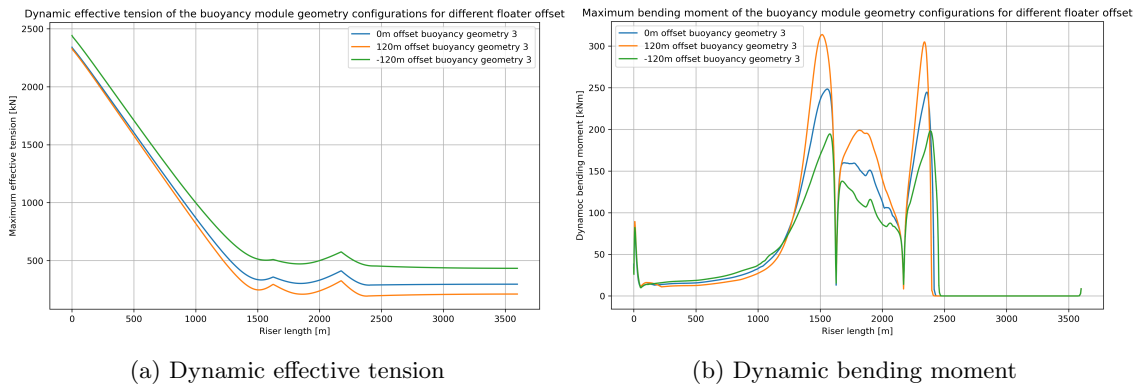


Figure 80: Dynamic results

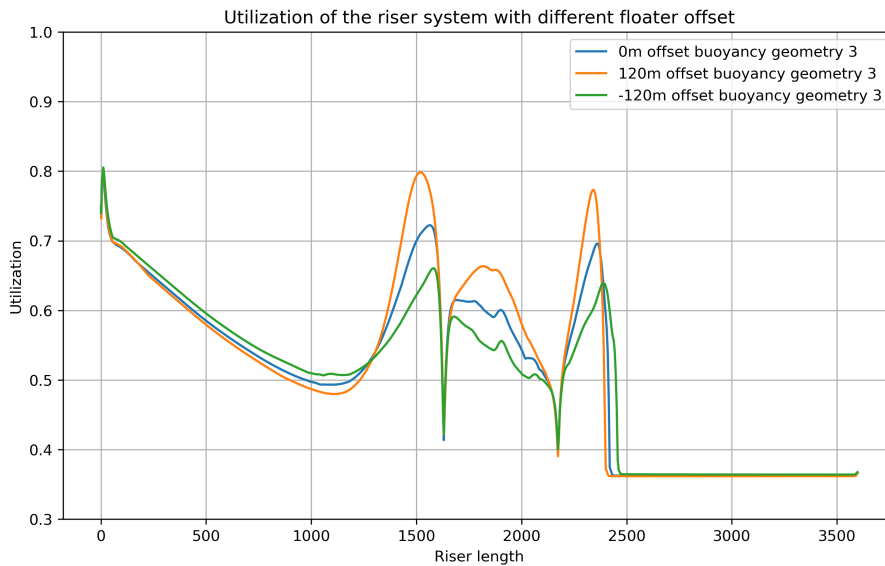


Figure 81: Utilization of buoyancy module geometry for different offsets

---

	<b>Maximum value in riser</b>	<b>Location on the riser</b>
Static bending moment	213.8 kNm	In the sag bend
Static effective tension	1960.8 kN	At the hang-off
Dynamic bending moment	248.4 kNm	In the sag bend
Dynamic effective tension	2341.3 kN	At the hang-off
Utilization	0.796	Near the hang-off

Table 31: Summary of the loads and utilization of the mean offset

	<b>Maximum value in riser</b>	<b>Location on the riser</b>
Static bending moment	290.3 kNm	In the sag bend
Static effective tension	1931.8 kN	At the hang-off
Dynamic bending moment	313.8 kNm	In the sag bend
Dynamic effective tension	2341.2 kN	At the hang-off
Utilization	0.805	Near the hang-off

Table 32: Summary of the loads and utilization of the near offset

	<b>Maximum value in riser</b>	<b>Location on the riser</b>
Static bending moment	150.8 kNm	In the sag bend
Static effective tension	2019.2 kN	At the hang-off
Dynamic bending moment	197.7 kNm	At the TDP
Dynamic effective tension	2442.6 kN	At the hang-off
Utilization	0.805	Near the hang-off

Table 33: Summary of the loads and utilization of the far offset

## F.4 Buoyancy module geometry 4

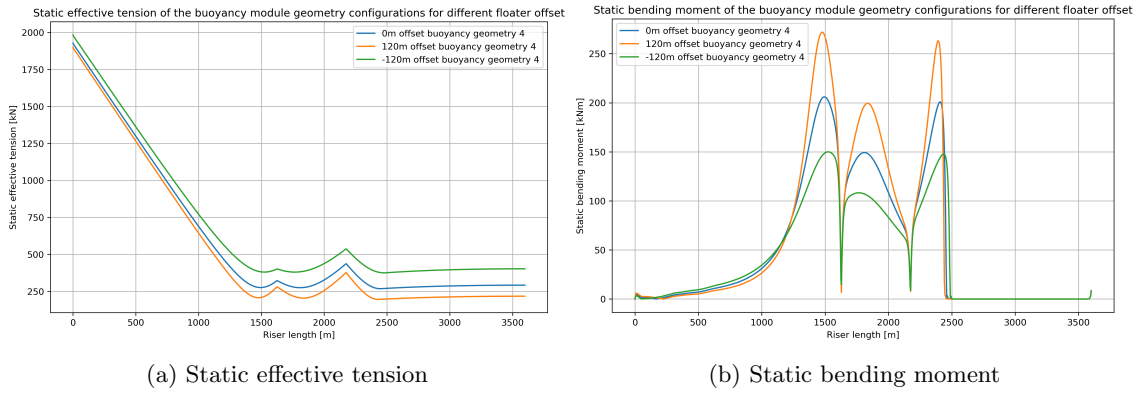


Figure 82: Static results

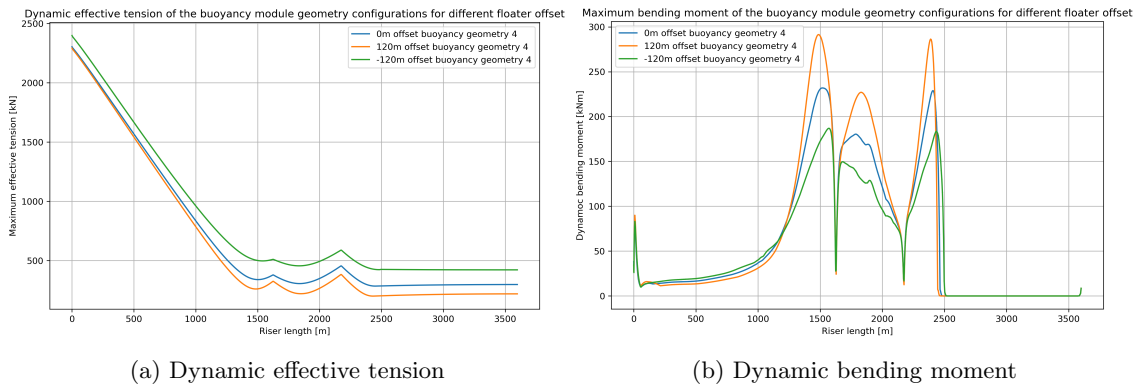


Figure 83: Dynamic results

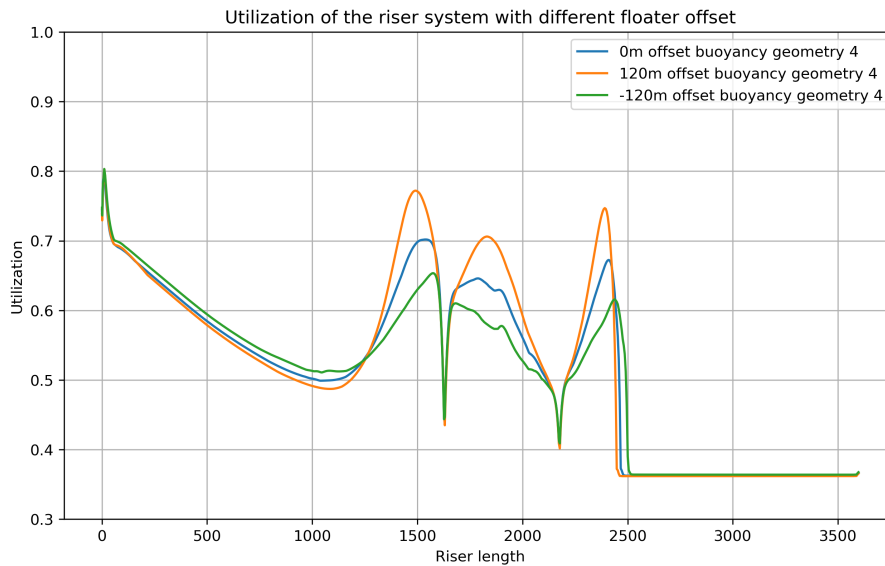


Figure 84: Utilization of buoyancy module geometry for different offsets

---

	<b>Maximum value in riser</b>	<b>Location on the riser</b>
Static bending moment	206.0 kNm	In the sag bend
Static effective tenison	1928.3 kN	At the hang-off
Dynamic bending moment	231.9 kNm	In the sag bend
Dynamic effective tension	2304.2 kN	At the hang-off
Utilization	0.794	Near the hang-off

Table 34: Summary of the loads and utilization of the mean offset

	<b>Maximum value in riser</b>	<b>Location on the riser</b>
Static bending moment	271.9 kNm	In the sag bend
Static effective tenison	1899.4 kN	At the hang-off
Dynamic bending moment	291.4 kNm	In the sag bend
Dynamic effective tension	2291.8 kN	At the hang-off
Utilization	0.803	Near the hang-off

Table 35: Summary of the loads and utilization of the near offset

	<b>Maximum value in riser</b>	<b>Location on the riser</b>
Static bending moment	150.0 kNm	In the sag bend
Static effective tenison	1983.1 kN	At the hang-off
Dynamic bending moment	186.9 kNm	In the sag bend
Dynamic effective tension	2399.0 kN	At the hang-off
Utilization	0.803	Near the hang-off

Table 36: Summary of the loads and utilization of the far offset

## F.5 Buoyancy module geometry 5

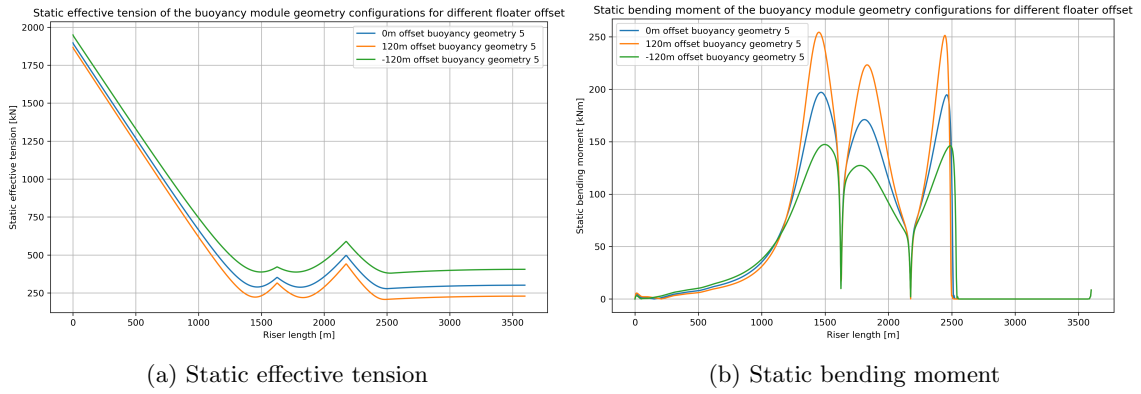


Figure 85: Static results

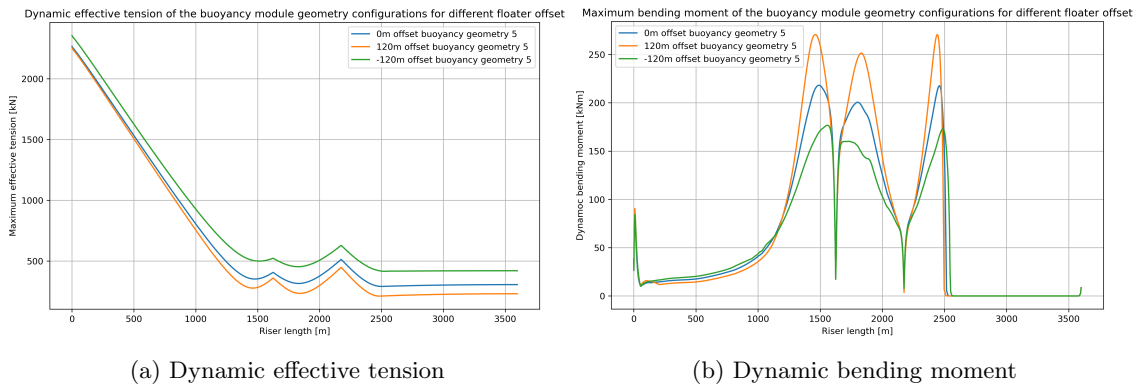


Figure 86: Dynamic results

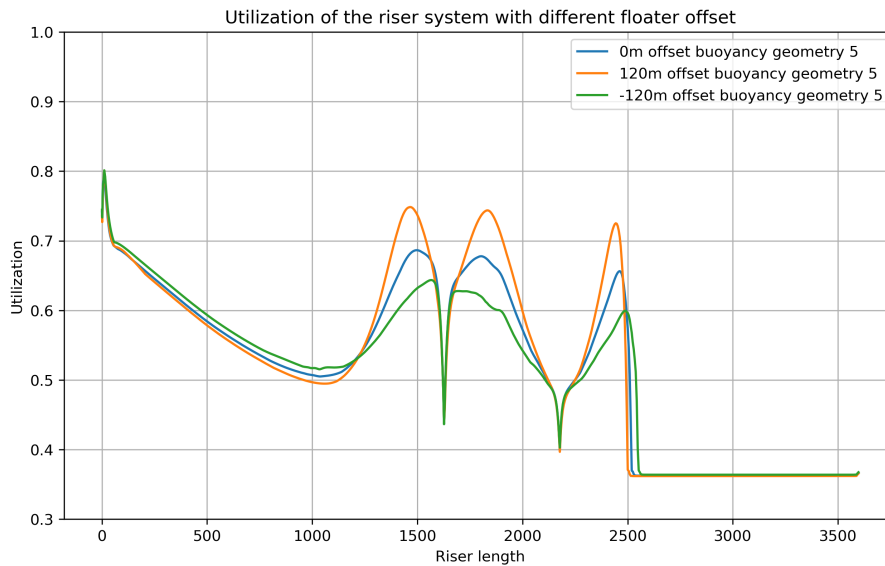


Figure 87: Utilization of buoyancy module geometry for different offsets



---

	<b>Maximum value in riser</b>	<b>Location on the riser</b>
Static bending moment	197.0 kNm	In the sag bend
Static effective tension	1896.6 kN	At the hang-off
Dynamic bending moment	218.1 kNm	In the sag bend
Dynamic effective tension	2267.8 kN	At the hang-off
Utilization	0.791	Near the hang-off

Table 37: Summary of the loads and utilization of the mean offset

	<b>Maximum value in riser</b>	<b>Location on the riser</b>
Static bending moment	254.3 kNm	In the sag bend
Static effective tension	1867.4 kN	At the hang-off
Dynamic bending moment	270.6 kNm	In the sag bend
Dynamic effective tension	2254.7 kN	At the hang-off
Utilization	0.801	Near the hang-off

Table 38: Summary of the loads and utilization of the near offset

	<b>Maximum value in riser</b>	<b>Location on the riser</b>
Static bending moment	147.3 kNm	In the sag bend
Static effective tension	1949.0 kN	At the hang-off
Dynamic bending moment	176.7 kNm	In the sag bend
Dynamic effective tension	2356.9 kN	At the hang-off
Utilization	0.801	Near the hang-off

Table 39: Summary of the loads and utilization of the far offset

## F.6 Buoyancy section length 500 meters

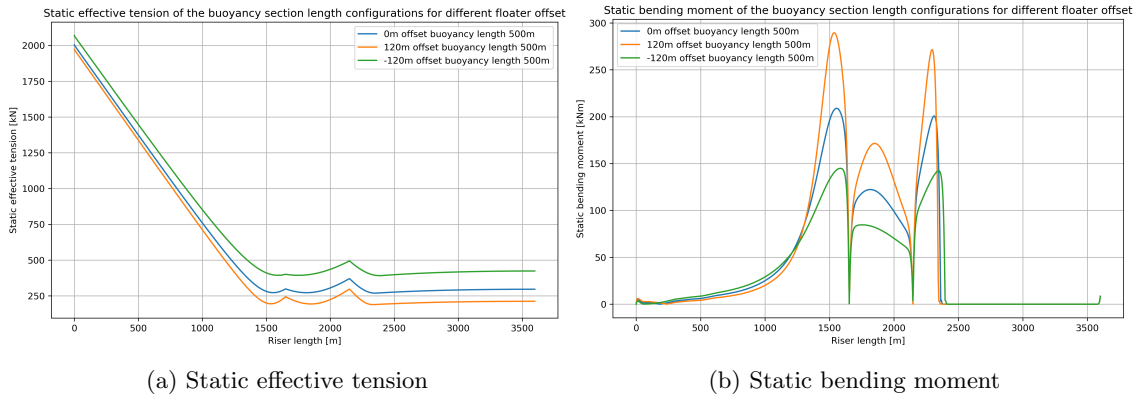


Figure 88: Static results

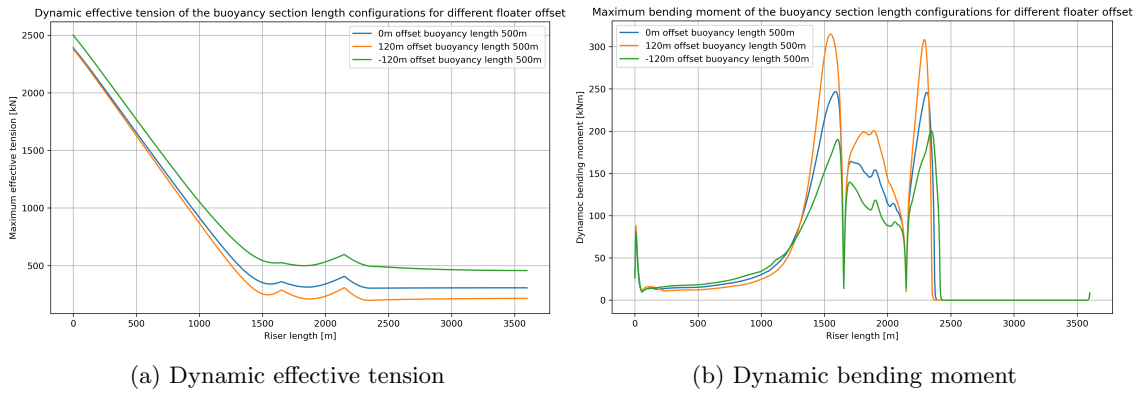


Figure 89: Dynamic results

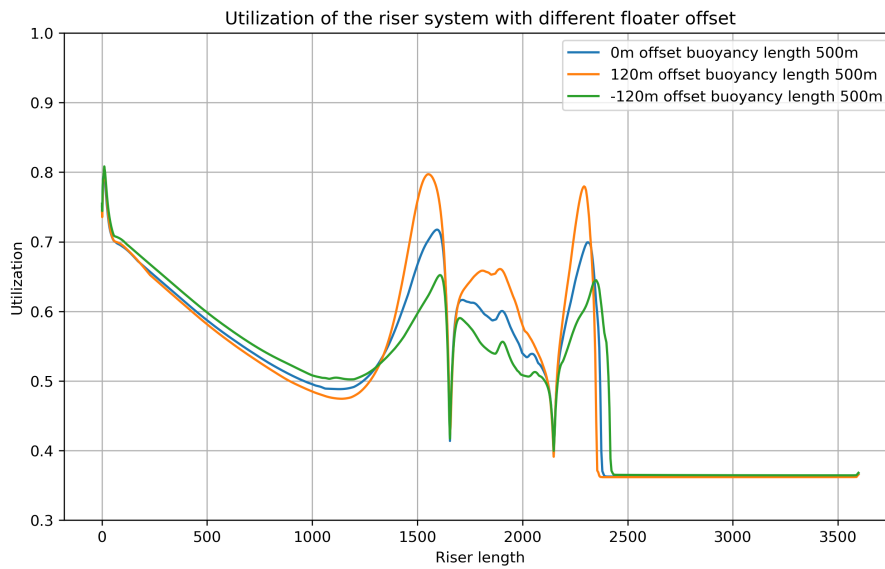


Figure 90: Utilization of buoyancy section length for different offsets

---

	<b>Maximum value in riser</b>	<b>Location on the riser</b>
Static bending moment	208.9 kNm	In the sag bend
Static effective tension	2005.4 kN	At the hang-off
Dynamic bending moment	246.9 kNm	In the sag bend
Dynamic effective tension	2391.3 kN	At the hang-off
Utilization	0.798	Near the hang-off

Table 40: Summary of the loads and utilization of the mean offset

	<b>Maximum value in riser</b>	<b>Location on the riser</b>
Static bending moment	289.4 kNm	In the sag bend
Static effective tension	1974.1 kN	At the hang-off
Dynamic bending moment	314.9 kNm	In the sag bend
Dynamic effective tension	2379.3 kN	At the hang-off
Utilization	0.807	Near the hang-off

Table 41: Summary of the loads and utilization of the near offset

	<b>Maximum value in riser</b>	<b>Location on the riser</b>
Static bending moment	144.9 kNm	In the sag bend
Static effective tension	2069.6 kN	At the hang-off
Dynamic bending moment	200.6 kNm	At the TDP
Dynamic effective tension	2501.1 kN	At the hang-off
Utilization	0.807	Near the hang-off

Table 42: Summary of the loads and utilization of the far offset

## F.7 Buoyancy section length 525 meters

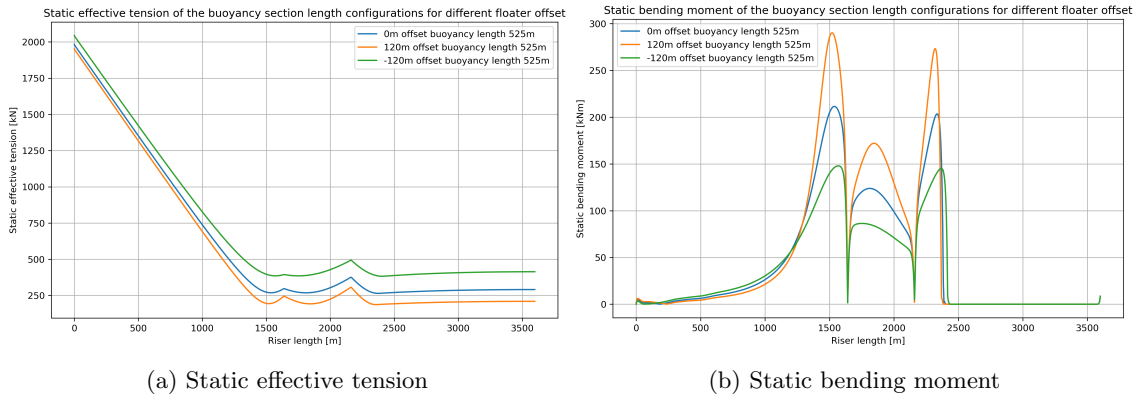


Figure 91: Static results

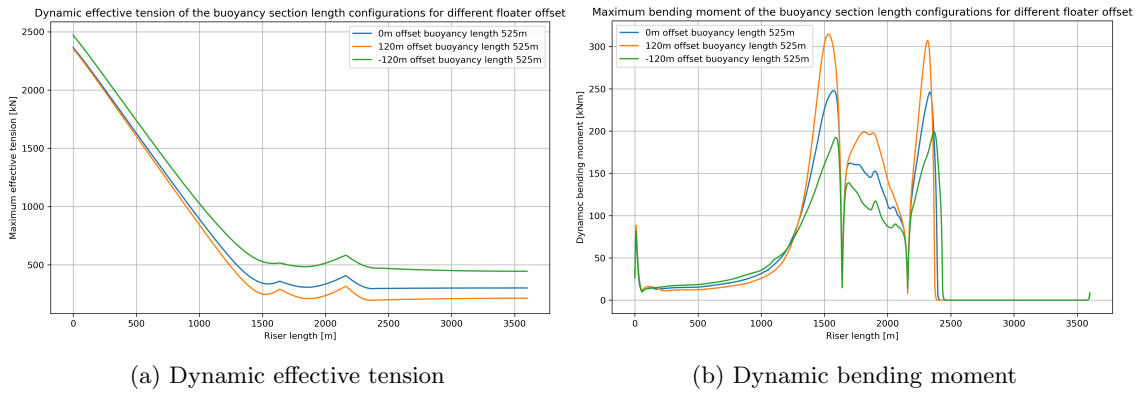


Figure 92: Dynamic results

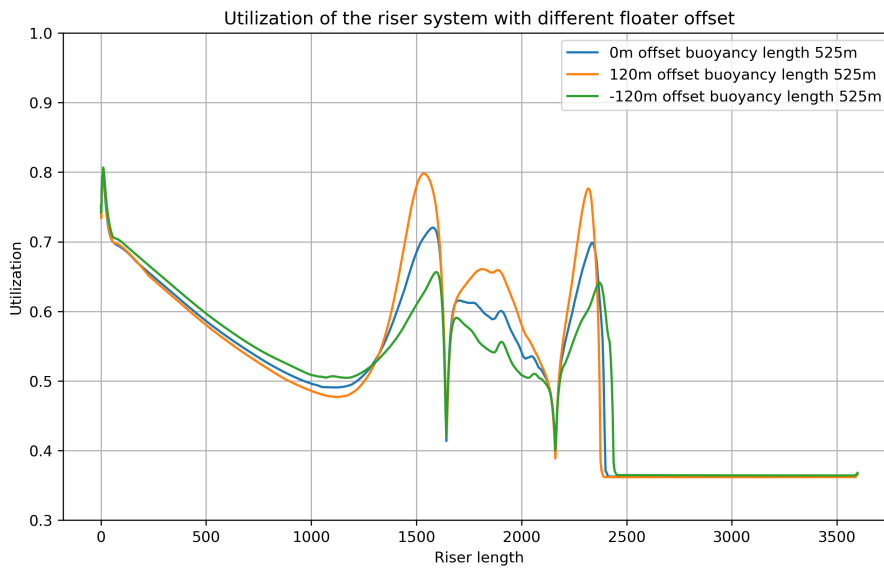


Figure 93: Utilization of buoyancy section length for different offsets

---

	<b>Maximum value in riser</b>	<b>Location on the riser</b>
Static bending moment	211.4 kNm	In the sag bend
Static effective tension	198.3 kN	At the hang-off
Dynamic bending moment	247.9 kNm	In the sag bend
Dynamic effective tension	2366.1 kN	At the hang-off
Utilization	0.797	Near the hang-off

Table 43: Summary of the loads and utilization of the mean offset

	<b>Maximum value in riser</b>	<b>Location on the riser</b>
Static bending moment	290.2 kNm	In the sag bend
Static effective tension	1952.9 kN	At the hang-off
Dynamic bending moment	314.6 kNm	In the sag bend
Dynamic effective tension	2354.4 kN	At the hang-off
Utilization	0.806	Near the hang-off

Table 44: Summary of the loads and utilization of the near offset

	<b>Maximum value in riser</b>	<b>Location on the riser</b>
Static bending moment	148.0 kNm	In the sag bend
Static effective tension	2069.6 kN	At the hang-off
Dynamic bending moment	199.2 kNm	At the TDP
Dynamic effective tension	2471.6 kN	At the hang-off
Utilization	0.807	Near the hang-off

Table 45: Summary of the loads and utilization of the far offset

## F.8 Buoyancy section length 550 meters

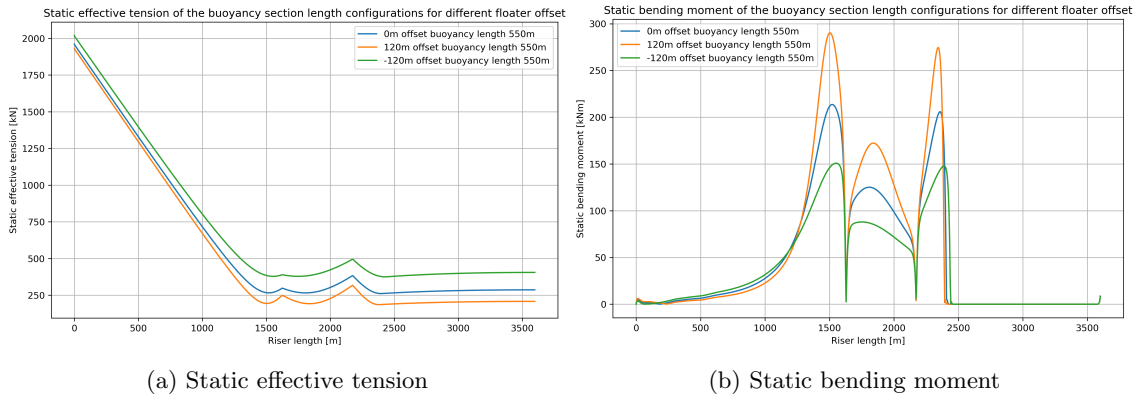


Figure 94: Static results

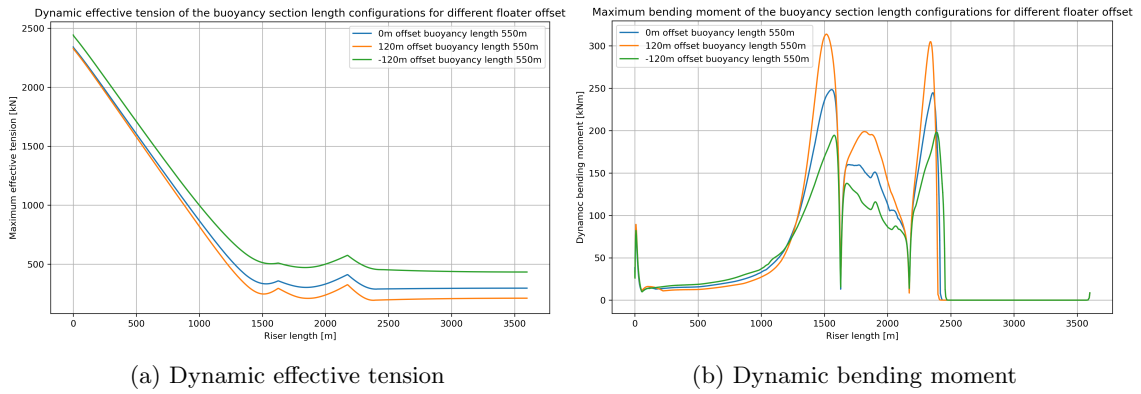


Figure 95: Dynamic results

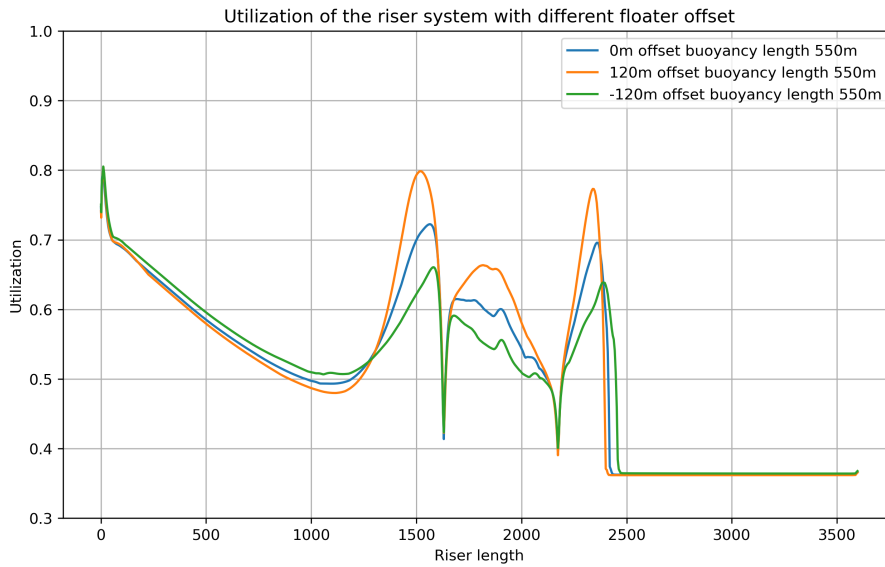


Figure 96: Utilization of buoyancy section length for different offsets

---

	<b>Maximum value in riser</b>	<b>Location on the riser</b>
Static bending moment	213.6 kNm	In the sag bend
Static effective tension	1960.8 kN	At the hang-off
Dynamic bending moment	248.4 kNm	In the sag bend
Dynamic effective tension	2341.2 kN	At the hang-off
Utilization	0.795	Near the hang-off

Table 46: Summary of the loads and utilization of the mean offset

	<b>Maximum value in riser</b>	<b>Location on the riser</b>
Static bending moment	290.3 kNm	In the sag bend
Static effective tension	1931.8 kN	At the hang-off
Dynamic bending moment	313.8 kNm	In the sag bend
Dynamic effective tension	2329.4 kN	At the hang-off
Utilization	0.805	Near the hang-off

Table 47: Summary of the loads and utilization of the near offset

	<b>Maximum value in riser</b>	<b>Location on the riser</b>
Static bending moment	150.8 kNm	In the sag bend
Static effective tension	2019.2 kN	At the hang-off
Dynamic bending moment	197.7 kNm	At the TDP
Dynamic effective tension	2442.6 kN	At the hang-off
Utilization	0.805	Near the hang-off

Table 48: Summary of the loads and utilization of the far offset

## F.9 Buoyancy section length 575 meters

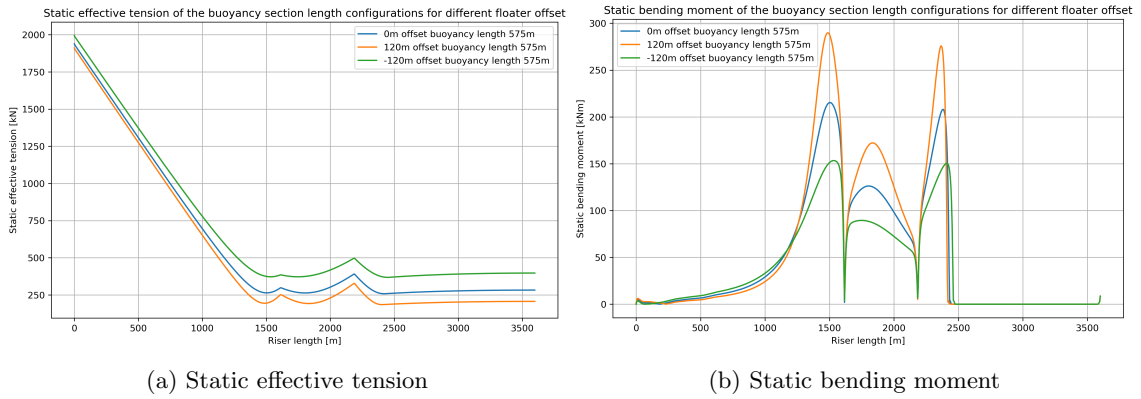


Figure 97: Static results

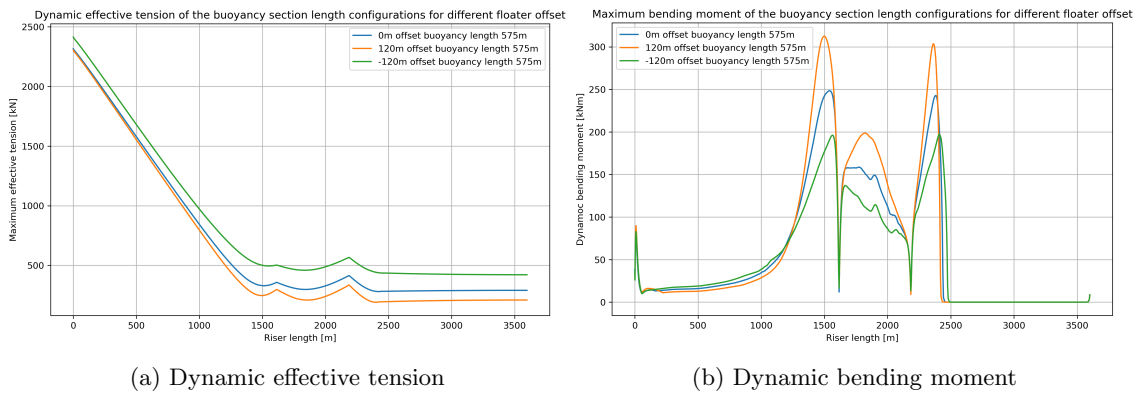


Figure 98: Dynamic results

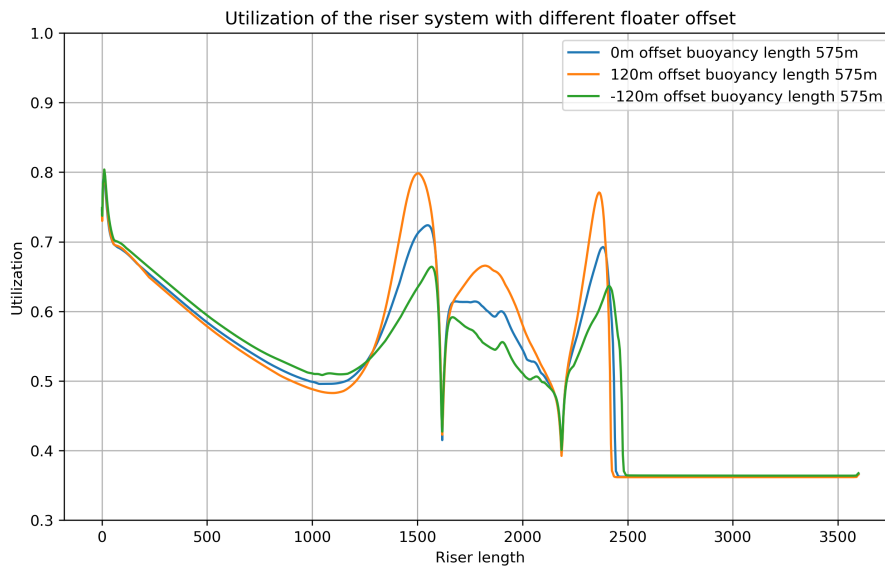


Figure 99: Utilization of buoyancy section length for different offsets



---

	<b>Maximum value in riser</b>	<b>Location on the riser</b>
Static bending moment	215.3 kNm	In the sag bend
Static effective tension	1938.8 kN	At the hang-off
Dynamic bending moment	248.4 kNm	In the sag bend
Dynamic effective tension	2315.8 kN	At the hang-off
Utilization	0.795	Near the hang-off

Table 49: Summary of the loads and utilization of the mean offset

	<b>Maximum value in riser</b>	<b>Location on the riser</b>
Static bending moment	289.8 kNm	In the sag bend
Static effective tension	1910.7 kN	At the hang-off
Dynamic bending moment	312.6 kNm	In the sag bend
Dynamic effective tension	2304.2 kN	At the hang-off
Utilization	0.804	Near the hang-off

Table 50: Summary of the loads and utilization of the near offset

	<b>Maximum value in riser</b>	<b>Location on the riser</b>
Static bending moment	153.4 kNm	In the sag bend
Static effective tension	1994.6 kN	At the hang-off
Dynamic bending moment	197.2 kNm	In the sag bend
Dynamic effective tension	2413.8 kN	At the hang-off
Utilization	0.804	Near the hang-off

Table 51: Summary of the loads and utilization of the far offset

## F.10 Buoyancy section length 600 meters

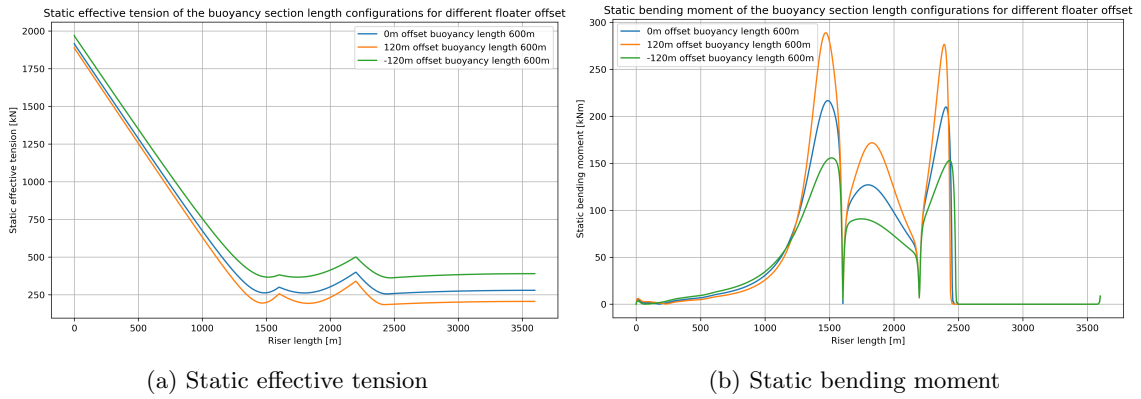


Figure 100: Static results

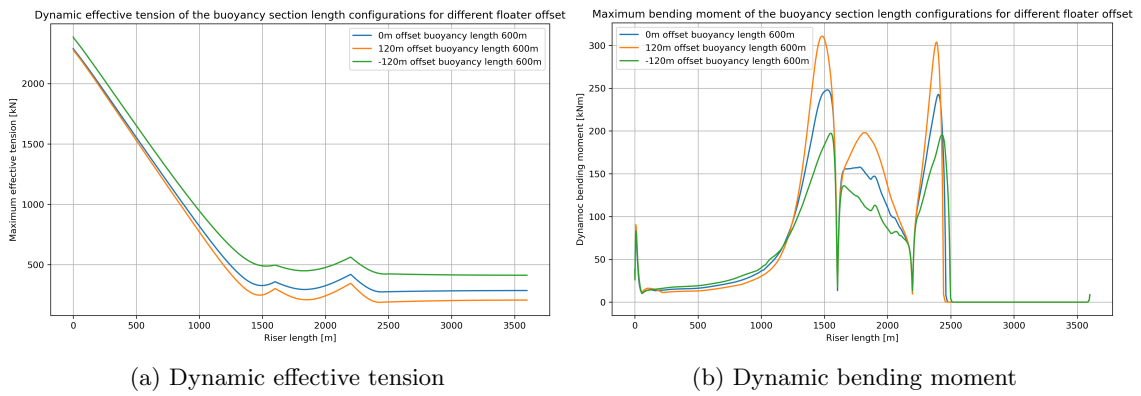


Figure 101: Dynamic results

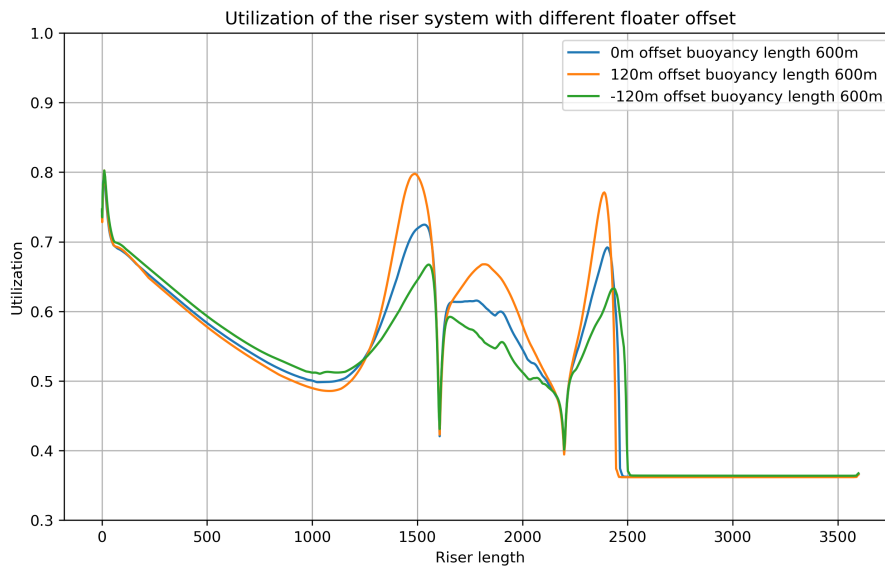


Figure 102: Utilization of buoyancy section length for different offsets

---

	<b>Maximum value in riser</b>	<b>Location on the riser</b>
Static bending moment	216.7 kNm	In the sag bend
Static effective tension	1916.9 kN	At the hang-off
Dynamic bending moment	248.0 kNm	In the sag bend
Dynamic effective tension	2290.3 kN	At the hang-off
Utilization	0.793	Near the hang-off

Table 52: Summary of the loads and utilization of the mean offset

	<b>Maximum value in riser</b>	<b>Location on the riser</b>
Static bending moment	288.9 kNm	In the sag bend
Static effective tension	1889.6 kN	At the hang-off
Dynamic bending moment	310.8 kNm	In the sag bend
Dynamic effective tension	2279.3 kN	At the hang-off
Utilization	0.803	Near the hang-off

Table 53: Summary of the loads and utilization of the near offset

	<b>Maximum value in riser</b>	<b>Location on the riser</b>
Static bending moment	155.7 kNm	In the sag bend
Static effective tension	1970.3 kN	At the hang-off
Dynamic bending moment	197.3 kNm	At the TDP
Dynamic effective tension	2385.1 kN	At the hang-off
Utilization	0.802	Near the hang-off

Table 54: Summary of the loads and utilization of the far offset

